University of Milano-Bicocca
School of Medicine and Surgery
PhD Program in Translational and Molecular Medicine DIMET

Angiotensin-(1-7) and Prone position: important strategies for the management of injury induced by mechanical ventilation

Paolo Delvecchio

Registration Number: 743047

Coordinator: Prof. Andrea Biondi, MD, PhD

Tutor: Prof. Giacomo Bellani, MD, PhD

XXXIII CYCLE
ACADEMIC YEAR
2019-2020

Ai miei genitori,
Ai loro sacrifici e al loro sudore.
Alla mia famiglia e ai miei amici.

Questa vittoria la dedico a voi.

Una volta in cima, non dimenticare mai chi ti ha aiutato a scalare la montagna.

The first part of this work was performed at the University of Milan-Bicocca, thanks to the support and mentorship of my tutor Prof. Giacomo Bellani and the assistance of Vanessa Zambelli while the second one at the University of Pennsylvania, Philadelphia, thanks to the supervision and help of Prof. Maurizio Cereda and Yi Xin.

TABLE OF CONTENTS

CHAPTER 1: INTRODUCTION

1.1 DEFINITION OF MECHANICAL VENTILATION

Mechanical ventilation (MV) is a life-saving intervention used to help patients breathe when they cannot maintain spontaneous ventilation to provide adequate oxygenation or carbon dioxide removal. The machine that providing this function is called ventilator.

Respiratory support is needed when occurs a dysfunction of the mechanisms of breathing or in the muscles that have to regulate it or in the airways or lung parenchyma or chest wall [1].

Most patients who need support from a ventilator because of a severe illness are cared in a hospital's intensive care unit (ICU). The primary goal of MV is the improvement of pulmonary gas exchange and it's crucial to maintain an adequate gas exchange in patients with pulmonary illness. MV is mainly used to support or replace the spontaneous breathing of a patient who has an acute respiratory failure, even if the clinical conditions leading to mechanical ventilation can be grouped into four areas as shown in table 1 [2,3].

Indication	Examples
Acute ventilatory failure	Apnea or Acute lung injury (ALI) or Acute respiratory distress syndrome (ARDS) pH <7.30, $PaCO_2$ >50 mmHg
Impending ventilatory failure	Progressive acidosis and Hypoventilation to pH <7.30 and $PaCO_2$ >50 mmHg Spontaneous frequency >30/min
Severe Hypoxemia	PaO_2 <40 mmHg, SaO_2 <75%, PaO_2 / F_IO_2 <300 mmHg for ALI, <200 mmHg for ARDS
Prophylactic ventilatory support	Post-anesthesia recovery Muscle fatigue Neuromuscular disease

Table 1. Indications for mechanical ventilation

1.2 RESPIRATORY CYCLE DURING SPONTANEOUS BREATHING

Pulmonary ventilation can be seen as the exchange, the flow of gas between the atmosphere and alveolar structure and vice versa. The diffusion of gases brings the partial pressures of Oxygen (O2) and carbonic dioxide (CO2) in blood and alveolar gas to an equilibrium at the pulmonary blood-gas barrier [4].

The alveolar pressure, according to Boyle's law, can change as a result of a volume change. Indeed, an increase in volume requires a reduction in pressure [4].

Alveolar PCO2 (PACO2) depends on the balance between the amount of CO2 being added by pulmonary blood and the amount being eliminated by alveolar ventilation (V̇A). In steady-state conditions, CO2output equals CO2elimination, but during non-steady-state conditions, phase issues and impaired tissue CO2clearance make CO2output less predictable [5]. The pressure value in the thoracic cage is negative in a normal spontaneous breathing act, throughout the ventilatory cycle (−5 cm H2O during exhalation to −8 cm H2O during inhalation). Alveolar pressure fluctuates from −1 cm H2O during inhalation to +1 cm H2O during exhalation [6]. The decrease in intrapleural pressure during inhalation facilitates lung inflation and venous return. It is this negative interpleural pressure that keeps the alveoli open and through the interaction of the lungs and chest wall interpleural pressure is altered, enabling the movement of gas into and out of the lungs (ventilation) (Figure 1). Transpulmonary pressure is the difference between proximal airway pressure and intrapleural pressure. The greatest transpulmonary pressure that can be generated normally during spontaneous inspiration is, normally about 30 cm H2O [7].

During inhalation, the contraction of the muscles of the rib cage and diaphragm increases the volume of the chest. When the diaphragm

contracts, it is able to increase the volume of the thoracic cavity and this leads to a decrease in alveolar pressure.

At the end of the inhalation, after relaxation of respiratory muscles, an elastic return of the lungs brings the diaphragm and the ribs back to the initial position. During exhalation, the volume of the thoracic cavity decreases and the alveolar pressure increases, up to a maximum value of 1 mmHg above atmospheric pressure. The alveolar pressure is now higher than atmospheric, so the air flow reverses and the air leaves the lungs.

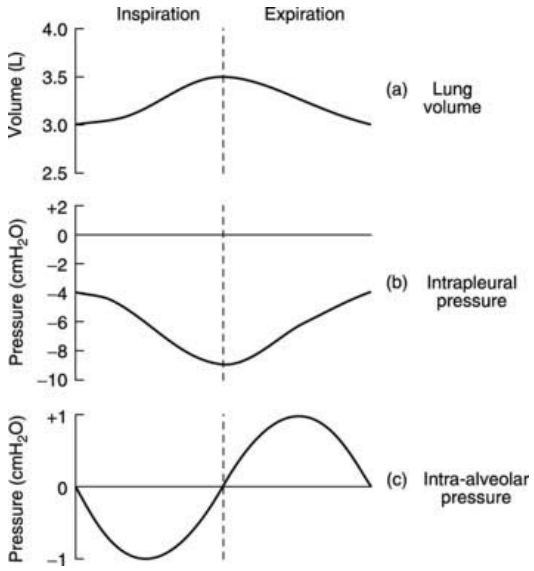

Figure 1. The relationship between (a) lung volume, (b) intrapleural pressure and (c) intra-alveolar pressure during quiet breathing.

In the alveolar structure the partial pressure of oxygen is 100 mmHg, while in the venous blood vessel the partial pressure of oxygen is 40 mmHg. Consequently, oxygen will move according to its partial pressure gradient moving from the alveoli towards the capillaries. The diffusion process achieves equilibrium and the PO_2 in the arterial blood equals that in the alveoli (100 mmHg) [7]. When arterial blood reaches the capillaries in the tissues, the gradient reverses. Indeed, cells continuously use oxygen for oxidative phosphorylation. In a cell at rest, intracellular PO_2 averages 40 mmHg. The arterial blood that irrigates the systemic capillaries has a PO2 partial pressure of 100 mmHg. Therefore, oxygen diffuses according to its gradient from the plasma to the cells. Once equilibrium is reached, PO2 in venous blood equals partial pressure in perfused cells [8].

1.3 VENTILATOR SETTING

When it becomes necessary to provide mechanical ventilation to a patient, the following main ventilator settings must be determined: mode, respiratory rate, Positive end expiratory pressure (PEEP), tidal volume, FIO2 and inspiratory/expiratory ratio. These initial ventilator settings are mainly based on a patient's body size, diagnosis, pathophysiology, and laboratory results. These settings only serve as a starting point and they

should be adjusted according to changes in the patient's condition and requirements [9].

MODE

In clinical practice a wide range of ventilator modes and set up options exist. The first classification is between the non-invasive ventilation and invasive ventilation; the first one is used when endotracheal intubation is not used, while when this is used the ventilation is termed invasive.

The ventilator blows gas (air plus oxygen as needed) into a person's lungs and it can deliver higher levels of oxygen than delivered by a mask or other devices (non-invasive ventilation).

The mechanical ventilation can be a positive pressure ventilation when is applied a positive pressure to the airway opening (comparative to atmospheric pressure) or in the case in which is used a negative pressure (always comparative to atmospheric pressure) to the abdomen of the patients, this ventilation is called negative pressure ventilation (non-invasive ventilation) [10,11].

Another differentiation is about the support's type, a patient can receive a total ventilatory support (FVS) or just partial ventilatory support (PVS) even in most of situations patients require full mechanical support.

Lastly, mechanical ventilation can be distinguished in ventilation at volume controlled (VCV) a desired tidal volume (a control variable) is set

and the pressure changes from breath to breath, and ventilation at pressure controlled (PCV) where the desired pressure (a control variable) is set and the delivered volume changed.

RESPIRATORY RATE

The respiratory rate is the number of breaths that the ventilator provides per minute and usually the initial frequency is set between 10 and 12/min and care should be taken when it exceeds 20/min as intrinsic PEEP can develop [12].

A possible way to select the initial frequency is to estimate the patient's minute volume requirement and divide the estimated minute volume by the tidal volume.

Frequency = Estimated minute volume/Tidal volume

The estimated minute volume for males is equal to 4.0 multiplied by the body surface area (BSA) (in square meters) and for females is equal to 3.5 multiplied by the BSA. In the case in which the concentration of the CO2 is elevated (e.g., due to an increase of metabolic rate) or the physiologic dead-space is increased (e.g., due to a decrease of pulmonary perfusion), the minute volume required to normalize the PaCO2 will need to be increased. Since increasing the tidal volume results in higher airway

pressures on a volume-limited ventilator, it is usually more appropriate to increase the minute volume by increasing the ventilator frequency [13].

PEEP

The ventilator can also provide what is called positive end expiratory pressure (PEEP). This helps to keep the alveoli stable and avoid collapse.
Positive end-expiratory pressure (PEEP) is the positive pressure that remains in the airways at the end of the respiratory cycle (end of exhalation) [14].

Positive end-expiratory pressure (PEEP) increases the functional residual capacity and is useful to treat hypoxemia (low PaO2 not responding to high FIO2). The initial PEEP level may be set at 5 cm H2O. Subsequent changes of PEEP should be based on the patient's blood gas results, FIO2 requirement, tolerance of PEEP, cardiovascular responses and mechanical responses [15].

TIDAL VOLUME

Tidal volume is the volume of gas delivered to the lungs in each breath by the mechanical ventilator.
For patients with no significant lung disease, such as patients who have experienced drug overdose or trauma and need mechanical ventilation

for airways protection, a maximum tidal volume of 10 ml/kg should be used for mechanical ventilation. Recent studies have shown decreased mortality with the use of lower tidal volume in patients with acute lung disease. Therefore, patients with an acute lung disease such as pneumonia, ARDS, fibrotic lung disease, or COPD should be ventilated with tidal volumes of 6–8 ml/kg [16].

I/E RATIO

The I:E ratio is the ratio of inspiratory time to expiratory time and it denotes the proportions of each breath cycle devoted to the inspiratory and expiratory phases. The total time of a respiratory cycle is determined by dividing 60 seconds by the respiratory rate. Inspiratory time and expiratory time are then determined by portioning the respiratory cycle based on the set ratio. For instance, a patient with a respiratory rate of 10 breaths per minute will have a breath cycle lasting 6 seconds. It is usually kept in the range between 1:2 and 1:4, if we apply this ratio to the patient above, the 6-second breath cycle will break down to 2 seconds of inspiration and 4 seconds of expiration [17].

F_IO_2

FiO2: Percentage of oxygen in the air mixture that is delivered to the patient. For patients with severe hypoxemia or abnormal cardiopulmonary functions (e.g., post-resuscitation, smoke inhalation, ARDS), the *initial* F_IO_2 may be set at 100%. The F_IO_2 should be evaluated by means of arterial blood gas analyses after stabilization of the patient. It should be adjusted accordingly to maintain a PaO_2 between 80 and 100mm Hg After stabilization of the patient, the FIO2 is best kept below 60% to avoid oxygen- induced lung injuries [12].

1.4 LUNG MECHANICS

During a mechanical ventilation a several data can be obtained, in order to monitor the lung mechanic trend.

Respiratory mechanics allows the readout of pulmonary function through measures of flow and pressure [18].

The lung function can be determined and influenced by a variety of a parameters, main ones being the pressure, the compliance and the resistance.

Compliance and resistance can be calculated, while pressure, flow and volume are continuously monitored.

The interaction between patient and ventilator can be constantly monitored on the ventilatory that displays all of these parameters.

PRESSURE

During a mechanical ventilation airway pressure, plateau pressure, and mean airway pressure are measured.

The pressure applied to the respiratory system (Prs) is described by the motion's equation:

$$Pr_s = Pa_o + (-P_{mus}) = V \times R + v/C + K$$

Where Pa_o is the pressure at the mouth v is the volume, V the flow over time, and K is a constant representing the alveolar end expiratory pressure. Respiratory pressure is the sum of the pressure generated by the ventilator Pa_o and the pressure developed by the respiratory muscles (P_{mus}) that provides a negative pressure [19].

Essentially, the airway pressure is detected by the ventilator measuring the pressure proximal to the expiratory valve during the inspiratory phase to approximate inspiratory proximal airway pressure and measuring the pressure distal to the inspiratory valve during the expiratory phase to approximate expiratory proximal airway pressure [20].

During the ventilation the most commonly technique for the measuring respiratory mechanics (specially compliance and resistance) is the rapid airway occlusion method. The airway pressure (P_{aw}) has a characteristic trend with the highest peak at end inspiration (P_{max}), followed by a rapid drop after the occlusion (P1), and a slow decay until a plateau is reached (P2) (Fig. 2). P2 is the static pressure of the respiratory system ($P_{st,\ rs}$) that, in the absence of flow, equals the alveolar pressure (P_{alv}), reflecting the elastic retraction of the entire respiratory system. The pressure drop from P_{max} to P1, represents the pressure required to move the inspiratory flow along the airways, thus representing the pressure dissipated by the flow-dependent resistances. Furthermore, the occlusion *manoeuvre* at end inspiration allows identification of the presence of a leak in the respiratory circuit, since the plateau pressure cannot be reached. At the end of a normal expiration, in a normal subject, the alveolar pressure is next to zero. Expiratory flow limitation, or an inadequate respiratory pattern (high tidal volume or high respiratory rate) causes PEEPi due to volume trapping. PEEPi is detectable during the post-expiratory occlusion manoeuvre (Fig. 2) [19,21,22,]

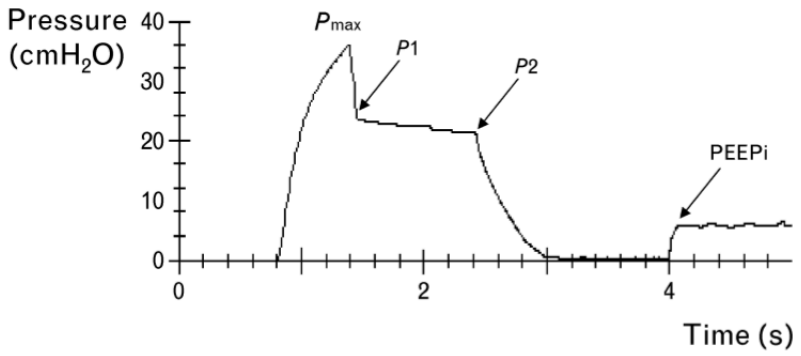

Figure 2. Post-inspiratory and expiratory occlusion is performed. Pmax is the maximum (peak) airway pressure. P1 points to the end of the rapid post-occlusion pressure drop. P2 points to the end of the slope pressure decay plateau. PEEPi, intrinsic positive end expiratory pressure. (*Lucangelo U et al., 2007*)

COMPLIANCE

Normally inspiration is a process, occurs through the expansion of the lungs and the thorax. The capacity with which the lungs and thorax can be distended is the lung compliance. The compliance is a measure of the ease with which the lungs can be inflated and is determined from the gradient of a plot of lung volume against distending pressure

Total compliance depends also on the thoracic cage, not only on the expansion capacity of the lung tissue.

The compliance is the volume change (lung expansion) per unit pressure change (work of breathing) so, this value can be calculated every time as a relationship between volume and pressure or C = DV/DP,

$C = \Delta V/\Delta P$

where C= compliance, DV = volume change, and DP = pressure change (Fig.3).

The patient's ability to maintain efficient gas exchange depends also on the compliance, which should remain within a physiologic range. Low compliance typically makes lung expansion difficult while high level of compliance can determinate an incomplete exhalation or can reduce the CO2 elimination capacity. Based on the previous relationship, low compliance means that the volume change is small per unit pressure change while high compliance is correlated with a sensible increase in volume per unit pressure change. Compliance is reduced by any factor such as pulmonary edema, fibrosis or any kind of restrictive lung diseases. High lung compliance is commonly seen in those patients with obstructive diseases, such of emphysema, in which destruction of the elastic tissue, mainly from cigarette smoke exposure, causes a loss of elastic recoil of the lung [23,24,25].

RESISTANCE

During each inspiration and expiration act air run into obstacles that generate a resistance in the flow route, this phenomenon is known as airway resistance. Airway resistance is an essential parameter of lung function and keep this value under control during mechanical ventilation is crucial.

This parameter is variable indeed airway resistance can change over time due to many factors.

The degree of this resistance may essentially depend on many variabilities such as the diameter of the airway, the type of flow (laminar or turbulent flow) and the surfactant's level in the lung [26]. Increasing in airway resistance, such as in some pulmonary diseases, may lead air trapped in the lungs, generating an obstruction in gas exchange with a possible severe consequence, such as pulmonary failure in severe cases [27]. Indeed, airway resistance is an essential parameter of lung function and keep this value under control during mechanical ventilation is crucial.

Airway resistance in the lung is determined by the delta pressure across the airways (mouth pressure (kPa) - alveoli pressure (kPa)) divided by the flow rate: ΔPressure/Flow

$$R = \Delta P/F$$

During Volume controlled ventilation: ΔPressure means Peak Inspiratory Pressure (PIP) - Plateau Pressure (Fig.3) [28].

Obstruction of airflow may be caused by changes inside the airway (e.g., retained secretions), changes in the diameter of the airway (e.g., hypertrophy of the bronchial muscle structure), or changes outside the airway (e.g., tumors surrounding and compressing the airway) [29].

When one of these conditions occurs, the size of the airway decreases and airway resistance increases.

Resistance to flow may be inspiratory or expiratory. Factors that can increase this obstruction include:

- Bronchial tone.
- Sputum.
- Oedema.
- External breathing circuits (eg ETT / tracheostomy tube and other circuit components).

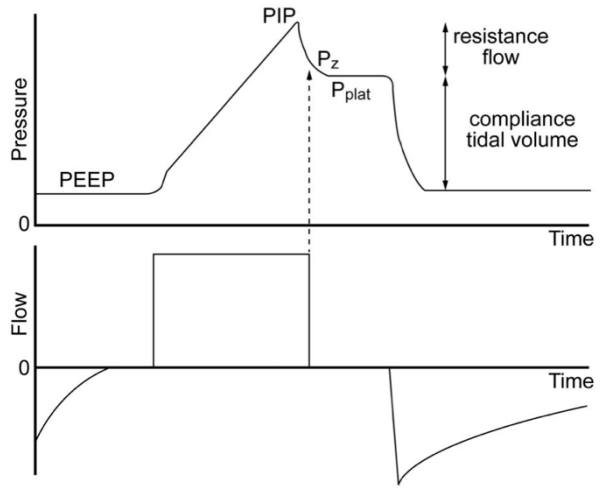

Figure 3. Airway pressure and flow waveforms during constant flow volume control ventilation, illustrating the effect of an end- inspiratory breath-hold. With a period of no flow, the pressure equilibrates to the plateau pressure (P_{plat}). P_{plat} represents the peak alveolar pressure. The difference between P_z and P_{plat} is due to time constant inhomogeneity within the lungs. The difference between the peak inspiratory pressure (PIP) and P_{plat} is deter- mined by resistance and flow. The difference between P_{plat} and PEEP is determined by tidal volume and respiratory system com- pliance. P_z pressure at zero flow (*Hess DR. 2014*).

1.5 THE RESPIRATORY MUSCLE

The respiratory muscles are morphologically and functionally skeletal muscles.

The respiratory act is supported and provided by a large number of muscles. According to which respiratory act they participate, these muscles divide in inspiratory and expiratory muscles (Fig.4).

These muscles are primarily responsible for changing the volume of the thoracic cavity during respiration. The group of expiratory muscles includes the rectus abdominis, external and internal oblique, internal intercostal and transverse abdominis muscles. The group of inspiratory muscles includes the external intercostal, rectus abdominis, external and internal oblique, and transverse abdominis muscles [30].

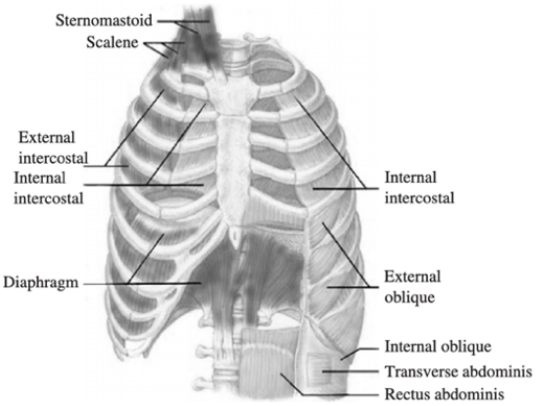

Figure 4. Respiratory muscles.

During low breathing effort (i.e., at rest) only the inspiratory muscles are active. During high breathing effort (i.e., exercise) the expiratory muscles become active as well [31].

The diaphragm is a dome-shaped muscle, with a tendon component, that separates the thorax and abdominal cavities. It is the principal component of respiratory muscle's pump, whose innervation is provided by the phrenic nerves that arise from the nerve roots at C3 through C5 and is primarily composed of fatigue-resistant slow-twitch type I and fast-twitch type II-a myofibers [32,33].

It is wider in the lateral side than in the anterior-posterior one and is higher on the right part due to the presence of the liver. The mammalian diaphragm is composed of three main segments a central noncontractile section, the central tendon (15-20% of the surface area), and two discrete muscular portions, the costal and crural diaphragm. The rat diaphragm is composed of the four major muscle fiber types that are distributed homogeneously within the diaphragm (Fig.3) [34]. The muscle portions are inserted at the vertebral, costal and sternal level and it is also connected through numerous ligaments with the heart, liver, stomach, intestines and other subdiaphragmatic viscera. The diaphragmatic muscle also has orifices through which pass the aorta, the esophagus and the inferior vena cava, the lymphatic system and neurovegetative system. In healthy and normal conditions, inspiration should take place mainly thanks to the intervention of the diaphragm.

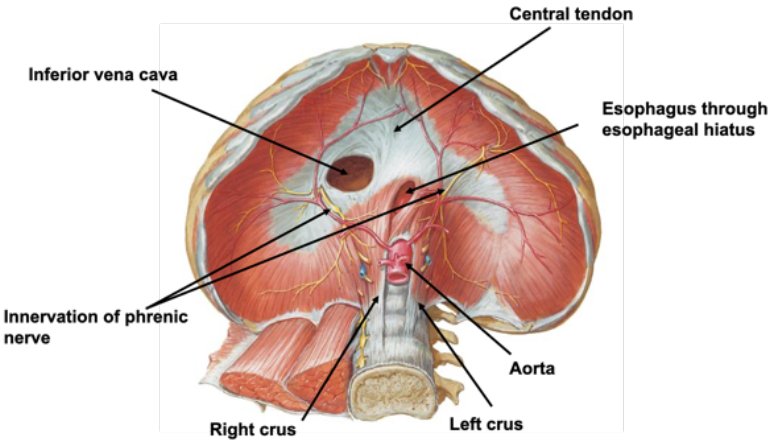

Figure 5. An inferior view of the diaphragmatic muscle.

By contracting it lowers and with the help of the intercostal muscles increases the thoracic volume allowing the inhalation of air into the lungs. The exhalation is instead an exclusively passive phenomenon, during which the diaphragm relaxes and returns to the initial position. The phrenic nerve provides innervation of the entire diaphragm, and the associated efferent projections exit the spinal cord from the mid-cervical ventral roots [35].

1.6 PROLONGED MECHANICAL VENTILATION AND OUTCOMES

Invasive mechanical ventilation is a life-saving intervention for people with acute respiratory failure. Unfortunately, it is also associated with several complications that may prolong the time spent on the ventilator and increase mortality.

Indeed, most patient centered outcomes, such as weaning success and mortality, are tightly correlated with the mechanical ventilation's duration [36].

In the near future, it is anticipated that a higher number of critically ill patients will require prolonged mechanical ventilation (PMV), with associated increases in mortality, morbidity, and costs [37].

Prolonged mechanical ventilation is defined in 2005, at the National Association for Medical Direction of Respiratory Care's conference, as a ventilation of ≥ 21 consecutive days, for ≥ 6 h/d, of invasive (via endotracheal tube or tracheostomy) and/or noninvasive (facial/nasal interface) methods of delivery [38]. Depending on the different criteria used, the definition of PMV, may change. For example, in the United States PMV is ≥ 96 h because this corresponds to the International Classification of Diseases (ICD) [39].

In 2017, Hill et al. have showed that ill patients ventilated for a time longer than 21 days have high in-hospital mortality and greater post-discharge mortality, health care utilization, and health care costs compared with

patients who undergo mechanical ventilation for a shorter period of time [40].

Definitely, the patient's liberation from the ventilator (weaning) as soon as it is feasible and safe, is recommended [41]. Prolonged mechanical ventilation has been recognized as a cause of several potential complications in the lung and diaphragm's function. Indeed, ventilation may cause damage to the lungs, a condition known as ventilator-induced lung injury or VILI, and to the diaphragm called ventilator-induced diaphragmatic dysfunction. It's understandable that the onset of these event can worsen the prognosis and other patient's outcome, such as weaning duration.

Indeed, patients with a dysfunction of the diaphragmatic muscle or with an overloaded secondary lung injury showed frequent early and delayed weaning failures [42,43].

1.7 VENTILATOR-INDUCED DIAPHRAGMATIC DYSFUNCTION

Mechanical ventilation itself can generate a diaphragmatic dysfunction by decreasing the force-generating capacity of the diaphragm, a condition known as ventilator-induced diaphragmatic dysfunction [44,45].

Recently, several studies have showed important evidence that respiratory muscle weakness may develop in ICU patients during a prolonged mechanical ventilation [46].

As stated, prolonged mechanical ventilation (PMV) can generate contractile dysfunction and atrophy of the diaphragmatic muscle result in the rapid development of the weakness (Fig.6), this condition called ventilator-induced diaphragmatic dysfunction or VIDD. Multiple recent studies have shown that VIDD is reported in up to 53% of mechanically ventilated patients within 24 h of intubation. An additional 26% may develop VIDD while on mechanical ventilation during their stay in the intensive care unit (ICU) [47].

From the first evidence of the correlation between MV and VIDD, several animal and human experiments consistently demonstrated that prolonged duration of mechanical ventilation resulting in an increment in the activity of oxidative stress and of the most important proteolytic pathways such ubiquitin-proteasome system, caspases and calpains (Fig. 7 and Fig.9) [48,49].

Numerous animal studies (mice, rats, rabbits, and pigs) have demonstrated that PMV results in significant atrophy of diaphragm muscle fibers [50-53].

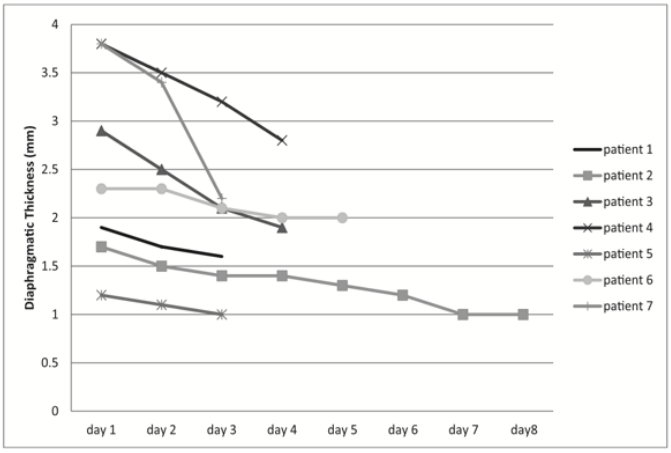

Figure 6. Diaphragm thickness over time for different patients (*Horiana B. Grosu et al 2012*).

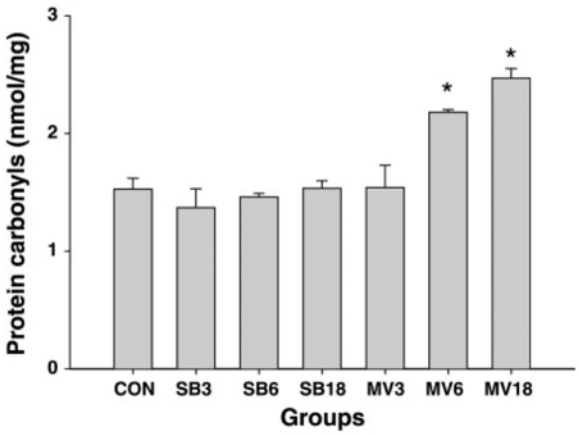

Figure 7. Differences about oxidative stress's component at different time of MV. *(Zergeroglu MA et al 2003).*

The composition of the fiber between rat and human is anatomically similar [54,55], for this reason rats are the most commonly used animal model to study MV-induced changes in diaphragm fiber size and function. The diaphragmatic atrophy occurring during MV a result of a decrease in protein synthesis and/or an increase in the rate of protein degradation. Mechanical ventilation generates a 30% decrease in mixed muscle protein synthesis in the diaphragm within the first 6 hours of MV, as shown is figure 8, and remained at this suppressed level during the following 12 hours of MV [56].

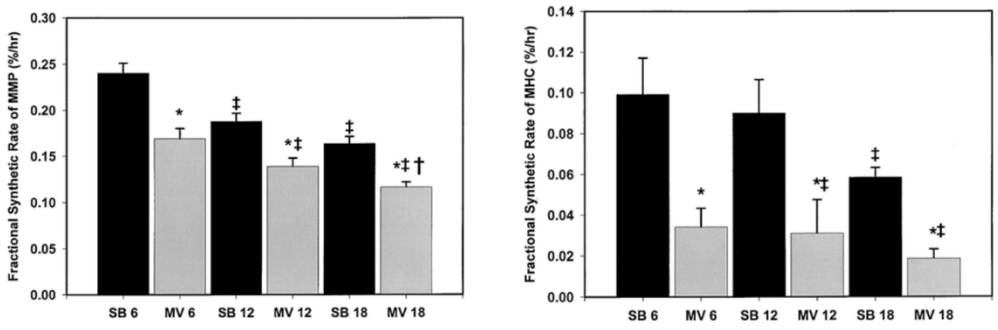

Figure 8. Fractional synthetic rates of mixed muscle protein (MMP) (top) and of myosin heavy chain (MHC) (bottom) *(R. Andrew Shanely 2004).*

It is important to observe that both partial and total MV results in diaphragmatic atrophy even if during a partial ventilation the development of this condition appears slower than during fully controlled MV. Inactivity and lack of mechanoreceptor stimulation dramatically affect muscle function, with a 12% to 40% loss of muscle function in one week [57,58]. The strength of fast-twitch (type II) fibers appears to decline at an accelerated rate compared to declines in strength measured within slow-twitch (type I) fibers, which implies that the diaphragm is one of most heavily affected muscles. Indeed, the diaphragm undergoes nearly 50% loss of muscle mass over the first 96 hours from the start of mechanical ventilation [59].

In fact, diaphragm dysfunction is highly prevalent. For instance, Dres and colleagues have demonstrated that at the time of the first spontaneous breathing trial in patients who had undergone mechanical ventilation, 63% of the patients had developed diaphragm dysfunction, which has recently been termed “critical illness–associated diaphragm weakness” [60].

Prolonged MV results in oxidative damage to the diaphragm through the generation of reactive oxygen species and their derivatives that have a significant effect on the contraction of the skeletal muscle. During prolonged MV, the oxidative modification of diaphragm contractile proteins leads to less efficient activation of diaphragm fibers induced by calcium.

Recently, Zergeroglu et al., showed that after 18 h of controlled MV there is in an increase in the protein carbonyls in the diaphragmatic muscle fibers that suggested an increase in oxidized proteins [61].

1.8 WEANING AND VIDD

The term "weaning" is used to describe the process that gradually leads to the decreasing in ventilation support. Before this process a successful degree can be predicted and a delayed weaning can lead to complications such as ventilator induced lung injury (VILI), ventilator associated pneumonia (VAP) or ventilator induced diaphragmatic dysfunction [62].

For patients undergoing prolonged mechanical ventilation, atrophy of the diaphragm muscles can occur as a result of muscle proteolysis and a decrease in myofiber content. Furthermore, the loss of diaphragm force is time dependent and because respiratory muscles play a crucial role in weaning and rehabilitation weaning from mechanical ventilation should be initiated as soon as feasible [63].

Most of the patients are weaned from the ventilator and the weaning failure, the inability to liberate a patient from the ventilator, occurs in a minority of patients but represents an important burden in term of days of mechanical ventilation morbidity and mortality [64].

The duration of the MV is crucial for the weaning process and after a prolonged time of mechanical ventilation weaning failure may occur. The

diaphragmatic thickness monitoring is very important to predict the weaning outcome. In 2014 Dinino et al. showed that, using ultrasonography, the difference in terms of diaphragmatic thickness between the end of inspiration and expiration could predict extubation failure with a sensitivity of 88% and a specificity of 71% [65].

Recent findings confirmed that diaphragm dysfunction is frequently involved during weaning failure and that it is associated with poor prognosis at time of liberation from mechanical ventilation [66-68].

Definitely, as Powers et al. have demonstrated, the clinical significance of VIDD resides in the belief that diaphragmatic weakness contributes to the inability to wean patients from MV (Fig.9). Difficult weaning is an important clinical problem and occurs in ∼30% of adult patients provided ventilator support for more than 3 days [69].

Ultimately, identifying the reason why a patient fails the weaning process might help to reduce the duration of mechanical ventilation and hence to improve patient outcomes.

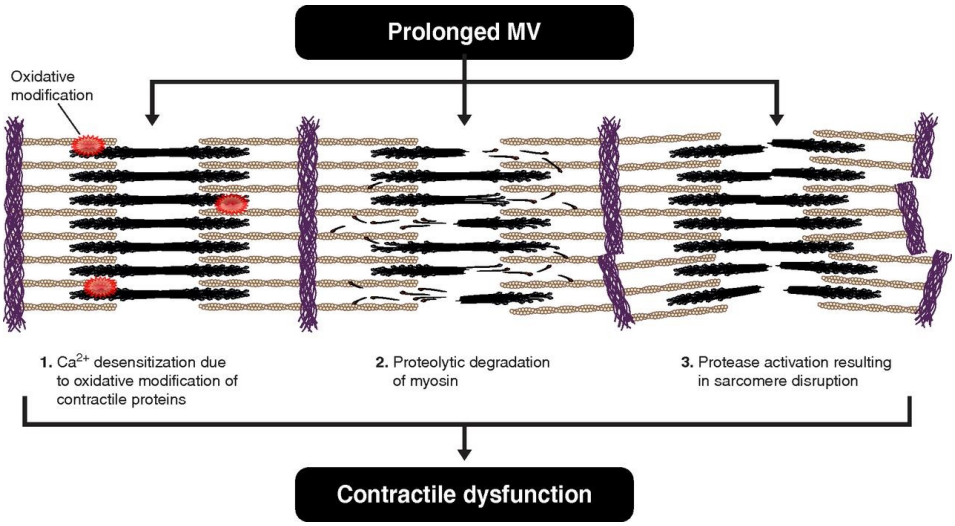

Figure 9. Potential mechanism under VIDD development *(Powers SK, 2013)*.

1.9 ANGIOTENSIN-(1-7)

The renin-angiotensin system (RAS) is a hormone system implicated in the regulation of blood pressure and fluid homeostasis. Many pathways are involved in the RAS system that plays an important role in several pathological processes, such as atherosclerosis, myocardial infarction, stroke, diabetes, tumorigenesis, and acute respiratory distress syndrome (ARDS) [70-72]. The main effector of the classical RAS system's axis is angiotensin II (Ang-II), which is originated by the proteolytic cleavage of

angiotensin I (Ang-I) by the angiotensin converting enzyme (ACE) (Fig.10). In parallel with the classical axis, RAS has counter-regulatory axis, which is composed by ACE2, the principal peptide angiotensin (1–7) (Ang (1–7)) and its receptor Mas (Fig.10) [73].

Beside hemodynamic process, it's known that RAS plays a relevant role in skeletal muscle diseases. Experimental studies showed that the infusion of Angiotensin-II can induce marked diaphragmatic muscle atrophy with an increase of atrophy, fibrosis and protein degradation [74].

In 2015, Kwon et al. have provided preclinical data in rats demonstrating that the treatment with losartan, an Ang-II receptor 1 (AT1R) antagonist, have clinical benefits to protect against ventilator-induced diaphragm weakness [75].

On the other hand, some evidence about the beneficial properties of Angiotensin-(1-7) has been published. Recently, Meneses et al. showed that Ang (1-7), through Mas, is able to prevent the effects induced by Ang II in the diaphragm muscles and decreases several events. [76]. In line with these results, experimental studies demonstrated that Ang-(1–7) lessens atrophy in models of endotoxin-related skeletal muscle wasting and disuse skeletal muscle atrophy [77,78]. The effects of the infusion of Angiotensin-(1-7) have been investigated by Sigurta' et al, in a rat model of VILI, suggesting beneficial effects in terms of improvement in oxygenation, inflammation, and lung fibrosis [73].

Nowadays, there aren't preclinical studies providing the effects of Ang-(1–7) on the diaphragmatic dysfunction, even if based on evidence, Ang-(1–7) may have an important role in the VIDD pathophysiology.

Verifying this hypothesis can help in understanding the processes involved in ventilator-induced diaphragmatic dysfunction pathophysiology and open new possibilities for its prevention and treatment.

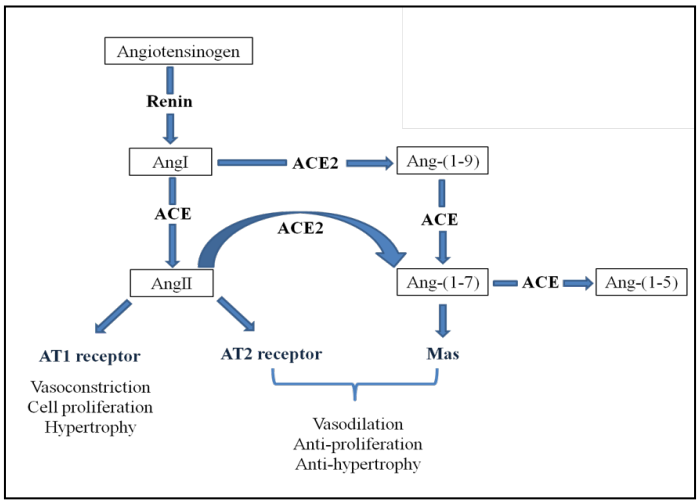

Figure 10. Renin-angiotensin system cascade. AngI: angiotensin I; ACE: angiotensin-converting enzyme; AT1 receptor: AngII type 1 receptor; AT2 receptor: AngII type 2 receptor; Mas: Ang-(1-7) receptor. *(Zambelli V., 2012)*.

1.10 ACUTE RESPIRATORY DISTRESS SYNDROME

The story of Acute Respiratory Distress Syndrome (ARDS) is very old, it's first description was illustrated in 1967 [79]. even if was more accurately defined in 1994 by the American-European Consensus Conference (AECC) [80].

Since then, over the years to improve the accuracy of clinical diagnosis a new definition has been proposed which describes ARDS as an acute lung injury correlated with an inflammatory condition, this definition is known as the Berlin definition [81].

According to the Berlin definition ARDS can be distinguished be the following points:

- Timing: the clinical picture within 7 days of a known clinical event (also a new or worsening respiratory symptoms),
- Chest imaging: Bilateral opacities—not fully explained by effusions, lobar/lung collapse, or nodules,
- Origin of edema: Respiratory failure not fully explained by cardiac failure or fluid overload Need objective assessment (eg, echocardiography) to exclude hydrostatic edema if no risk factor present,
- Oxygenation: the severity of ARDS is so defined:
    - Mild: $200 < PaO_2/FiO_2 < 300$ con CPAP o PEEP > $5cmH_2O$

- Moderate: 100< PaO_2/FiO_2 <200 con PEEP > 5cmH2O
- Severe: PaO_2/FiO_2 < 100 con PEEP > 5cmH_2O

According to this new definition, ARDS is a diffuse inflammatory lesion, characterized by an increase in the permeability of pulmonary vessels and a reduction in the aerated lung volume due to the presence of bilateral infiltrates.

The main consequence of ARDS is the presence the onset of a different degrees of hypoxemic situation with an increasing in alveolar shunt and not aerated lung regions.

The classification of ARDS into three increasing stages of severity—mild, moderate, and severe—according to the level of hypoxemia, significantly reflected an increased mortality rate (respectively: 27%, 95% CI, 24–30%; 32%, 95% CI, 29–34%; and 45%, 95% CI, 42–48%) [82].

Puybasset et al., have showed, using chest X-ray and CT scan, that several differences in lung morphology, are correlated with different distribution of gas and opacities within the pulmonary regions and these different patterns are observed in patients whose clinical condition was in line with the ARDS definition [83].

Nowadays, lung CT scan is the pivotal tool for the diagnosis of extrapulmonary causes of ARDS, the most frequent are pneumonia, extrapulmonary sepsis, and aspiration [84].

Mechanical ventilation has always been the main tool for the ARDS management even id over the years it was discovered that MV can cause

a secondary overlap lung injury, known as ventilatory induced lung injury (VILI).

1.11 VENTILATOR-INDUCED LUNG INJURY

Since the first introduction of the mechanical ventilation, clinicians have suspected that tidal volume and the airway pressure required to maintain and adequate pulmonary gas exchange might contribute to the lung injury, although the term VILI was introduced in 1993 [85].

VILI is defined as an acute lesion of the lung parenchyma caused by the mechanical ventilation. Several factors have been recognized as possible triggers of VILI. Indeed, a clinically significant VILI may occur from volutrauma, barotrauma, atelectrauma and biotrauma [86].

In 2000, the landmark ARDS Network trial showed that limiting tidal volume (6 vs. 12 mL/kg predicted body weight [PBW]) and plateau airway pressure (≤ 30 vs. ≤ 50 cmH_2O) improves survival in patients with acute respiratory distress syndrome [87].

- Barotrauma: is a mechanical damage caused by an excessive pressure gradient applied on the alveolar walls that leads to a rupture of lung parenchyma. This event may result in phenomena

such as pneumothorax, pneumomediastinum, pneumoperitoneum and subcutaneous emphysema [88]. The mechanism behind the development of barotrauma is excessive transpulmonary pressure (PTP), that is the difference between the pressure applied inside the lung, i.e. the alveolar pressure and the pressure present outside the lung, i.e. the pleural pressure.

- Volutrauma: is a lung damage caused by high tidal volume, which lead to an excessive distension of the alveolar units and small airways. For much of the last thirty years, barotrauma (high inflation pressure-mediated lung injury) and volutrauma (overdistension-mediated lung injury) were viewed as distinct albeit related entities [89]. Instead, this kind of lung injury, caused by excessive strain, is strictly connected to barotrauma, as Dreyfuss et al. have showed in experimental studies on rat model of VILI. Furthermore, an excessive pulmonary transpulmonary pressure can be determined both by the application of an excessive peak inspiratory pressure (PIP) and by an excessive tidal volume compared to the lung volume [90,91].

- Atelectotrauma: is a parenchymal lesion caused by the cycling opening and closing (recruitment/de-recruitment) of the small airways and alveoli during each act of ventilation. The idea that

lung injury can be also determined by repeated opening and closing of airway alveolar duct units was introduced for the first time in 1994 by Muscedere [92]. This concept was later confirmed by Arthur Slutsky, after observing the marked increase in inflammatory cytokines in *in vivo* experiments on rats, when the lungs were allowed to cyclically collapse and re-inflate [93]. The risk of atelectotrauma development is greater if lung volumes are lower and if PEEP is set to a low value, because PEEP prevents active shear stress on the bronchial and alveolar walls. Definitely, clinically low tidal volume ventilation may minimize atelectotrauma by maintaining low airway driving pressures, decreasing likelihood of exceeding the critical opening pressure of collapsed lung units [94,95].

- Biotrauma: is an extended biological response that occur in the lung during the mechanical ventilation. The excessive alveolar distension and the continuous opening and closing of the small airways determine the activation of an inflammatory response, including activation of a monocyte macrophages and lymphocytes [96].

  This proinflammatory response can also become systemic and promotes extrapulmonary organ injury, predisposing to multiorgan failure that carries increased risk of death [97,98].

1.12 LUNG INJURY AND PRONE POSITION

The goal of mechanical ventilation for patients with a pulmonary failure is minimize the side effects (ventilator-induced lung injury) while providing acceptable oxygenation and carbon dioxide (CO_2) clearance [99].

As previous reported, pulmonary stress during mechanical ventilation accelerates acute respiratory distress syndrome (ARDS) progression and may diminish the efficacy of therapeutic strategies, reducing the success's opportunities [100].

Prone ventilation improves gas exchange compared with the supine position via better matching of ventilation and perfusion and decreases the mortality of severe ARDS. The effects of positional therapy on regional lung mechanics might explain its outcome effects: for example, pulmonary gas distribution is more homogeneous when a patient is prone, as improved recruitment of collapsed lung and reduced regional tissue stress compared to supine ventilation may mitigate injury [101-104].

Prone-ventilation in patients may lead to a more uniform distribution of lung stress and strain, leading to improved ventilation-perfusion matching and regional improvement in lung and chest wall mechanics [105].

Indeed, since the first clinical trial in 1997, many preclinical and clinical studies have supported and confirmed the idea that prone position not only improves oxygenation in patients with ARDS, but also decreases the

duration of ventilation and the mortality in these ventilated patients [106].

Supporting this hypothesis, serial computed tomography (CT) scans showed that prone ventilation limited the early propagation of experimental lung injury by stabilizing posterior inflation. In fact, Imaging studies suggest that pulmonary aeration, pleural pressures, and regional strain are more homogeneous in patient in prone versus supine position, due to the apparent attenuation of the gravity-related forces that compress and deform the lungs [107-110].

Based on these data, ventilation in the prone position is recommended for the first week in moderate to severe ARDS patients.

REFERENCES

1. Mehta S, Hill NS. Noninvasive ventilation. Am J Respir Crit Care Med 2001: 163: 540-77
2. Brown BR. Understanding mechanical ventilation: indications for and initiation of therapy. J Okla State Med Assoc. 1994 Aug;87(8):353-7.
3. Otto CW. Ventilatory management in the critically ill. Emerg Med Clin North Am. 1986 Nov;4(4):635-54.
4. Powers KA, Dhamoon AS. Physiology, Pulmonary Ventilation and Perfusion. 2020 Sep 29.
5. Tortora, G. & Grabowski, S.R., 2003, Principles of Anatomy and Physiology, 10th ed, John Wiley & Sons, Inc, New York.
6. Wagner PD, Laravuso RB, Uhl RR, West JB. Continuous distributions of ventilation-perfusion ratios in normal subjects breathing air and 100 per cent O2. J Clin Invest. 1974 Jul;54(1):54-68.
7. West, J 2011, Respiratory Physiology, the Essentials, 9th edition, Williams & Wilkins Co. Baltimore.
8. Cook D, Meade M, Guyatt G, et al. Criteria for Weaning from Mechanical Ventilation. Rockville (MD): Agency for Healthcare Research and Quality (US); 2000 Nov.

9. Pham T, Brochard LJ, Slutsky AS. Mechanical Ventilation: State of the Art. Mayo Clin Proc. 2017 Sep;92(9):1382-1400.
10. Walter JM, Corbridge TC, Singer BD. Invasive Mechanical Ventilation. South Med J. 2018 Dec;111(12):746-753.
11. Esteban A, Anzueto A, Alía I, Gordo F, Apezteguía C, Pálizas F, Cide D, Goldwaser R, Soto L, Bugedo G, Rodrigo C, Pimentel J, Raimondi G, Tobin MJ. How is mechanical ventilation employed in the intensive care unit? An international utilization review. Am J Respir Crit Care Med. 2000 May;161(5):1450-8.
12. Shapiro BA. A historical perspective on ventilator management. New Horiz. 1994 Feb;2(1):8-18.
13. Brown, B. R. (1994). Understanding mechanical ventilation: Indications for and initiation of therapy. Journal of the Oklahoma State Medical Association, 87, 353–357.
14. Acosta P, Santisbon E, Varon J. "The use of positive end-expiratory pressure in mechanical ventilation". Crit Care Clin. 2007 Apr;23(2):251-61.
15. Rezoagli E, Bellani G. How I set up positive end-expiratory pressure: evidence and physiology-based! Crit Care. 2019 Dec 16;23(1):412.
16. Mark A. Warner, Bela Patel, Chapter 48 - Mechanical Ventilation, Editor(s): Carin A. Hagberg, Benumof and Hagberg's Airway

Management (Third Edition), W.B. Saunders, 2013, Pages 981-997.e3.

17. Sembroski E, Sanghavi D, Bhardwaj A. Inverse Ratio Ventilation. 2020 Jul 6. In: StatPearls [Internet]. Treasure Island (FL): StatPearls Publishing; 2020 Jan–. PMID: 30571016. Shapiro BA. A historical perspective on ventilator management. New Horiz. 1994 Feb;2(1):8-18.
18. Hess DR, Medoff BD, Fessler MB. Pulmonary mechanics and graphics during pressure ventilation. Int Anesthesiol Clin 1999;37(3):15-34.
19. Lucangelo U, Bernabé F, Blanch L. Lung mechanics at the bedside: make it simple. Curr Opin Crit Care 2007;13(1):64–72.
20. Hess DR. Respiratory mechanics in mechanically ventilated patients. Respir Care. 2014 Nov;59(11):1773-94.
21. Brochard L. Intrinsic (or auto-) positive end-expiratory pressure during spontaneous or assisted ventilation. Intensive Care Med. 2002 Nov;28(11):1552-4.
22. Ranieri VM, Giuliani R, Cinnella G, Pesce C, Brienza N, Ippolito EL, Pomo V, Fiore T, Gottfried SB, Brienza A. Physiologic effects of positive end-expiratory pressure in patients with chronic obstructive pulmonary disease during acute ventilatory failure and controlled mechanical ventilation. Am Rev Respir Dis. 1993 Jan;147(1):5-13.

23. West, J 2011, Respiratory Physiology, the Essentials, 9th edition, Williams & Wilkins Co. Baltimore.
24. Mauri T, Lazzeri M, Bellani G, Zanella A, Grasselli G. Respiratory mechanics to understand ARDS and guide mechanical ventilation. Physiol Meas. 2017 Nov 30;38(12):R280-H303.
25. Singer BD, Corbridge TC. Basic invasive mechanical ventilation. South Med J. 2009 Dec;102(12):1238-45.
26. Kaminsky DA. What does airway resistance tell us about lung function? Respir Care. 2012 Jan;57(1):85-96; discussion 96-9.
27. Hurley JJ, Hensley JL. Physiology, Airway Resistance. 2020 Sep 27. In: StatPearls [Internet]. Treasure Island (FL): StatPearls Publishing; 2020 Jan–. PMID: 31194340.
28. Criée CP, Sorichter S, Smith HJ, Kardos P, Merget R, Heise D, Berdel D, Köhler D, Magnussen H, Marek W, Mitfessel H, Rasche K, Rolke M, Worth H, Jörres RA; Working Group for Body Plethysmography of the German Society for Pneumology and Respiratory Care. Body plethysmography--its principles and clinical use. Respir Med. 2011 Jul;105(7):959-71.
29. Hogg JC, Paré PD, Hackett TL. The Contribution of Small Airway Obstruction to the Pathogenesis of Chronic Obstructive Pulmonary Disease. Physiol Rev. 2017 Apr;97(2):529-552.
30. Sieck GC, Ferreira LF, Reid MB, Mantilla CB. Mechanical properties of respiratory muscles. Compr Physiol. 2013 Oct;3(4):1553-67.

31. Aliverti A. The respiratory muscles during exercise. Breathe (Sheff). 2016 Jun;12(2):165-8.
32. Hlastala MP, Berger AJ. Physiology of Respiration. New York, NY: Oxford University Press; 2001.
33. Macklem PT. The Thorax; Part A: Physiology, Chapter 15 The Act of Breathing. New York, NY: Marcel Dekker, Inc.; 1995.
34. Poole DC, Sexton WL, Farkas GA, Powers SK, Reid MB. Diaphragm structure and function in health and disease. Med Sci Sports Exerc. 1997 Jun;29(6):738-54.
35. Nair J, Streeter KA, Turner SMF, Sunshine MD, Bolser DC, Fox EJ, Davenport PW, Fuller DD. Anatomy and physiology of phrenic afferent neurons. J Neurophysiol. 2017 Dec 1;118(6):2975-2990.
36. Sansone GR, Frengley JD, Vecchione JJ, Manogaram MG, Kaner RJ. Relationship of the duration of ventilator support to successful weaning and other clinical outcomes in 437 prolonged mechanical ventilation patients. J Intensive Care Med 2017;32(4):283–291.
37. Zilberberg MD, de Wit M, Shorr AF. Accuracy of previous estimates for adult prolonged acute mechanical ventilation volume in 2020: update using 2000-2008 data. Crit Care Med. 2012 Jan;40(1):18-20.
38. MacIntyre NR, Epstein SK, Carson S, Scheinhorn D, Christopher K, Muldoon S, National Association for Medical Direction of Respiratory Care. Management of patients requiring prolonged

mechanical ventilation: report of a NAMDRC consensus conference. Chest 2005;128(6):3937–3954.

39. Variation in Definition of Prolonged Mechanical Ventilation. Louise Rose, Michael McGinlay, Reshma Amin, Karen EA Burns, Bronwen Connolly, Nicholas Hart, Philippe Jouvet, Sherri Katz, David Leasa, Cathy Mawdsley, Danny F McAuley, Marcus J Schultz and Bronagh Blackwood Respiratory Care October 2017, 62 (10) 1324-1332.
40. Hill AD, Fowler RA, Burns KE, Rose L, Pinto RL, Scales DC. Long-Term Outcomes and Health Care Utilization after Prolonged Mechanical Ventilation. Ann Am Thorac Soc. 2017 Mar;14(3):355-362.
41. Difficulty weaning from mechanical ventilation; Failure to wean, respiratory failure, ventilator dependence. Scott Epstein Critical care medicine 2019.
42. Kim WY, Suh HJ, Hong SB, Koh Y, Lim CM. Diaphragm dysfunction assessed by ultrasonography: influence on weaning from mechanical ventilation. Crit Care Med. 2011 Dec;39(12):2627-30.
43. Wawrzeniak IC, Regina Rios Vieira S, Almeida Victorino J. Weaning from Mechanical Ventilation in ARDS: Aspects to Think about for Better Understanding, Evaluation, and Management. Biomed Res Int. 2018 Oct 9;2018:5423639.

44. Zhu EC, Yu RJ, Sassoon CS: Ventilator-induced diaphragm dysfunction and its prevention [in Chinese]. Zhonghua Jie He He Hu Xi Za Zhi 2008; 31:616–619).
45. Schild K, Neusch C, Schönhofer B. Ventilator induzierter Zwerchfellschaden [Ventilator-induced diaphragmatic dysfunction (VIDD)]. Pneumologie. 2008 Jan;62(1):33-9. German.
46. Levine S, Nguyen T, Taylor N, Friscia ME, Budak MT, Rothenberg P, Zhu J, Sachdeva R, Sonnad S, Kaiser LR, Rubinstein NA, Powers SK, Shrager JB. Rapid disuse atrophy of diaphragm fibers in mechanically ventilated humans. N Engl J Med. 2008 Mar 27;358(13):1327-35.
47. Johns Hopkins Medicine | Armstrong Institute for Patient Safety and Quality Baltimore, Mechanically ventilated patients, AHRQ Publication No. 16(17)-0018-1-EF January 2017
48. Zergeroglu MA, McKenzie MJ, Shanely RA, Van Gammeren D, DeRuisseau KC, Powers SK. Mechanical ventilation-induced oxidative stress in the diaphragm. J Appl Physiol (1985). 2003 Sep;95(3):1116-24.
49. Powers SK, Wiggs MP, Sollanek KJ, Smuder AJ. Ventilator-induced diaphragm dysfunction: cause and effect. Am J Physiol Regul Integr Comp Physiol. 2013 Sep;305(5):R464-77.
50. Capdevila X, Lopez S, Bernard N, Rabischong E, Ramonatxo M, Martinazzo G, Prefaut C. Effects of controlled mechanical

ventilation on respiratory muscle contractile properties in rabbits. Intensive Care Med. 2003 Jan;29(1):103-10.

51. Jung B, Constantin JM, Rossel N, Le Goff C, Sebbane M, Coisel Y, Chanques G, Futier E, Hugon G, Capdevila X, Petrof B, Matecki S, Jaber S. Adaptive support ventilation prevents ventilator-induced diaphragmatic dysfunction in piglet: an in vivo and in vitro study. Anesthesiology. 2010 Jun;112(6):1435-43.
52. Mrozek S, Jung B, Petrof BJ, Pauly M, Roberge S, Lacampagne A, Cassan C, Thireau J, Molinari N, Futier E, Scheuermann V, Constantin JM, Matecki S, Jaber S. Rapid onset of specific diaphragm weakness in a healthy murine model of ventilator-induced diaphragmatic dysfunction. Anesthesiology. 2012 Sep;117(3):560-7.
53. Tang H, Lee M, Sharpe O, Salamone L, Noonan EJ, Hoang CD, Levine S, Robinson WH, Shrager JB. Oxidative stress-responsive microRNA-320 regulates glycolysis in diverse biological systems. FASEB J. 2012 Nov;26(11):4710-21.
54. Poole DC, Sexton WL, Farkas GA, Powers SK, Reid MB. Diaphragm structure and function in health and disease. Med Sci Sports Exerc. 1997 Jun;29(6):738-54.
55. Nguyen T, Shrager J, Kaiser L, Mei L, Daood M, Watchko J, Rubinstein N, Levine S. Developmental myosin heavy chains in the

adult human diaphragm: coexpression patterns and effect of COPD. J Appl Physiol (1985). 2000 Apr;88(4):1446-56.

56. Shanely RA, Van Gammeren D, Deruisseau KC, Zergeroglu AM, McKenzie MJ, Yarasheski KE, Powers SK. Mechanical ventilation depresses protein synthesis in the rat diaphragm. Am J Respir Crit Care Med. 2004 Nov 1;170(9):994-9.
57. Jiricka, M.K. (2008) Activity Tolerance and Fatigue pathophysiology: Concepts of Altered Health States, Eighth Edition: International Edition by Carol Mattson Porth Kannus P, Jozsa L, Järvinen TLN, Kvist M, Vieno T, Jarvinen TAH, Natri A, Jarvinen M. (1998) Free mobilization and low- to high-intensity exercise in immobilization-induced muscle atrophy. J Appl Physiol 84: 1418–1424.
58. Topp R, Ditmyer M, King K, Doherty K, Hornyak J 3rd. The effect of bed rest and potential of prehabilitation on patients in the intensive care unit. AACN Clin Issues. 2002 May;13(2):263-76.
59. Nguyen T, Rubinstein NA, Vijayasarathy C, Rome LC, Kaiser LR, Shrager JB, Levine S. Effect of chronic obstructive pulmonary disease on calcium pump ATPase expression in human diaphragm. J Appl Physiol (1985). 2005 Jun;98(6):2004-10.
60. Dres M, Dubé BP, Mayaux J, Delemazure J, Reuter D, Brochard L, *et al*. Coexistence and impact of limb muscle and diaphragm weakness at time of liberation from mechanical ventilation in

medical intensive care unit patients. Am J Respir Crit Care Med 2017;195:57–66.

61. Zergeroglu MA, McKenzie MJ, Shanely RA, Van Gammeren D, DeRuisseau KC, Powers SK. Mechanical ventilation-induced oxidative stress in the diaphragm. J Appl Physiol (1985). 2003 Sep;95(3):1116-24.
62. Zein H, Baratloo A, Negida A, Safari S. Ventilator Weaning and Spontaneous Breathing Trials; an Educational Review. *Emerg (Tehran)*. 2016;4(2):65-71.
63. Haitsma JJ. Diaphragmatic dysfunction in mechanical ventilation. Curr Opin Anaesthesiol. 2011 Apr;24(2):214-8.
64. Béduneau G, Pham T, Schortgen F, et al. Epidemiology of weaning outcome according to a new definition. The WIND study. Am J Respir Crit Care Med. 2017;195:772–78.
65. DiNino E, Gartman EJ, Sethi JM, McCool FD. Diaphragm ultrasound as a predictor of successful extubation from mechanical ventilation. Thorax. 2014;69(5):423–7.
66. Jung B, Moury PH, Mahul M, et al. Diaphragmatic dysfunction in patients with ICU-acquired weakness and its impact on extubation failure. Intensive Care Med. 2016;42:853–86.
67. Dubé BP, Dres M, Mayaux J, Demiri S, Similowski T, Demoule A. Ultrasound evaluation of diaphragm function in mechanically

ventilated patients: comparison to phrenic stimulation and prognostic implications. Thorax. 2017;72:811–818.

68. Vassilakopoulos T, Petrof BJ. Ventilator-induced diaphragmatic dysfunction. Am J Respir Crit Care Med. 2004;169:336–34.
69. Powers SK, Wiggs MP, Sollanek KJ, Smuder AJ. Ventilator-induced diaphragm dysfunction: cause and effect. Am J Physiol Regul Integr Comp Physiol. 2013 Sep;305(5):R464-77.
70. Husain K, Hernandez W, Ansari RA, Ferder L. Inflammation, oxidative stress and renin angiotensin system in atherosclerosis. *World J Biol Chem.* 2015;6:209–217.
71. Macconi D, Remuzzi G, Benigni A. Key fibrogenic mediators: old players. Renin-angiotensin system. *Kidney Int Suppl (2011)* 2014;4:58–64.
72. Miyajima A, Kosaka T, Kikuchi E, Oya M. Renin-angiotensin system blockade: its contribution and controversy. *Int J Urol.* 2015;22:721–730.
73. Sigurta' A, Zambelli V, Bellani G. Renin-angiotensin system in ventilator-induced diaphragmatic dysfunction: Potential protective role of Angiotensin (1-7). Med Hypotheses. 2016 Sep;94:132-7.
74. Cabello-Verrugio C, Morales MG, Rivera JC, Cabrera D, Simon F Med Res Rev. 2015 May; 35(3):437-63.

75. Kwon OS, Smuder AJ, Wiggs MP, Hall SE, Sollanek KJ, Morton AB, Talbert EE, Toklu HZ, Tumer N, Powers SK. AT1 receptor blocker losartan protects against mechanical ventilation-induced diaphragmatic dysfunction. J Appl Physiol (1985). 2015 Nov 15;119(10):1033-41.
76. Meneses C, Morales MG, Abrigo J, Simon F, Brandan E, Cabello-Verrugio C. The angiotensin-(1-7)/Mas axis reduces myonuclear apoptosis during recovery from angiotensin II-induced skeletal muscle atrophy in mice. *Pflugers Arch.* 2015;467:1975–1984.
77. Morales MG, Olguín H, Di Capua G, Brandan E, Simon F, Cabello-Verrugio C. Endotoxin-induced skeletal muscle wasting is prevented by angiotensin-(1-7) through a p38 MAPK-dependent mechanism. *Clin Sci (Lond)* 2015;129:461–476.
78. Morales MG, Abrigo J, Acuña MJ, Santos RA, Bader M, Brandan E, Simon F, Olguin H, Cabrera D, Cabello-Verrugio C. Angiotensin-(1-7) attenuates disuse skeletal muscle atrophy in mice via its receptor, Mas. *Dis Model Mech.* 2016;9:441–449.
79. Ashbaugh DG, Bigelow DB, Petty TL, Levine BE. Acute respiratory distress in adults. Lancet (London, England) 1967; 2(7511): 319-23.
80. Bernard GR, Artigas A, Brigham KL, et al. The American-European Consensus Conference on ARDS. Definitions, mechanisms, relevant outcomes, and clinical trial coordination. American

journal of respiratory and critical care medicine 1994; 149(3 Pt 1): 818-24.

81. ARDS Definition Task Force, Ranieri VM, Rubenfeld GD, Thompson BT, Ferguson ND, Caldwell E, Fan E, Camporota L, Slutsky AS. Acute respiratory distress syndrome: the Berlin Definition. JAMA. 2012 Jun 20;307(23):2526-33.
82. Rezoagli E, Fumagalli R, Bellani G. Definition and epidemiology of acute respiratory distress syndrome. Ann Transl Med. 2017 Jul;5(14):282.
83. Puybasset L, Cluzel P, Gusman P, Grenier P, Preteux F, Rouby JJ. Regional distribution of gas and tissue in acute respiratory distress syndrome. I. Consequences for lung morphology. CT Scan ARDS Study Group. Intensive Care Med. 2000 Jul;26(7):857-69.
84. Cochi SE, Kempker JA, Annangi S, Kramer MR, Martin GS. Mortality Trends of Acute Respiratory Distress Syndrome in the United States from 1999 to 2013. Ann Am Thorac Soc. 2016 Oct;13(10):1742-1751.
85. Parker JC, Hernandez LA, Peevy KJ. Mechanisms of ventilator-induced lung injury. Crit Care Med. 1993 Jan;21(1):131-43.
86. Beitler JR, Malhotra A, Thompson BT. Ventilator-induced Lung Injury. Clin Chest Med. 2016 Dec;37(4):633-646.
87. Acute Respiratory Distress Syndrome Network. Ventilation with lower tidal volumes as compared with traditional tidal volumes

for acute lung injury and the acute respiratory distress syndrome. N Engl J Med. 2000;342(18):1301–1308.

88. Kumar A, Pontoppidan H, Falke KJ, et al. Pulmonary barotrauma during mechanical ventilation. Crit Care Med 1973;1: 181-6.
89. Beitler JR, Malhotra A, Thompson BT. Ventilator-induced Lung Injury. Clin Chest Med. 2016 Dec;37(4):633-646.
90. Slutsky AS. Lung injury caused by mechanical ventilation. Chest. 1999;116(1 Suppl):9S–15S.
91. Dreyfuss D, Soler P, Basset G, Saumon G. High inflation pressure pulmonary edema. Respective effects of high airway pressure, high tidal volume, and positive end-expiratory pressure. Am Rev Respir Dis. 1988;137(5):1159–1164.
92. Muscedere JG, Mullen JB, Gan K, Slutsky AS. Tidal ventilation at low airway pressures can augment lung injury. Am J Respir Crit Care Med. 1994 May;149(5):1327-34
93. Tremblay L, Valenza F, Ribeiro SP, et al. Injurious ventilatory strategies increase cytokines and c-fos m-RNA expression in an isolated rat lung model. J Clin Invest 1997;99: 944-52. 10.1172/JCI119259.
94. Malhotra A. Low-tidal-volume ventilation in the acute respiratory distress syndrome. N Engl J Med. 2007;357(11):1113–1120.

95. Caironi P, Cressoni M, Chiumello D, et al. Lung opening and closing during ventilation of acute respiratory distress syndrome. Am J Respir Crit Care Med. 2010;181(6):578–586.
96. Ranieri VM, Giunta F, Suter PM, Slutsky AS. Mechanical ventilation as a mediator of multisystem organ failure in acute respiratory distress syndrome. JAMA. 2000;284(1):43–44
97. Tremblay L, Valenza F, Ribeiro SP, Li J, Slutsky AS. Injurious ventilatory strategies increase cytokines and c-fos m-RNA expression in an isolated rat lung model. J Clin Invest. 1997;99(5):944–952.
98. Imai Y, Parodo J, Kajikawa O, et al. Injurious mechanical ventilation and end-organ epithelial cell apoptosis and organ dysfunction in an experimental model of acute respiratory distress syndrome. JAMA. 2003;289(16):2104–2112.
99. Koulouras V, Papathanakos G, Papathanasiou A, Nakos G. Efficacy of prone position in acute respiratory distress syndrome patients: A pathophysiology-based review. World J Crit Care Med. 2016 May 4;5(2):121-36.
100. Network TARDS. Ventilation with Lower Tidal Volumes as Compared with Traditional Tidal Volumes for Acute Lung Injury and the Acute Respiratory Distress Syndrome. *New England Journal of Medicine* 2000;342:1301–8.

101. Richter T, Bellani G, Harris RS, *et al.* Effect of Prone Position on Regional Shunt, Aeration, and Perfusion in Experimental Acute Lung Injury. *Am J Respir Crit Care Med* 2005;172:480–7.

102. Guerin C, Reignier J, Richard JC, *et al.* Prone positioning in severe acute respiratory distress syndrome. *The New England journal of medicine* 2013; 368: 2159–68.

103. Motta-Ribeiro GC, Hashimoto S, Winkler T, *et al.* Deterioration of Regional Lung Strain and Inflammation during Early Lung Injury. *Am J Respir Crit Care Med* 2018;198: 891–902.

104. Xin Y, Cereda M, Hamedani H, *et al.* Unstable Inflation Causing Injury. Insight from Prone Position and Paired Computed Tomography Scans. *American Journal of Respiratory and Critical Care Medicine* 2018;198: 197–207.

105. Koulouras V, Papathanakos G, Papathanasiou A, Nakos G. Efficacy of prone position in acute respiratory distress syndrome patients: A pathophysiology-based review. World J Crit Care Med. 2016 May 4;5(2):121-36.

106. Blanch L, Mancebo J, Perez M, Martinez M, Mas A, Betbese AJ, Joseph D, Ballús J, Lucangelo U, Bak E. Short-term effects of prone position in critically ill patients with acute respiratory distress syndrome. Intensive Care Med. 1997;23: 1033–1039.

107. Guérin C, Reignier J, Richard JC, Beuret P, Gacouin A, Boulain T, Mercier E, Badet M, Mercat A, Baudin O, Clavel M,

Chatellier D, Jaber S, Rosselli S, Mancebo J, Sirodot M, Hilbert G, Bengler C, Richecoeur J, Gainnier M, Bayle F, Bourdin G, Leray V, Girard R, Baboi L, Ayzac L; PROSEVA Study Group. Prone positioning in severe acute respiratory distress syndrome. N Engl J Med. 2013; 368:2159–68.

108. Gattinoni L, Pelosi P, Vitale G, Pesenti A, D'Andrea L, Mascheroni D. Body position changes redistribute lung computed-tomographic density in patients with acute respiratory failure. Anesthesiology. 1991; 74:15–23.

109. Mutoh T, Guest J, Lamm JE, Albert RK. Prone position alters the effect of volume overload on regional pleural pressures and improves hypoxemia in pigs in ViV01, 2. Am Rev Respir Dis. 1992; 146:300–6.

110. Xin Y, Cereda M, Hamedani H, Martin KT, Tustison NJ, Pourfathi M, Kadlecek S, Siddiqui S, Amzajerdian F, Connell M, Abate N, Kajanaku A, Duncan I, Gee JC, Rizi RR. Positional Therapy and Regional Pulmonary Ventilation. Anesthesiology. 2020 Nov 1;133(5):1093-1105.

SCOPE OF THESIS

The two topics covered in this work are strictly correlated to the professional experiences performed during the three years of my PhD program, regarding the main field of the prolonged mechanical ventilation.

Particularly, I spent the first period at the University of Milan-Bicocca in the preclinical ICU laboratory directed by Prof. Giacomo Bellani, where my work has been focused on the diaphragm dysfunction during a mechanical ventilation; in particular, in the effectiveness study of a therapeutical treatment with Angiotensin-(1-7) in a rat model of VIDD.

In the second part of my PhD course, I had a chance to rotate at the University of Pennsylvania to conduct a similar research but in the progression of lung injury.

In the anesthesia laboratory of Prof. Maurizio Cereda, the main purpose has been investigating and evaluating the effects of pronation in a large model of ARDS.

Regarding the future prospective, my goals will be to combine the competences and the knowledges acquired from my heterogenous research path to study the effects of the prone position on the ventilatory induced diaphragmatic dysfunction.

AIM OF THE FIRST STUDY

The aim of the first phase of my PhD project is to evaluate the effects of a pharmacological treatment with Angiotensin 1-7 in a rat model of ventilatory induced diaphragmatic dysfunction.

CHAPTER 2: ANGIOTENSIN-(1–7) EXERTS A PROTECTIVE ACTION IN A RAT MODEL OF VENTILATOR-INDUCED DIAPHRAGMATIC DYSFUNCTION

ANGIOTENSIN-(1–7) EXERTS A PROTECTIVE ACTION IN A RAT MODEL OF VENTILATOR-INDUCED DIAPHRAGMATIC DYSFUNCTION

Vanessa Zambelli, Anna Sigurtà, Laura Rizzi, Letizia Zucca, Paolo Delvecchio, Elena Bresciani, Antonio Torsello and Giacomo Bellani.

Intensive Care Med Exp. 2019 Jan 18;7(1):8.

Abstract

Background: Ventilator-induced diaphragmatic dysfunction (VIDD) is a common event during mechanical ventilation (MV) leading to rapid muscular atrophy and contractile dysfunction. Recent data show that renin-angiotensin system is involved in diaphragmatic skeletal muscle atrophy after MV. In particular, Angiotensin-II can induce marked diaphragm muscle wasting, whereas Angiotensin-(1-7) (Ang-(1-7)) could counteract this activity. This study was designed to evaluate the effects of the treatment with Ang-(1-7) in a rat model of VIDD with neuromuscular blocking agent infusion. Moreover, we studied whether the administration of A-779, an antagonist of Ang-(1-7) receptor (Mas), alone or in combination with PD123319, an antagonist of AT2 receptor, could antagonize the effects of Ang-(1-7).

Methods: Sprague Dawley rats underwent prolonged MV (8 hours), while receiving an iv infusion of sterile saline 0.9% (Vehicle) or Ang-(1-7) or Ang-(1-7)+A-779 or Ang-(1-7)+A-779+PD123319. Diaphragms were collected

for ex vivo contractility measurement (with electric stimulation), histological analysis, quantitative real-time PCR and Western blot analysis.
Results: MV resulted in a significant reduction of diaphragmatic contractility in all groups of treatment. Ang-(1-7)-treated rats showed higher muscular fibers cross sectional area and lower Atrogin-1 and Myogenin mRNA levels, compared to Vehicle treatment. Treatment with the antagonists of Mas and AT2R caused a significant reduction of muscular contractility and an increase of Atrogin-1 and MuRF-1 mRNA levels, not affecting the cross sectional fiber area and Myogenin mRNA levels.
Conclusions: Systemic Ang-(1-7) administration during MV exerts a protective role on the muscular fibers of the diaphragm preserving muscular fibers anatomy, and reducing atrophy. The involvement of Mas and AT2R in the mechanism of action of Ang-(1-7) still remains controversial.

Keywords: Ventilation – Diaphragm – Angiotensin-(1-7)

Background

Mechanical ventilation (MV) is an important tool in the achievement of an optimal pulmonary gas exchange in ICU patients. However, prolonged MV is also associated with numerous potential complications affecting both the lungs and the diaphragm. MV can worsen the injury in previously

damaged lung (Ventilator Induce Lung Injury - VILI) [1] and is associated with adverse effects on multiple aspects of diaphragmatic structure and function (Ventilator Induced Diaphragm Dysfunction - VIDD) [2]. The injurious impact of prolonged MV on the diaphragm is tightly related with problems in weaning patients from the ventilator, whose incidence can reach 30% of patients exposed to prolonged MV, with subsequent increase in morbidity and mortality [2, 3]. Several experimental and clinical studies have shown a rapid muscular atrophy and contractile dysfunction in the diaphragm during prolonged MV [4], through the reduction of protein synthesis, the increase of proteolysis and the activation of oxidative stress. Indeed animal studies revealed that protein synthesis decreases rapidly already after the first 6 hours of MV, and remains low throughout the next 12 hours [5]. Simultaneously, the following proteolytic systems initiate: macroautophagy, calpains, caspases and the ubiquitin-proteasome system [2]. Prolonged MV results in oxidative damage to the diaphragm through the generation of reactive oxygen species (ROS) and their derivatives that have a significant effect on the contraction of the skeletal muscle [6]. During prolonged MV the oxidative modification of diaphragm contractile proteins leads to less efficient activation of diaphragm fibers induced by calcium [7].

Renin-angiotensin system (RAS) is a hormonal system implicated in the regulation of blood pressure and fluid and salt balance. Moreover, RAS plays an important role in several pathologies, such as atherosclerosis,

myocardial infarction, stroke, diabetes, nephrosclerosis, tumorigenesis and Acute Respiratory Distress Syndrome (ARDS) [8-12]. The classical axis is composed by ACE and Angiotensin-II, but, concurrently, RAS has a counter-regulatory one, in which ACE2, the principal peptide Angiotensin (1–7) (Ang-(1–7)) and its receptor Mas [13] are involved. RAS could play a relevant role in skeletal muscle diseases, since ACE could act in skeletal muscle, inducing negative effects on myogenesis [14]. The infusion of Ang-II in experimental studies causes marked diaphragm muscle wasting and respiratory muscle dysfunction [15]. Recently, Kwon et al. [16] showed that the treatment with losartan, an Ang-II receptor 1 (AT1R) antagonist, prevented ventilator induced oxidative stress and diaphragm contractile dysfunction. On the other hand, Ang-(1-7) reduces extracellular matrix proteins, TGF-β levels and oxidative stress in skeletal muscles [17, 18], thus decreasing fibrosis in muscular dystrophy mouse models. Moreover, Ang-(1–7) and its Mas receptor can maintain muscle strength by preserving fiber diameter, and reduce Atrogin-1 and Muscle RING-Finger Protein 1 (MuRF-1) levels during the muscle wasting induced by Ang-II [19]. In line with these results, experimental studies demonstrated that Ang-(1–7) lessens atrophy in models of endotoxin-related skeletal muscle wasting [20] and disuse skeletal muscle atrophy [21]. We conceived the hypothesis that the administration of Ang-(1-7) might have beneficial effects on diaphragm functions by preserving the anatomical structure of muscular fibers [22], in a rat model of VIDD with the use of neuromuscular

blocking agent. In this study we used a rat model, since the human and rat diaphragmatic muscle are anatomically close. Indeed the composition of fiber types are comparable between the two species [23]. Moreover we have previously studied the effects of the infusion of Ang-(1-7) in a rat model of VILI [24], showing improvement in terms of oxygenation, inflammation and lung fibrosis. We also demonstrated that the infusion of Ang-(1-7) is well tolerated by rats during prolonged MV without adverse effects. Ang-(1-7) can bind to the AT2R, even if with lower affinity than Ang-II [25]. Moreover Mas and AT2R have very similar physiological and pathophysiological actions and are able to form dimers with AT1R, leading to its inhibition [26].To better characterized the mechanisms of action of Ang-(1-7) we used a Mas receptor (A-779) antagonist and an inhibitor of Ang-II receptor 2 (AT2R) (PD 123319).

Material and Methods

Animals and husbandry

60 Sprague-Dawley rats (250-300 g) were employed (Envigo S.r.l., San Pietro al Natisone, UD, Italy). Animals were housed 2 per cage in a limited access animal facility, with the following condition: the room temperature was 20 ± 2°C and the relative humidity set at 55 ± 10%. Artificial lighting provided a 12 h light/12 h dark (7 a.m.–7 p.m.) cycle. The general

condition of the animals before the experiment was assessed daily. The care and husbandry of animals were in conformity with the institutional guidelines in compliance with national (D. L.vo 26/2014, Gazzetta Ufficiale della Repubblica Italiana, n.61, March 14th 2014) and international laws and policies (European Union directive 2010/63/UE; Guide for the Care and Use of Laboratory Animals, U.S. National Research Council, 1996). The experimental protocol was approved by the Italian Ministry of Health (531/2016-PR) and by the Animal Care Unit of the University of Milano-Bicocca, Monza, Italy. In full respect of the Reduction principle of the 3Rs, the number of animal/group was selected to obtain reliable results and enough biological samples to perform the analysis planned. Some analysis could not be performed in some animals because of technical problems (e.g., electric stimulator malfunctioning or during histologic procedures); however, the total number of analyses performed in each group is reported in the captions.

Experimental protocol

Rats were anesthetized with ketamine (100mg/kg) (Ketavet 100, Intervet Productions, Aprilia, Latina, Italy) and xilazine (4mg/kg) (Rompun 2%, Bayer, Milano, Italy), orotracheally intubated and ventilated for eight hours (Inspira ASV, Harvard Apparatus, Holliston, MA, USA) with following parameters: Tidal Volume: 10ml/kg; Respiratory Rate: 80/min; PEEP: 2-2.5 cmH_2O; fraction of inspired oxygen [FiO_2: 0.5]). Deep anesthesia and

paralysis were maintained throughout the whole procedure by infusion in the right femoral artery of propofol (13mg/kg/h) (Propofol Kabi, Fresenius Kabi Italia, Isola della Scala, Verona, Italy) and ketamine (5mg/kg/h) and in the right jugular vein of rocuronium bromide (1.5mg/kg/h) (Rocuronio, Fresenius Kabi Italia, Isola della Scala, Verona, Italy) and ringer acetate (1.8ml/h). In the left jugular vein, rats received treatment (50µl/h) depending on the randomly assigned experimental group: 1. sterile saline solution NaCl 0.9% (**Vehicle**), 2. 60µg/kg/h Angiotensin-(1-7) (Angiotensin Fragment 1-7 acetate salt hydrate, A9202, Sigma Aldrich, St. Louis, MO, USA) (**Ang-(1-7)**), 3. 60µg/kg/h Angiotensin-(1-7) + 120µg/kg/h A-779 (A-779 trifluoroacetate salt, SML1370, Sigma Aldrich, St. Louis, MO, USA) (**Ang-(1-7)+A-779**), 4. 60µg/kg/h Angiotensin-(1-7)+ 120µg/kg/h A-779 + 120µg/kg/h PD123319 (PD 123,319 di(trifluoroacetate) salt hydrate, P186, Sigma Aldrich, St. Louis, MO, USA) (**Ang-(1-7)+A-779+PD**). Airway pressure and hemodynamic parameters were monitored using pressure transducers in ventilator and arterial catheter, during the whole experimental procedure. A recruitment maneuver (30cmH_2O for 10 sec) was performed every 60 minutes, and the plateau pressure and respiratory system static compliance were recorded every hour. A group of unventilated rats was used as control (CTRL).

Assessment of the injury

The primary outcomes of the study were: the anatomical structure of muscular fibers and the levels of atrophy and autophagy. The secondary outcome was to evaluate the effects of Mas and AT2R antagonists.

Respiratory mechanics.

For the lung mechanical properties, a Pressure to Volume (PV) curve was calculated. After a recruitment maneuver, five steps of inspiratory volumes (2.5ml) were delivered into the lungs. For each step, the plateau pressure was recorded in order to calculate the static compliance.

Diaphragmatic contractile properties.

The diaphragm muscle was excised after animal sacrifice, placed in Krebs solution and a 2mm wide strip was dissected. The strip was mounted into a jacketed tissue bath chamber filled with Krebs solution, containing two stimulation electrodes connected to a stimulator (Grass S88, Grass technologies, Quincy, MA, USA). Tissues were allowed a thermo-equilibration period of 15 min before initiating contractile measurements at 27°C. The following measurements were made:

- Optimal length (L0) (the muscle length at which the maximal force is recorded): muscle was stimulated at 70V 100Hz with 2ms single pulse and L0 was obtained by systematically adjusting the length of the muscle by

using a micrometer while evoking contractions. Thereafter, all contractile measurements were performed at L0;

- Peak tetanic tension: the force produced at L0 when diaphragms were stimulated at 70V 100Hz with 1000ms stimulation trains;
- Force-frequency relationship: the force-frequency relationship at L0 was determined by sequential 1000ms stimulation trains of 70V at different frequency (from 10 to 150Hz), with 2 min intervals after each stimulation;

Muscle force was normalized to tissue cross-sectional area, calculated by the algorithm: [muscle mass/(fiber length x 1.056)], where the muscle mass is the weight of the muscle strip, the fiber length is the L0 and 1.056g/cm^3 is the muscle density [27].

Fiber cross sectional area and muscle structure.

After dissection, right hemidiaphragm tissue was rinsed, embedded in OCT (Optimal Cutting Temperature) and immediately frozen on dry ice. Several 10µm-thick sections were cut and stained with hematoxylin and eosin. The cross sectional area (CSA) of the muscular fibers was determined by manually tracing the fiber contour on digitized images. The mean CSA value was calculated on at least 150 fibers per diaphragm. The fiber disorganization of the muscular tissue was evaluated by converting the digitized images into binary images using a fixed intensity threshold

and by measuring the tissue to air ratio. The analysis was performed by two blinded operators.

Real Time Polymerase Chain Reaction.

Total RNA was extracted from a frozen section of diaphragm muscle using Eurogold trifast reagent (Euroclone S.p.A., Pero, Milano, Italy) according to the kit protocol, and quantified using a NanoDrop 1000 spectrophotometer (ThermoScientific, Waltham, MA, USA). 1000 ng of total RNA were incubated with rDNase I (Ambion, Austin, TX, USA) for 20 minutes at 37° C to digest contaminating genomic DNA. 400 ng of total digested RNA of each sample were reverse transcribed to cDNA using M-MLV Reverse Transciptase (Invitrogen, Carlsbad, CA, USA). cDNA was amplified by PCR using GoTaq G2 DNA Polymerase (Promega, Milano, Italy) with an Applied Biosystems 7900HT Fast Real-Time PCR System. MuRF-1, Atrogin-1 and Myogenin were assayed using probe sequences Taqman® Gene Expression Assay (MuRF-1: Fbxo-32 Rn00591730_m1, Atrogin-1: Trim63 Rn00590197_m1, Myogenin Rn01490689_g1, β–actin Rn00667869_m1). Gene expression was measured by the ΔΔCT method and was normalized to β-actin mRNA levels. Data are shown as the fold change of the gene of interest relative to that of control animals.

Western blot analysis.

A section of the diaphragm was immediately frozen in liquid nitrogen and stored at -80°C. The cytoplasmic extraction was prepared using an NE-PER Nuclear Cytoplasmic Extraction Reagent kit (Pierce, Rockford, IL, USA) according to the manufacturer's instruction. Total protein concentrations were quantified by the bicinchoninic acid assay (BCA assay, Pierce, Rockford, IL, USA) and each sample was analyzed according to standard Western blotting protocols. Briefly, 40 µg total proteins of each sample were separated by 4-12% SDS-Page and transferred onto a PVDF membrane (Thermo Fisher Scientific, Rockford, IL, USA). After blocking with 5% skim milk, PVDF membranes were incubated with specific antibody against LC3B (Light chain 3, isoform B II, 2775, Cell signaling technology, Danvers, MA, USA) and Tubulin (2125, Cell signaling technology, Danvers, MA, USA) as loading control. After the incubation with horseradish-peroxidase conjugated goat anti-rabbit antibody (7074, Cell signaling technology, Danvers, MA, USA), the final reaction was visualized using enhanced chemiluminescence (Amersham ECL Western Blotting Detection Reagent, GE Healthcare, Buckinghamshire, UK). Images were densitometrically analyzed with ImageJ software (ImageJ 1.50b, National Institutes of Health, USA).

Statistical analysis

Shapiro-Wilk test was used to assay the population distribution. Comparisons between Vehicle and Ang-(1-7) treatment were made by t-test or Mann Whitney U test, in normally or not-normally distributed data, respectively. Comparisons between Ang-(1-7) treatment and A-779 and PD group were made by a one-way analysis of variance (ANOVA) or by Kruskal Wallis. If the group effect was significant, a Tukey post-hoc test was used for pairwise comparisons between groups. Data are shown as means ± SD for normally distributed data and as median [interquartile range] when non-normally distributed. In order to calculate the sample size, we started from the study of Kwon et al [16] and we considered that if we wanted to find a 10% reduction in diaphragm contractile properties with a 80% power and a 0.05 significance level we had to use 10 animals per group. Significance was established at $p<0.05$ (IBM SPSS Statistics software, version 24.0.0.1)

Results

Systemic Response

We found no difference in survival in all experimental groups: all rats survived the eight hours of MV, except two rats (one in Vehicle and one in Ang-(1-7) group) that were sacrificed after seven hours because of hypotension. The body weight before the experiment and the oxygenation were not different between groups (Table 1). The mean blood pressure was similar between groups at the beginning of the experiment, whereas at the end of the MV it was significantly higher in Ang-(1-7)+A-779+PD compared to the other two treatment groups (Table 1). Eight hours of MV induced a significant decrease in compliance with no difference between groups.

Table 1.

	Body Weight (g)	*PaO_2 (mmHg)*	*Mean Blood Pressure (mmHg)*		*Respiratory System Static Compliance (ml/cmH_2O)*	
			Start	End	Start	End
CTRL	282 ± 34	-	-	-	0.44 ± 0.04	
Vehicle	279 ± 32	94 ± 15	101 ± 22	91 ± 35	0.41 ± 0.03	0.33 ± 0.05
Ang-(1-7)	275 ± 37	100 ± 6	96 ± 18	91 ± 36	0.41 ± 0.08	0.32 ± 0.05
Ang-(1-7)+A-779	277 ± 30	91 ± 9	99 ± 16	95 ± 43	0.40 ± 0.06	0.32 ± 0.03
Ang-(1-7)+A-779+PD	276 ± 16	102 ± 11	103 ± 25	139 ± 17*	0.42 ± 0.05	0.34 ± 0.05
ANOVA	NS	NS	NS	0.022	NS	NS

Table 1. Body weight, oxygenation, blood pressure and compliance during the mechanical ventilation. CTRL (n=10): unventilated controls; Vehicle (n=18): VIDD + saline treatment; Ang-(1-7) (n=14): VIDD + Ang-(1-7) treatment; Ang-(1-7)+A-779 (n=10): VIDD + Ang-(1-7) + A-779

treatment; Ang-(1-7)+A-779+PD (n=8): VIDD + Ang-(1-7) + A-779 + PD123319 treatment; *p=0.018 vs Ang-(1-7), p=0.044 vs Ang-(1-7)+A-779.

Diaphragm contractile dysfunction

After eight hours of MV all groups showed a significant reduction in diaphragmatic contractility in response to *in vitro* electric stimulation. As shown in Fig 1, increasing the frequency of stimulation the diaphragmatic muscle strip of MV rats generated less force than the unventilated (CTRL) diaphragm ($p<0.05$ for all frequencies and versus all ventilated groups). Ang-(1-7) treatment did not improve the diaphragmatic contraction if compared to Vehicle group but, notably, the two groups of rats treated with Mas and AT2R antagonists showed a greater contractility dysfunction, with less force developed at every frequency of stimulation. Indeed Ang-(1-7)+A-779 and Ang-(1-7)+A-779+PD groups always showed significantly lower ($p<0.05$ at 20, 30, 40 and 50 Hz; $p<0.01$ at the other frequencies) force compared to Ang-(1-7)-treated rats.

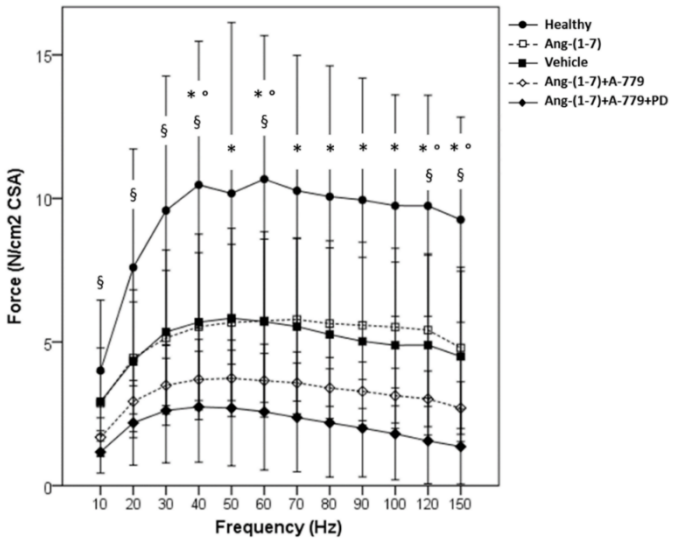

Fig 1. Diaphragm force frequency relationship. Healthy (n=8): unventilated controls; Vehicle (n=10): VIDD + saline treatment; Ang-(1-7) (n=10): VIDD + Ang-(1-7) treatment; Ang-(1-7)+A-779 (n=10): VIDD + Ang-(1-7) + A-779 treatment; Ang-(1-7)+A-779+PD (n=7): VIDD + Ang-(1-7) + A-779 + PD123319 treatment; *p<0.05 Healthy vs Vehicle; °p<0.05 Healthy vs Ang-(1-7); §p<0.05 Healthy vs Ang-(1-7)+A-779 and vs Ang-(1-7)+A-779+PD.

Histological analysis

Ang-(1-7) administration protected diaphragm muscle fiber from MV-induced cellular atrophy (2990 ± 760 μm^2). As shown in Fig 2, in Vehicle

group there was a significant decrease (p=0.001) in cross sectional fiber area (2427 ± 397 μm^2) if compared to CTRL rats (3159 ± 430 μm^2). Similar results were obtained in rats treated with Ang-(1-7)+A-779 (2976 ± 455 μm^2) and Ang-(1-7)+A-779+PD (3001 ± 595 μm^2). Interestingly, all Ang-(1-7)-treated rats (with or without antagonists) showed preserved muscular cell structure.

Real Time PCR

MV induced an increase in mRNA levels of two important muscle-specific E3 ligases (Atrogin-1 and MuRF-1) belonging to the ubiquitin-proteasome system of proteolysis (Fig 4). Interestingly, treatment with Angiotensin-(1-7) lowered the expression of these two mRNA (2.82 ± 2.20 and 20.27 ± 23.81 respectively), even if the difference was statistically significant only for Atrogin-1 mRNA levels (p=0.035), if compared to Vehicle group (6.58 ± 4.62 and 29.43 ± 30.97 respectively). In Ang-(1-7)+A-779 and Ang-(1-7)+A-779+PD groups, Atrogin-1 mRNA levels did not differ from Vehicle group, whereas MuRF-1 mRNA levels seemed to have a reduction more pronounced in Ang-(1-7)+A-779 group.

Analogously to CSA results, levels of Myogenin mRNA significantly (p=0.041) decreased in Ang-(1-7)-treated rats compared to Vehicle group (3.42 ± 2.62 versus 10.25 ± 8.37), and rats treated with antagonists of Mas and AT2R receptor, as already seen in histological analysis, had low Myogenin mRNA levels.

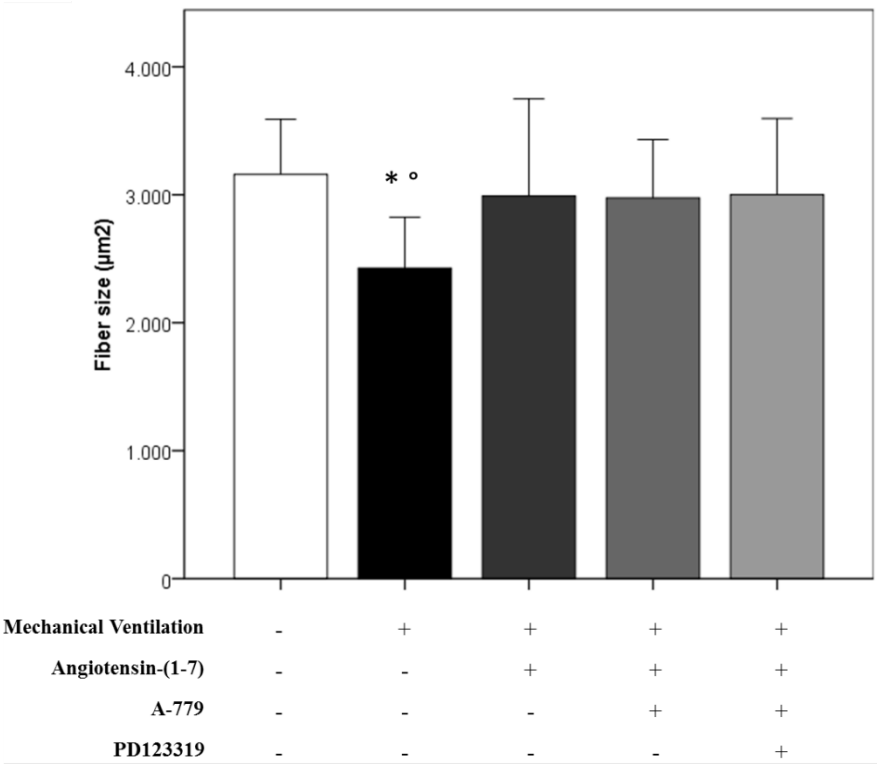

Fig 2. Diaphragm fiber size. Healthy (n=9): unventilated controls; Vehicle (n=10): VIDD + saline treatment; Ang-(1-7) (n=13): VIDD + Ang-(1-7) treatment; Ang-(1-7)+A-779 (n=10): VIDD + Ang-(1-7) + A-779 treatment; Ang-(1-7)+A-779+PD (n=8): VIDD + Ang-(1-7) + A-779 + PD123319 treatment; *p=0.001 vs Healthy; °p=0.028 vs Ang-(1-7).

Western blot

LC3B II levels were non-significantly (p=0.051) lower in rats treated with Angiotensin-(1-7) compared to Vehicle group (Fig 5). Similar levels were found in rats treated with both receptors inhibitor. The group treated with Mas inhibitor had LC3B II levels similar to Vehicle.

Discussion

The RAS is involved in skeletal muscle atrophy, indeed Ang-II acts as key peptide in the regulation of skeletal muscle function, by affecting the tissue structure and muscular contraction in muscle diseases [28, 29]. Conversely, Ang-(1-7) with its receptor Mas [30] can increase muscle strength in dystrophic mice [17] and reduce the muscle atrophy induced by Ang-II. Therefore, the aim of this study was to test the effects of Ang-(1-7) treatment on the diaphragmatic injury induced by the prolonged MV with neuromuscular blocking agent. We have recently [24] demonstrated beneficial effects on the lungs of Ang-(1-7) in a rat model of ARDS. Ang-(1-7) administration during prolonged MV was safe and well tolerated, with no effects on hemodynamics.

Diaphragm contractile properties.

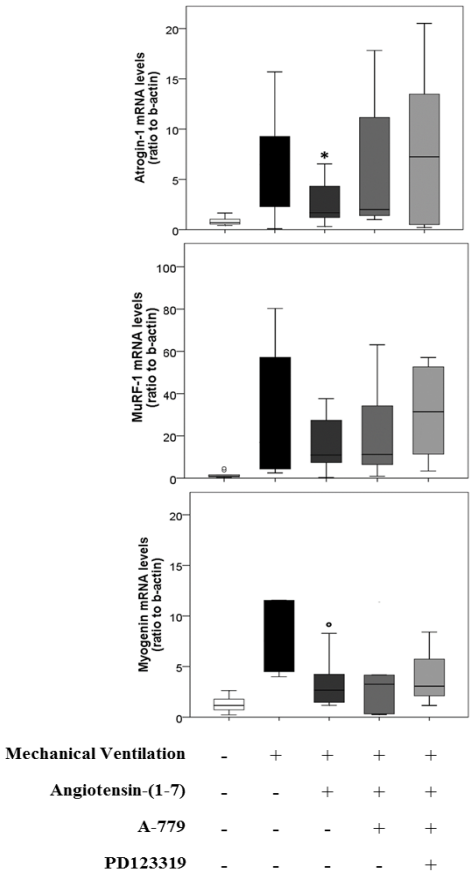

In this study, we decided to ventilate the rats only for eight hours, in order to evaluate the early changes in contractility of the diaphragm and the potential effect of the treatment of Ang-(1-7) on the diaphragm functions. As expected, MV induced a significant reduction in diaphragmatic contractility in response to electric stimulation, as shown in Fig 1, where the force-frequency curves from all four ventilated groups were shifted towards the bottom of the graph.

Fig. 3 Real-time PCR. CTRL (n = 6): unventilated controls; vehicle (n = 6): VIDD + saline treatment; Ang-(1–7) (n = 6): VIDD + Ang-(1–7) treatment; Ang-(1–7) + A-779 (n = 6): VIDD + Ang-(1–7) + A-779 treatment; Ang- (1–

7) + A-779 + PD (n = 6): VIDD + Ang-(1–7) + A-779 + PD123319 treatment; *p = 0.035 vs vehicle; °p = 0.041 vs vehicle

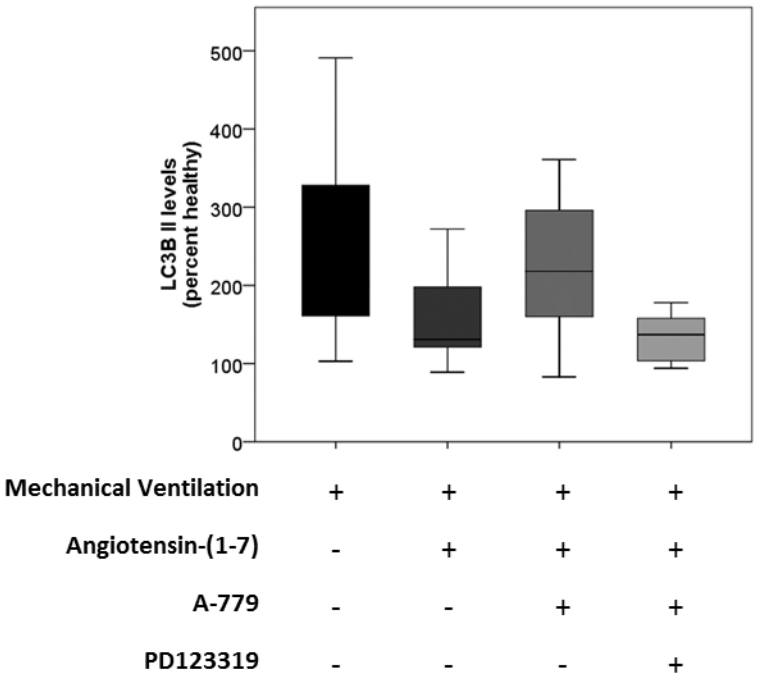

Fig 4. Western Blot analysis: autophagy-related protein (LC3B II). Vehicle (n=11): VIDD + saline treatment; Ang-(1-7) (n=10): VIDD + Ang-(1-7) treatment; Ang-(1-7)+A-779 (n=9): VIDD + Ang-(1-7) + A-779 treatment; Ang-(1-7)+A-779+PD (n=7): VIDD + Ang-(1-7) + A-779 + PD123319 treatment.

Main effects of Angiotensin-(1-7) treatment.

From the functional standpoint, Ang-(1-7) did not induce an improvement of the contractility force. The main finding of this study is the protective role of Ang-(1-7) treatment on the muscular fibers of the diaphragm: the CSA and the Myogenin mRNA levels were significantly higher and lower, respectively, than in Vehicle group. The reduced CSA is an index of diaphragmatic atrophy, that occurs also in clinical settings in the first hours of MV. The muscle disorganization was apparently prevented by Ang-(1-7) treatment. Myogenin is a muscle regulatory factors, whose levels are pronounced after MV [31], and is implicated as modulator of fiber phenotype [32]. Myogenin mRNA is mainly found in slow-twitch muscle [33], so its high levels are correlated to fibers switching from fast to slow [32]. Since the balance between protein degradation and protein synthesis regulates skeletal muscle fiber size, the reduction in muscular atrophy may depend on the levels of Atrogin-1 and MuRF-1. Eight hours of MV induced an increase of their mRNA levels, as shown in Fig 4, but they were reduced in Ang-(1-7) group. Atrogin-1 and MuRF-1 are specific E3 ligases, belonging to ubiquitin-proteasome system, that plays an important role in muscle protein degradation and in skeletal muscle atrophy [34, 35]. Numerous studies in humans and animals demonstrated that MV stimulated the expression of E3 ligases along with an increase in ubiquitinated proteins [36-38]. In order to evaluate autophagy, we measured the protein levels of LC3B II, a microtubule-associated protein.

Autophagy is an important cellular process that involves sequestration of proteins and cell organelles in autophagosomes and degradation in lysosomes, which is activated in response to a variety of stress-related diseases [39]. In our study LC3B II levels tended ($p=0.051$) to be reduced in Ang-(1-7) group compared to Vehicle, showing an anti-autophagic effect.

Unfortunately, the preservation of fiber structure and the decreased protein degradation was not associated to an improvement in force generation, as compared to Vehicle treatment. This finding questions the potential clinical relevance of Ang-(1-7) but deserves further scrutiny, since might be related to the timing of our analysis. It is possible that if MV would have been prolonged beyond the eight hours, the Vehicle group would should show a further decrease in contractility caused by the atrophy of muscle fibers, prevented by Ang-(1-7).

Use of antagonists of Ang-(1-7) receptors.

The inhibition of the two receptors Mas and AT2R affected in part the diaphragm contractility function: both treatments led to significant lower force developed in comparison to Ang-(1-7) treated rats. Interestingly, also Mas (A-779) and AT2R (PD123319) receptor antagonists preserved diaphragm fibers in a way similar to Ang-(1-7). As expected, LC3B II levels remained high with A-779 treatment, whereas in the group treated with PD123319 levels were similar to those of Ang-(1-7)-treated rats. This is in

contrast with a study of Jiang et al [40] that demonstrated that both A-779 and PD123319 were capable to revert the anti-autophagic effect of Ang-(1-7).

The controversial results obtained in the rats treated with the antagonists of Mas and AT2R did not clarify the mechanism of action of Ang-(1-7) and they are in line with Villela et al [26], that described the unclear nature of the interaction between these two receptors. At the hemodynamic level we found that, as expected from our previous study [24], no difference was evident between CTRL, Vehicle and Ang-(1-7) groups, whereas the treatment with PD123319 induced a significant increase of blood pressure. From the functional point of view, the diaphragm in A-779 and A-779+PD123319 groups were characterized by a significant reduction in contractile capability, demonstrating an important role of Ang-(1-7) for the contraction. This aspect could suggest that the RAS shifts the action on the “dark side” of the system, composed by Ang-II and AT1R, with negative effects. Histological analysis and quantification of Myogenin mRNA indicated that muscle fibers are protected from atrophy in all three groups treated with Ang-(1-7) with or without antagonists. It is possible that in presence of the two blocked receptors, Ang-(1-7) circulating levels increased and its alternative metabolites, such as Alamandine, are synthesized and can act through different receptors [41]. Indeed Alamandine can be produced directly from Ang-(1-7) through decarboxylation of N-terminal aspartate amino acid residue [42]. These

two peptides have high similarity and the biological actions seem to be closely related to each other, although each compound acts through different receptors [41].

Experimental limitations.

This study has some limitations which should be acknowledged. First, during the MV period, the rats received an infusion of rocuronium bromide, that could probably affect the diaphragmatic muscle. Indeed it is known that, concurrently to mechanical ventilation, some drugs, such as neuromuscular blocking agents, may worsen diaphragm dysfunction, albeit data on their effects are not univocal [43-46]. Second, we obtained quite low values of force during *in vitro* electric stimulation if compared to other studies in literature [5, 47-49]. This could be due to the relatively young age of rats used in the present study: we used 8-week-old rats. The age-related changes in contractile properties of diaphragm are known [50], and it could have influenced our measures. Third, we did not distinguish the different type of muscle fiber in the histological analysis, but for the measure of the cross sectional area (CSA) we used hematoxylin and eosin staining instead of immunohistochemistry. Fourth, we anesthetized the animals with propofol and ketamine even if it was demonstrated that these anesthetics could affect *per se* the diaphragm contractility and autophagy [51-53]. Fifth, we did not include a group or rats treated with losartan (AT1R blocker), that was already demonstrated

to have beneficial effect on VIDD [16]. Finally, we did not evaluate the effects of Ang-(1-7) on the oxidative stress.

Conclusions

To our knowledge, no studies investigated the role of Ang-(1-7) on the diaphragmatic dysfunction. Our results show that Ang-(1-7) preserved the muscle fibers from atrophy, probably by reducing the expression of the two major E3 ligases, Atrogin-1 and MuRF-1 as confirmed by the lower levels of Myogenin mRNA, typically expressed by slow fibers. These beneficial effects on fiber structure, however, were not mirrored by an increased force generation capability. These results encourage further studies preliminary to the use of Angiotensin-(1-7) in humans.

Declarations

Ethics approval

The care and husbandry of animals were in conformity with the institutional guidelines in compliance with national (D. L.vo 26/2014, Gazzetta Ufficiale della Repubblica Italiana, n.61, March 14th 2014) and international laws and policies (European Union directive 2010/63/UE; Guide for the Care and Use of Laboratory Animals, U.S. National Research Council, 1996). The experimental protocol was approved by the Italian

Ministry of Health (531/2016-PR) and by the Animal Care Unit of the University of Milano-Bicocca, Monza, Italy.

Funding

The present study was completely supported by departmental funding (School of Medicine and Surgery, University of Milano-Bicocca).

References

1. Dreyfuss D, Saumon G, (1998) Ventilator-induced lung injury: lessons from experimental studies. Am J Respir Crit Care Med 157: 294-323
2. Powers SK, Wiggs MP, Sollanek KJ, Smuder AJ, (2013) Ventilator-induced diaphragm dysfunction: cause and effect. Am J Physiol Regul Integr Comp Physiol 305: R464-477
3. Vassilakopoulos T, Petrof BJ, (2004) Ventilator-induced diaphragmatic dysfunction. Am J Respir Crit Care Med 169: 336-341
4. Knisely AS, Leal SM, Singer DB, (1988) Abnormalities of diaphragmatic muscle in neonates with ventilated lungs. J Pediatr 113: 1074-1077
5. Shanely RA, Van Gammeren D, Deruisseau KC, Zergeroglu AM, McKenzie MJ, Yarasheski KE, Powers SK, (2004) Mechanical ventilation depresses protein synthesis in the rat diaphragm. Am J Respir Crit Care Med 170: 994-999
6. Powers SK, Jackson MJ, (2008) Exercise-induced oxidative stress: cellular mechanisms and impact on muscle force production. Physiol Rev 88: 1243-1276
7. Andrade FH, Reid MB, Westerblad H, (2001) Contractile response of skeletal muscle to low peroxide concentrations: myofibrillar

calcium sensitivity as a likely target for redox-modulation. FASEB J 15: 309-311

8. Husain K, Hernandez W, Ansari RA, Ferder L, (2015) Inflammation, oxidative stress and renin angiotensin system in atherosclerosis. World J Biol Chem 6: 209-217

9. Macconi D, Remuzzi G, Benigni A, (2014) Key fibrogenic mediators: old players. Renin-angiotensin system. Kidney Int Suppl (2011) 4: 58-64

10. Miyajima A, Kosaka T, Kikuchi E, Oya M, (2015) Renin-angiotensin system blockade: Its contribution and controversy. Int J Urol 22: 721-730

11. Suzuki Y, Ruiz-Ortega M, Lorenzo O, Ruperez M, Esteban V, Egido J, (2003) Inflammation and angiotensin II. Int J Biochem Cell Biol 35: 881-900

12. Marshall RP, Webb S, Bellingan GJ, Montgomery HE, Chaudhari B, McAnulty RJ, Humphries SE, Hill MR, Laurent GJ, (2002) Angiotensin converting enzyme insertion/deletion polymorphism is associated with susceptibility and outcome in acute respiratory distress syndrome. Am J Respir Crit Care Med 166: 646-650

13. Ferrario CM, Trask AJ, Jessup JA, (2005) Advances in biochemical and functional roles of angiotensin-converting enzyme 2 and angiotensin-(1-7) in regulation of cardiovascular function. Am J Physiol Heart Circ Physiol 289: H2281-2290

14. Cabello-Verrugio C, Morales MG, Rivera JC, Cabrera D, Simon F, (2015) Renin-angiotensin system: an old player with novel functions in skeletal muscle. Med Res Rev 35: 437-463
15. Rezk BM, Yoshida T, Semprun-Prieto L, Higashi Y, Sukhanov S, Delafontaine P, (2012) Angiotensin II infusion induces marked diaphragmatic skeletal muscle atrophy. PLoS One 7: e30276
16. Kwon OS, Smuder AJ, Wiggs MP, Hall SE, Sollanek KJ, Morton AB, Talbert EE, Toklu HZ, Tumer N, Powers SK, (2015) AT1 receptor blocker losartan protects against mechanical ventilation-induced diaphragmatic dysfunction. J Appl Physiol (1985) 119: 1033-1041
17. Acuña MJ, Pessina P, Olguin H, Cabrera D, Vio CP, Bader M, Muñoz-Canoves P, Santos RA, Cabello-Verrugio C, Brandan E, (2014) Restoration of muscle strength in dystrophic muscle by angiotensin-1-7 through inhibition of TGF-β signalling. Hum Mol Genet 23: 1237-1249
18. Sabharwal R, Cicha MZ, Sinisterra RD, De Sousa FB, Santos RA, Chapleau MW, (2014) Chronic oral administration of Ang-(1-7) improves skeletal muscle, autonomic and locomotor phenotypes in muscular dystrophy. Clin Sci (Lond) 127: 101-109
19. Meneses C, Morales MG, Abrigo J, Simon F, Brandan E, Cabello-Verrugio C, (2015) The angiotensin-(1-7)/Mas axis reduces myonuclear apoptosis during recovery from angiotensin II-induced skeletal muscle atrophy in mice. Pflugers Arch 467: 1975-1984

20. Morales MG, Olguín H, Di Capua G, Brandan E, Simon F, Cabello-Verrugio C, (2015) Endotoxin-induced skeletal muscle wasting is prevented by angiotensin-(1-7) through a p38 MAPK-dependent mechanism. Clin Sci (Lond) 129: 461-476

21. Morales MG, Abrigo J, Acuña MJ, Santos RA, Bader M, Brandan E, Simon F, Olguin H, Cabrera D, Cabello-Verrugio C, (2016) Angiotensin-(1-7) attenuates disuse skeletal muscle atrophy in mice via its receptor, Mas. Dis Model Mech 9: 441-449

22. Sigurta' A, Zambelli V, Bellani G, (2016) Renin-angiotensin system in ventilator-induced diaphragmatic dysfunction: Potential protective role of Angiotensin (1-7). Med Hypotheses 94: 132-137

23. Powers SK, Demirel HA, Coombes JS, Fletcher L, Calliaud C, Vrabas I, Prezant D, (1997) Myosin phenotype and bioenergetic characteristics of rat respiratory muscles. Med Sci Sports Exerc 29: 1573-1579

24. Zambelli V, Bellani G, Borsa R, Pozzi F, Grassi A, Scanziani M, Castiglioni V, Masson S, Decio A, Laffey JG, Latini R, Pesenti A, (2015) Angiotensin-(1-7) improves oxygenation, while reducing cellular infiltrate and fibrosis in experimental Acute Respiratory Distress Syndrome. Intensive Care Med Exp 3: 44

25. Bosnyak S, Jones ES, Christopoulos A, Aguilar MI, Thomas WG, Widdop RE, (2011) Relative affinity of angiotensin peptides and

novel ligands at AT1 and AT2 receptors. Clin Sci (Lond) 121: 297-303

26. Villela D, Leonhardt J, Patel N, Joseph J, Kirsch S, Hallberg A, Unger T, Bader M, Santos RA, Sumners C, Steckelings UM, (2015) Angiotensin type 2 receptor (AT2R) and receptor Mas: a complex liaison. Clin Sci (Lond) 128: 227-234

27. Powers SK, Shanely RA, Coombes JS, Koesterer TJ, McKenzie M, Van Gammeren D, Cicale M, Dodd SL, (2002) Mechanical ventilation results in progressive contractile dysfunction in the diaphragm. J Appl Physiol (1985) 92: 1851-1858

28. Cabello-Verrugio C, Morales MG, Cabrera D, Vio CP, Brandan E, (2012) Angiotensin II receptor type 1 blockade decreases CTGF/CCN2-mediated damage and fibrosis in normal and dystrophic skeletal muscles. J Cell Mol Med 16: 752-764

29. Henriksen EJ, Prasannarong M, (2013) The role of the renin-angiotensin system in the development of insulin resistance in skeletal muscle. Mol Cell Endocrinol 378: 15-22

30. Cisternas F, Morales MG, Meneses C, Simon F, Brandan E, Abrigo J, Vazquez Y, Cabello-Verrugio C, (2015) Angiotensin-(1-7) decreases skeletal muscle atrophy induced by angiotensin II through a Mas receptor-dependent mechanism. Clin Sci (Lond) 128: 307-319

31. Rácz GZ, Gayan-Ramirez G, Testelmans D, Cadot P, De Paepe K, Zádor E, Wuytack F, Decramer M, (2003) Early changes in rat diaphragm biology with mechanical ventilation. Am J Respir Crit Care Med 168: 297-304

32. Talmadge RJ, (2000) Myosin heavy chain isoform expression following reduced neuromuscular activity: potential regulatory mechanisms. Muscle Nerve 23: 661-679

33. Hughes SM, Taylor JM, Tapscott SJ, Gurley CM, Carter WJ, Peterson CA, (1993) Selective accumulation of MyoD and myogenin mRNAs in fast and slow adult skeletal muscle is controlled by innervation and hormones. Development 118: 1137-1147

34. Bodine SC, Latres E, Baumhueter S, Lai VK, Nunez L, Clarke BA, Poueymirou WT, Panaro FJ, Na E, Dharmarajan K, Pan ZQ, Valenzuela DM, DeChiara TM, Stitt TN, Yancopoulos GD, Glass DJ, (2001) Identification of ubiquitin ligases required for skeletal muscle atrophy. Science 294: 1704-1708

35. Gomes MD, Lecker SH, Jagoe RT, Navon A, Goldberg AL, (2001) Atrogin-1, a muscle-specific F-box protein highly expressed during muscle atrophy. Proc Natl Acad Sci U S A 98: 14440-14445

36. DeRuisseau KC, Kavazis AN, Deering MA, Falk DJ, Van Gammeren D, Yimlamai T, Ordway GA, Powers SK, (2005) Mechanical ventilation induces alterations of the ubiquitin-proteasome pathway in the diaphragm. J Appl Physiol (1985) 98: 1314-1321

37. Jaber S, Petrof BJ, Jung B, Chanques G, Berthet JP, Rabuel C, Bouyabrine H, Courouble P, Koechlin-Ramonatxo C, Sebbane M, Similowski T, Scheuermann V, Mebazaa A, Capdevila X, Mornet D, Mercier J, Lacampagne A, Philips A, Matecki S, (2011) Rapidly progressive diaphragmatic weakness and injury during mechanical ventilation in humans. Am J Respir Crit Care Med 183: 364-371

38. Levine S, Nguyen T, Taylor N, Friscia ME, Budak MT, Rothenberg P, Zhu J, Sachdeva R, Sonnad S, Kaiser LR, Rubinstein NA, Powers SK, Shrager JB, (2008) Rapid disuse atrophy of diaphragm fibers in mechanically ventilated humans. N Engl J Med 358: 1327-1335

39. Klionsky DJ, Emr SD, (2000) Autophagy as a regulated pathway of cellular degradation. Science 290: 1717-1721

40. Jiang T, Gao L, Zhu XC, Yu JT, Shi JQ, Tan MS, Lu J, Tan L, Zhang YD, (2013) Angiotensin-(1-7) inhibits autophagy in the brain of spontaneously hypertensive rats. Pharmacol Res 71: 61-68

41. Etelvino GM, Peluso AA, Santos RA, (2014) New components of the renin-angiotensin system: alamandine and the MAS-related G protein-coupled receptor D. Curr Hypertens Rep 16: 433

42. Lautner RQ, Villela DC, Fraga-Silva RA, Silva N, Verano-Braga T, Costa-Fraga F, Jankowski J, Jankowski V, Sousa F, Alzamora A, Soares E, Barbosa C, Kjeldsen F, Oliveira A, Braga J, Savergnini S, Maia G, Peluso AB, Passos-Silva D, Ferreira A, Alves F, Martins A, Raizada M, Paula R, Motta-Santos D, Klempin F, Kemplin F,

Pimenta A, Alenina N, Sinisterra R, Bader M, Campagnole-Santos MJ, Santos RA, (2013) Discovery and characterization of alamandine: a novel component of the renin-angiotensin system. Circ Res 112: 1104-1111

43. Dres M, Demoule A (2018) Diaphragm dysfunction during weaning from mechanical ventilation: an underestimated phenomenon with clinical implicationsCrit Care

44. Testelmans D, Maes K, Wouters P, Gosselin N, Deruisseau K, Powers S, Sciot R, Decramer M, Gayan-Ramirez G, (2006) Rocuronium exacerbates mechanical ventilation-induced diaphragm dysfunction in rats. Crit Care Med 34: 3018-3023

45. Testelmans D, Maes K, Wouters P, Powers SK, Decramer M, Gayan-Ramirez G, (2007) Infusions of rocuronium and cisatracurium exert different effects on rat diaphragm function. Intensive Care Med 33: 872-879

46. (2018) Ovid: The role of neuromuscular blockers in ARDS: benefits and risks. In: Editor (ed)^(eds) Book Ovid: The role of neuromuscular blockers in ARDS: benefits and risks., City, pp.

47. McClung JM, Kavazis AN, Whidden MA, DeRuisseau KC, Falk DJ, Criswell DS, Powers SK, (2007) Antioxidant administration attenuates mechanical ventilation-induced rat diaphragm muscle atrophy independent of protein kinase B (PKB Akt) signalling. J Physiol 585: 203-215

48. Bruells CS, Breuer T, Maes K, Bergs I, Bleilevens C, Marx G, Weis J, Gayan-Ramirez G, Rossaint R, (2016) Influence of weaning methods on the diaphragm after mechanical ventilation in a rat model. BMC Pulm Med 16: 127

49. Bruells CS, Maes K, Rossaint R, Thomas D, Cielen N, Bleilevens C, Bergs I, Loetscher U, Dreier A, Gayan-Ramirez G, Behnke BJ, Weis J, (2013) Prolonged mechanical ventilation alters the expression pattern of angio-neogenetic factors in a pre-clinical rat model. PLoS One 8: e70524

50. Imagita H, Yamano S, Tobimatsu Y, Miyata H, (2009) Age-related changes in contraction and relaxation of rat diaphragm. Biomed Res 30: 337-342

51. Bruells CS, Maes K, Rossaint R, Thomas D, Cielen N, Bergs I, Bleilevens C, Weis J, Gayan-Ramirez G, (2014) Sedation using propofol induces similar diaphragm dysfunction and atrophy during spontaneous breathing and mechanical ventilation in rats. Anesthesiology 120: 665-672

52. Li X, Li Y, Zhao J, Li L, Wang Y, Zhang Y, Chen Y, Liu W, Gao L, (2018) Administration of Ketamine Causes Autophagy and Apoptosis in the Rat Fetal Hippocampus and in PC12 Cells. Front Cell Neurosci 12: 21

53. Hackl W, Winkler M, Mauritz W, Steinbereithner K, (1989) [The action of ketamine on muscle contractile behavior. In vitro studies

on the musculature of subjects susceptible to malignant hyperthermia]. Anaesthesist 38: 681-685

AIM OF THE SECOND STUDY

Prone positioning improves ARDS survival, likely by improving the distribution of pulmonary gas. Progression of lung injury seems to reduce the ability of respiratory care maneuvers to improve lung aeration and could also decrease the efficacy of prone positioning. Does progression of lung injury reduce the ability of prone positioning to improve lung aeration in the acute respiratory distress syndrome (ARDS)?

CHAPTER 3: DIMINISHING EFFICACY OF PRONE POSITIONING WITH LATE APPLICATION IN EVOLVING LUNG INJURY

DIMINISHING EFFICACY OF PRONE POSITIONING WITH LATE APPLICATION IN EVOLVING LUNG INJURY

Authors: Yi Xin,Kevin Martin, Caio C.A. Morais, Paolo Delvecchio, Sarah E. Gerard, Hooman Hamedani, Jacob Herrmann, Nicholas Abate, Austin Lenart, Shiraz Humayun, Uday Sidhu, Mihail Petrov, Kristan Reutlinger, Tal Mandelbaum, Ian Duncan, Nicholas Tustison, Stephen Kadlecek, Shampa Chatterjee, James C. Gee, Rahim R. Rizi, Lorenzo Berra, Maurizio Cereda

Submitted Thorax 2020

ABSTRACT

Background: It is not known how lung injury progression during mechanical ventilation modifies pulmonary responses to prone positioning. We compared the efficacy of prone positioning on regional lung aeration in late vs. early stages of lung injury.

Methods: Injury was induced by bronchial hydrochloric acid (HCl, 3.5 ml/kg) in 10 ventilated Yorkshire pigs and worsened by supine non-protective ventilation for 24 hours. Whole-lung computed tomography was performed in both prone and supine positions 2 hours after HCl (Day 1) and repeated at 24 hours (Day 2). Prone and supine images were registered (superimposed) in pairs to measure the effects of positioning on the aeration of each tissue unit. Two patients with early acute

respiratory distress syndrome (ARDS) were compared with two patients with late ARDS, using electrical impedance tomography to measure the effects of body position on regional lung mechanics.

Results: Gas exchange and respiratory mechanics worsened over 24 hours, indicating ventilator-induced injury progression. On Day 1, prone positioning reinflated 18.9 ± 5.2% of lung mass in the posterior-caudal lung regions. On Day 2, position-associated dorsal reinflation was reduced to 7.3 ± 1.5% ($P<0.05$). Prone positioning decreased aeration in the anterior lungs on both days. In the early ARDS patients, prone positioning improved posterior lung compliance, but it had no effect in late ARDS subjects.

Conclusions: The effects of prone positioning on lung aeration may depend on the stage of lung injury and duration of ventilation; this may limit the clinical efficacy of this treatment if applied late.

INTRODUCTION

While the morphologic and functional characteristics of lungs with acute respiratory distress syndrome (ARDS) change over time [1,2], this evolution is poorly characterized. Pulmonary stress during mechanical ventilation accelerates ARDS progression [3] and may diminish the efficacy of therapeutic strategies, narrowing the opportunity for success. Better understanding the evolution of ARDS could therefore help refine both indications and timing of treatment.

Prone ventilation improves gas exchange compared with the supine position via better matching of ventilation and perfusion [4], and decreases the mortality of severe ARDS [5]. The effects of positional therapy on regional lung mechanics might explain its effects on outcome: for example, pulmonary gas distribution is more homogeneous when a patient is prone [6], as improved recruitment of collapsed lung and reduced regional tissue stress [7] compared to supine ventilation may mitigate injury. Supporting this hypothesis, serial computed tomography (CT) scans showed that prone ventilation contained the early propagation of experimental lung injury by stabilizing posterior inflation [8].

Despite strong evidence supporting positional therapy, only 16 to 33% of patients with severe ARDS receive such treatment [9,10]. Clinicians may view prone positioning as a rescue maneuver [10] and attempt other strategies first, such as higher positive end-expiratory pressure (PEEP) or inhaled vasodilators to increase arterial oxygenation, but these strategies

do not uniformly improve ARDS outcomes [11,12]. If injury progression due to pulmonary stress diminishes the lung's ability to redistribute regional mechanics, delayed initiation could decrease the positive clinical impact of positional therapy. While ARDS lungs may become resistant to recruitment by airway pressures after prolonged ventilation [13], no human or experimental studies have prospectively assessed the evolving responses to positional therapy.

In a large animal model of early lung injury, we previously visualized the effects of prone positioning on the aeration of each voxel of lung tissue in paired prone-supine CT images [14]. We found that reaeration and recruitment by the prone position were chiefly localized in posterior lung regions near the diaphragm. In the current study, we used a similar imaging approach to test the hypothesis that lung injury progression diminishes prone positioning's ability to reaerate the lungs. For this purpose, we performed longitudinal CT scans in pigs with evolving lung injury triggered by acid aspiration and worsened during 24 hour-long non-protective ventilation while supine. With high spatial resolution, we compared imaging of early vs. late responses to positional therapy and for comparison, to high airway pressures. Finally, using electrical impedance tomography (EIT), we compared the effects of prone positioning on regional lung mechanics in two patients with late vs. two patients with earlier ARDS. Overall, the results suggest that injury progression in

ventilated lungs might lessen prone positioning's ability to improve aeration and to recruit posterior lung regions.

METHODS

All studies were approved by the Animal Care and Use Committee of the University of Pennsylvania and by the Investigational Review Board of the Massachusetts General Hospital. Detailed methods are described in the Online Supplementary Material; **Figure 1A** outlines the animal experiments.

Animal Preparation and Protocol

Ten Yorkshire pigs (30.7±1.1 kg) were intravenously anesthetized, intubated, instrumented, and mechanically ventilated. 3.5 ml/kg of hydrochloric acid (HCl, pH 1.0) was instilled via bronchoscopy into the lobar bronchi. After two-hours stabilization period, CT scans were obtained (Day 1). All animals were then ventilated supine for 24 hours on volume-controlled ventilation with non-protective settings: PEEP 3 cmH_2O and tidal volume (V_T) 12 ml/kg. Inspired fraction of oxygen and respiratory rate were set at 0.5 and 25 bpm, then adjusted to arterial oxygen saturation (>90%) and $PaCO_2$ (35–45 mmHg). After 24 hours, CT was repeated (Day 2). Hemodynamic and respiratory variables were monitored continuously; hypotension was treated with fluids and epinephrine infusion. Respiratory mechanics and arterial blood gases

were measured serially. Animals were euthanized after Day 2 imaging, at which time lung tissue samples were obtained and processed.

Image Acquisition and Analysis

CT images and physiologic measurements were obtained after supine and prone ventilation with each of two settings that were randomly applied for 15 minutes in-scanner: low PEEP (3 cmH_2O) non-protective ventilation (V_T 12 ml/kg, rate 25 bpm), and high PEEP (15 cmH_2O) ventilation chosen to maximize lung recruitment. At high PEEP, V_T 6 ml/kg and rate 40 bpm were dialed to avoid barotrauma. Recruitment maneuvers were performed after each position change. Pigs lay unsupported when in the prone position. Lungs were scanned during 5-second end-expiratory pauses, and images were reconstructed to a resolution of 1x1x1 mm.

To quantitatively analyze aeration changes, we first segmented lung images via validated deep-learning methodology [15] and calculated lung weights [16] and end-expiratory lung volumes (EELV) [17]. We then registered (warped) segmented CT scans obtained in the prone position to the supine images (**Figure 1B**) using deformable registration to align lung borders and internal features between images, thus placing corresponding voxels on the same reference system [18]. This allowed us to measure the effects of positioning and PEEP on the density (aeration) of each voxel. Voxels were then classified as 'recruitment' or

'derecruitment' if their density respectively decreased or increased across a threshold of -100 Hounsfield units (HU) when turning prone and/or increasing PEEP [14]. Aeration changes were mapped and spatially analyzed in 10 anterior-posterior and 10 cranio-caudal equal-weight bins.

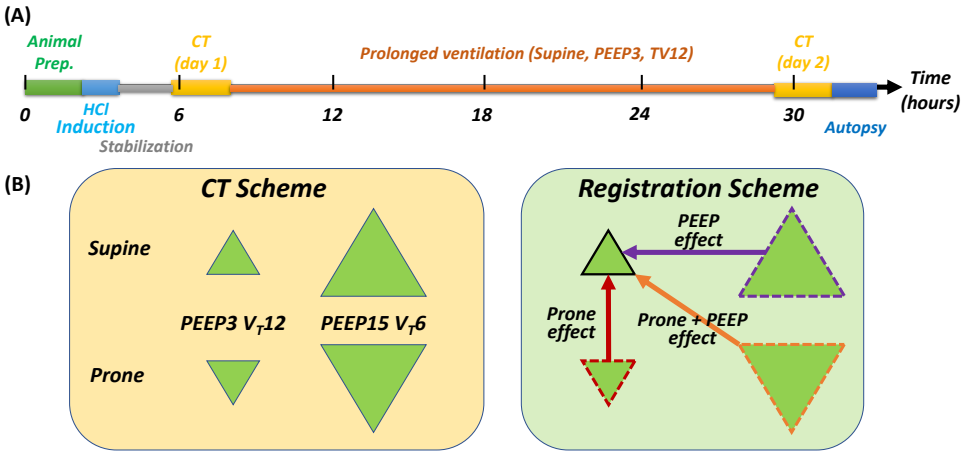

Figure 1. A) Experimental timeline in supine pigs ventilated with non-protective settings after hydrochloric acid (HCl) instillation in the bronchi. After animal preparation and HCl administration, pigs were stabilized for two hours, followed by early (Day 1) computed tomography (CT) scans. All pigs were then ventilated with tidal volume (V_T) 12 ml/kg and positive end-expiratory pressure (PEEP) 3 cmH_2O. After 24 hours, CT scans were repeated (Day 2), followed by euthanasia and tissue retrieval. B) On both

days, CT scans were obtained during end-expiratory pauses following 15-minute-long periods of ventilation in prone or supine position with low (3 cmH_2O) or high (15 cmH_2O) PEEP, applied in random order. For image processing, CT scans in the prone (at low and high PEEP) and supine (at high PEEP) positions were registered to (superimposed on) the supine-low PEEP scans.

Patients

Two patients with early (<7 days from onset) and two with late (>7 days from onset) ARDS [19] were imaged with electrical impedance tomography (EIT) in the prone and in supine position while volume-controlled ventilated with V_T 5–6 ml/kg and PEEP 15 cmH_2O. Images were reconstructed according to a 3D finite element model, plotted in a matrix of 32 x 32 pixels, and partitioned into 32 anterior-posterior bins [20]. For each bin, tidal ventilation was calculated by impedance changes and divided by the driving pressure, yielding regional compliance (Online Supplement).

Statistical Analysis

Data was prepared in Jupyter Notebook using Python 3.6. Statistical analysis was performed using RStudio 1.2.5001 (R Foundation for Statistical Computing; Vienna, Austria). Two-tailed paired T-tests with

Bonferroni correction were performed for comparisons between the two time points. A mixed-effect regression model (lme4, R package) [21,22] was used to study the effects of PEEP, positioning, and their combination (fixed terms) on physiologic and imaging variables. 'Individual subject' was retained as random effect. Each estimate was reported with its confidence intervals. An experiment-wide $P<0.05$ was selected as the threshold for statistical significance.

RESULTS

Lung Injury Progression

Acid aspiration caused a decrease in both PaO_2/FiO_2 ($P<0.001$) and respiratory system compliance ($P<0.001$) and an increase in $PaCO_2$ ($P=0.019$) between healthy baseline and the first post-injury time point (**Figure 2**)**.** We observed further decreases in PaO_2/FiO_2 ($P<0.001$) and compliance ($P=0.015$) over the next 24 hours, while $PaCO_2$ continued to increase ($P=0.042$) (**Figure 2**)**.** Additional trends of physiological and laboratory parameters are shown in **Table 1**, Online Supplement. Analysis of tissue samples confirmed injury (**Figure 3 A-C**), which was more severe in the middle and lower lobes than in the upper lobe (**Figure 3D**). Unprocessed expiratory CT images on Day 1 showed consolidations and ground glass opacities, which became more prominent on Day 2 (**Figure**

4, left panels). Density analysis of segmented, non-registered images showed that lung weight increased from 764.6±74.7 to 859.9±92.0 grams of tissue (P<0.001) between Days 1 and 2.

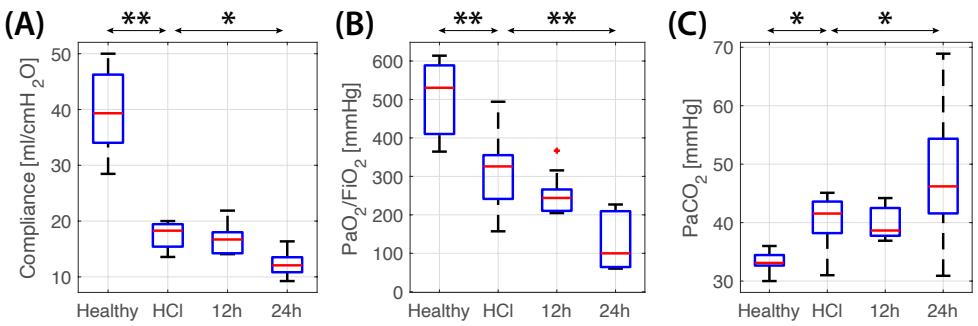

Figure 2. Effects of initial lung injury and its subsequent progression (mean and standard deviation) on: A) respiratory system compliance, B) PaO_2/FiO_2, C) $PaCO_2$. All measurements were taken during ventilation at V_T 12 ml/kg and PEEP 3 cmH_2O: at healthy baseline, 2 hours after instillation of hydrochloric acid (HCl), and after 12 and 24 hours of ventilation. ** P<0.01, * P<0.05.

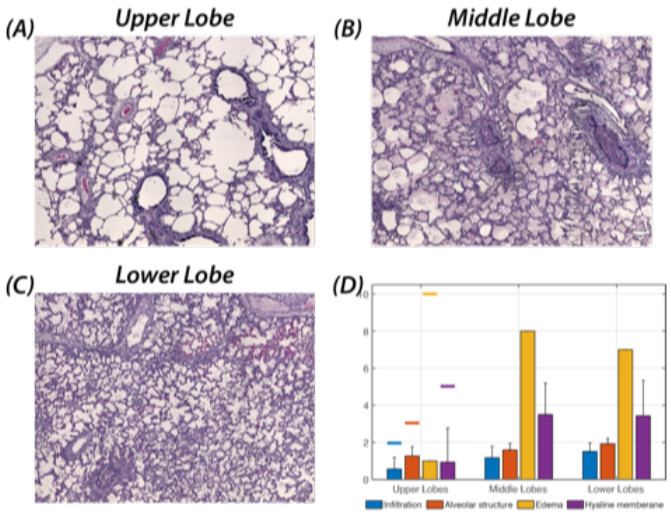

Figure 3. Effects of Positioning and PEEP

Respiratory Parameters: On Day 1, prone vs. supine positioning increased PaO_2/FiO_2 (mean difference = 101.7 mmHg, 95%CI = [61.5, 141.8 mmHg], P<0.001, Cohen's *d* = 1.87) and compliance (mean difference = 3.9 ml/cmH_2O, 95%CI = [2.3, 5.6 ml/cmH_2O], P<0.001, Cohen's *d* = 1.74), while high vs. low PEEP decreased both variables (**Table 1**). On Day 2, prone positioning slightly worsened PaO_2/FiO_2 (mean difference = -23.5 mmHg, 95%CI = [-37.7, -9.3 mmHg], P=0.003, Cohen's *d* = -1.22) while still increasing compliance (mean difference = 2.3 ml/cmH_2O, 95%CI = [1.1, 3.5 ml/cmH_2O], P=0.001, Cohen's d = 1.46); high PEEP had no significant effect on PaO_2/FiO_2, but, similar to Day 1, it worsened compliance (mean

difference = -5.1 ml/cmH_2O, 95%CI = [-6.3, -3.9 ml/cmH_2O], P<0.001, Cohen's *d* = -3.19) (**Table 1**). $PaCO_2$ was unaffected by positioning on Day 1, but slightly increased on Day 2 in the prone position. The increase in $PaCO_2$ at high vs. low PEEP was likely caused by the use of lower V_T. EELV was stable between positions on Day 1 but was on Day 2 it was lower in the prone position compared to supine (mean difference = -106.0 ml, 95%CI = [-142.7, -69.2 ml], P<0.001, Cohen's *d* = -2.13) (**Table 1**). Also see **Table 2** in the Online Supplement for the complete results of the statistical analysis.

Regional Aeration: After segmentation and registration, the warped images showed anatomic correspondence with the supine images at low PEEP (**Figure 4**, right panels), except for the effects of PEEP and positioning on regional lung aeration. These were calculated by subtracting density values between each voxel of the warped image and the spatially corresponding voxel of the low-PEEP supine scan (**Figure 1B**). The resulting subtraction maps show that, on Day 1, proning at low PEEP caused density to decrease (improved aeration) in the posterior-caudal lung (blue) and to increase (worse aeration) in the anterior regions (red) (**Figure 5A**). Raising PEEP in the supine animal improved aeration predominantly in the posterior lung, while gas content remained relatively stable in the anterior regions. Joint application of high PEEP and prone positioning further enhanced the posterior improvement of aeration, while the anterior decrease of aeration was smaller compared to prone

positioning alone (**Figure 5A**). On Day 2, the prone position and high PEEP (both alone and in combination) were unable to meaningfully improve posterior and caudal aeration (**Figure 5C**), while their effects on the anterior lung were similar to Day 1. Population averages of anterior-posterior and cranio-caudal distributions of CT densities, as well as of their shifts caused by positioning and PEEP, confirm these visual patterns (**Figure 1**, Online Supplementary Material).

Lung Recruitment: After identifying those voxels in which density shifts indicated recruitment or derecruitment in each tested condition (**Figure 5B, D**), we quantified them as fractions of total lung volumes and mass (**Table 2**). The anterior-posterior (**Figure 6A**) and cranio-caudal (**Figure 6B**) distributions of recruitment show that most voxels recruited by the prone position were in the posterior and caudal lung regions on Day 1, but that this recruitment was diminished on Day 2 (**Table 2,** P<0.001). Voxels recruited by high PEEP were also distributed in the posterior-caudal territories on Day 1, but their distribution shifted from posterior to more anterior bins on Day 2 (**Figures 5D, 6A**). Combining prone position and high PEEP enhanced recruitment vs. high PEEP alone on Day 1 (mean difference = 5.8%, 95%CI = [3.75-7.92%], P<0.001, Cohen's *d* = 2.58), while this additional effect was smaller on Day 2 (mean difference = 1.9%, 95%CI = [-0.04-3.83%], P=0.072, Cohen's *d* = 0.90). On both days, the prone position was associated with a quota of derecruitment (**Table 2**) which was mostly localized in anterior lung regions (**Figures 5D, 6A**) and was

attenuated by the addition of high PEEP. Also see **Table 3** in the Online Supplement for the complete results of the mixed-effect model analysis.

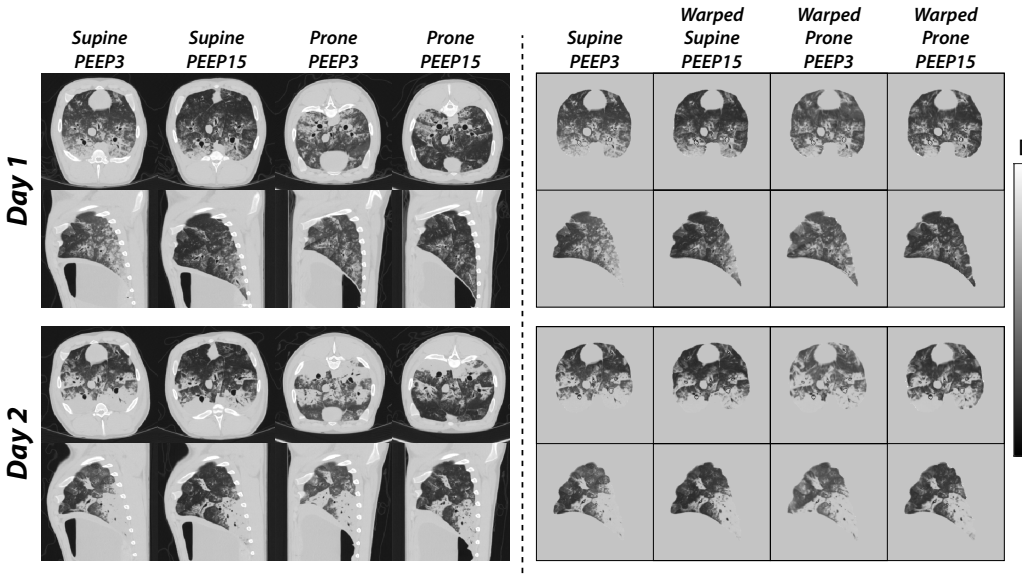

Figure 4. Representative axial and coronal images obtained in early acid aspiration injury (Day 1) and after 24 hours of ventilation with non-protective settings (Day 2). The left panels show the unprocessed images, which were obtained during expiratory pauses after ventilation in both supine and prone positions, at two levels of PEEP. Day 2 images show the radiological progression of lung injury, with expansion of high-attenuation

areas. The right panels show the same images after segmentation and registration (warping). All images were registered to the supine-low PEEP scans obtained on the same day, which were used as a reference to create high-resolution maps of the changes in aeration resulting from the tested treatments. In this figure, the warped prone images are shown inverted to facilitate anatomic comparisons.

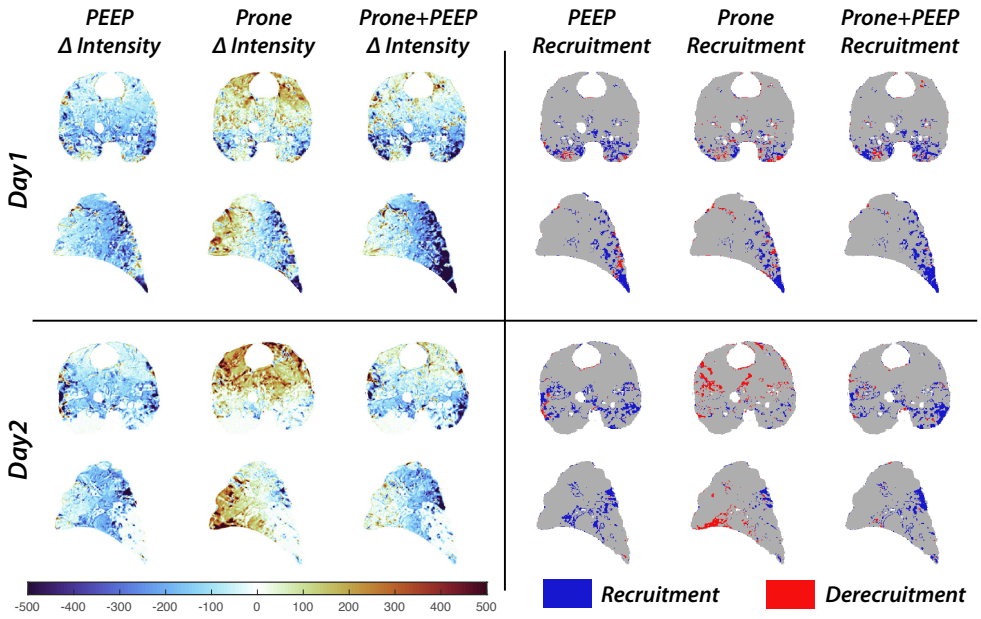

Figure 5. Subtraction maps display voxel-by-voxel density changes (left panels) and lung recruitment-derecruitment (right panels) on Day 1 (A, B)

and Day 2 (C, D) of the experiment. The density changes were calculated by subtracting CT densities of the warped images from those of the supine-low PEEP images, which were used as a reference to calculate the effects of high PEEP alone, prone position alone, and their joint application on the gas content of each voxel. Recruitment and derecruitment were mapped by identifying voxels where the CT density changes due to PEEP or positioning crossed a threshold (-100 Hounsfield Units) indicating near complete loss of aeration. Recruited voxels are shown in blue; derecruitment is shown in red.

ARDS Patients

Patients were 35 to 69-year-old and were ventilated for 6 to 60 days (see Online Supplementary Material for additional details). In the patients with "early ARDS" (patients 1 and 2 in **Figure 7**), prone position increased both global respiratory system compliance and the EIT-measured compliance of the posterior bins, suggesting lung recruitment in the same areas. In the "late ARDS" patients (patients 3 and 4 in **Figure 7**), global compliance was reduced in prone position compared to supine position. EIT images revealed a lack of compliance improvement in the posterior bins and a concomitant decrease in the anterior regions.

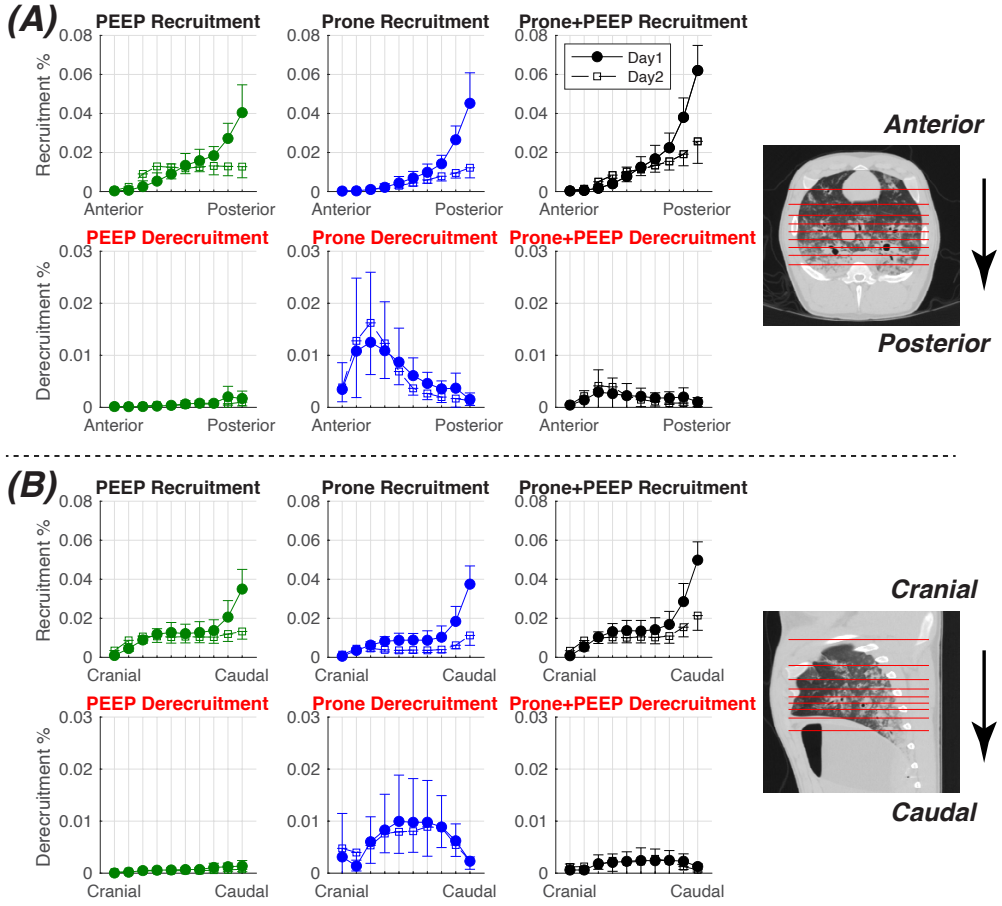

Figure 6. The regional distributions of recruitment and derecruitment were analyzed by partitioning the lung into 10 segments of equal voxels along the A) Anterior-Posterior axis and B) Caudal-Cranial axis, as exemplified in the images on the right. Each value (mean±SD) represents the amount of recruited or derecruited tissue (as a % fraction of the total

lung volume) contained in each bin. Day 1 (closed circles) and Day 2 (open squares) are shown in each plot.

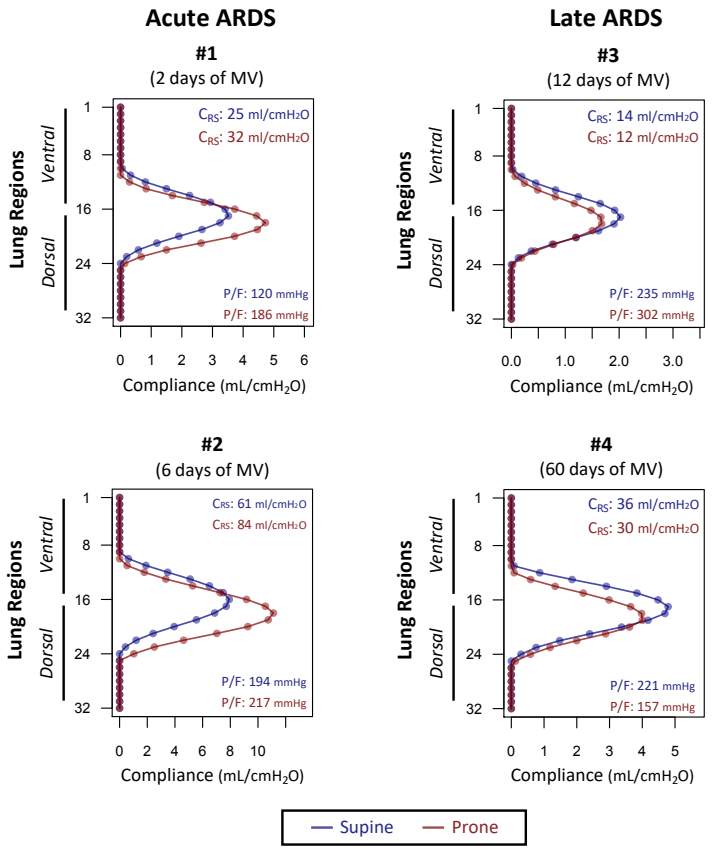

Figure 7. Changes in regional compliance measured by electrical impedance tomography (EIT) with in 32 horizontal bins (region 1 most

anterior, region 32 most posterior) in patients with acute and late ARDS imaged in supine (blue) and in prone (in red) positions. Global respiratory system compliance (CRS) and PaO_2/FIO_2 ratio (P/F) was added to each graph for each position. The insert shows an EIT image of regional ventilation reconstructed in a 32 x 32 matrix. Regional compliance was measured in each horizontal pixel layer of the EIT matrix (exemplified by the red rectangle). Please note that regional ventilation and compliance are mostly measurable in the central bins (e.g. 8–24), as the more peripheral bin values reflect extrapulmonary tissue impedance.

	Day1						Day2					
	PEEP3 V_T12		PEEP15 V_T6		P-value		PEEP3 V_T12		PEEP15 V_T6		P-value	
	Supine	Prone	Supine	Prone	PEEP effect	Prone effect	Supine	Prone	Supine	Prone	PEEP effect	Prone effect
Compliance	17.4±2.5	21.8±3.8	11.8±3.1	15.2±2.9	**<0.001**	**<0.001**	13.6±4.4 †	15.8±5.0 †	8.4±3.4 †	10.8±4.6 †	**<0.001**	**0.001**
PaO_2/FiO_2	363.6±136.5	440.8±107.6	292.8±152.5	418.9±110.0	**0.032**	**<0.001**	124.9±71.0 †	103.9±61.2 †	141.1±81.0 †	115.1±52.4 †	0.069	**0.003**
$PaCO_2$	37.2±5.0	37.8±5.3	50.5±8.4	50.6±13.9	**<0.001**	0.835	51.0±14.2 †	60.1±18.6 †	70.3±18.2 †	73.1±21.5 †	**<0.001**	0.017
Lung Volume	876.4±70.6	840.5±120.4	1108.2±130.1	1086.0±148.7	**<0.001**	0.163	859.9±118.2	732.7±92.3 †	988.2±166.2 †	903.5±171.7 †	**<0.001**	**<0.001**
Average Intensity	-542.7±34.5	-518.8±46.4	-591.1±37.1	-580.4±43.7	**<0.001**	**0.001**	-497.4±44.9	-461.3±40.8 †	-531.9±53.4 †	-509.9±55.0 †	**<0.001**	**<0.001**

Table 1. Physiological characteristics of pigs at different PEEP levels and positions on different study days. Between-day comparisons were made by paired t-test. Within-day comparisons were made using a mixed-effect regression model (see table E2 for complete analysis results). †: P<0.05 between Day 1 vs. Day 2.

		Recruitment % by mass	Derecruitment % by mass
Day1	PEEP	22.5 ± 5.7%	0.9 ± 0.5%
	Prone	18.9 ± 5.2% ‡	5.9 ± 3.0% ‡
	PEEP+Prone	28.3 ± 6.1% ¶	2.0 ± 1.1%
Day2	PEEP	15.8 ± 2.9% †	0.6 ± 0.2%
	Prone	7.3 ± 1.5% †‡	6.5 ± 2.8% ‡
	PEEP+Prone	17.7±4.2% †	1.8±1.4%

Table 2. The amount of recruited and derecruited lung tissue (as a percent of whole-lung mass) as a result of applying high PEEP, prone position, and the combination of both in early (Day 1) and late (Day 2) injury. Between-day comparisons were made by paired t-test. Within-day comparisons were made using a mixed-effect regression model (see table E3 for compete analysis results). †: $P<0.05$ Day 1 vs. Day 2; ‡: $P<0.05$ effect of PEEP vs. prone; ¶: $P<0.05$ effect of PEEP alone vs. the combination of PEEP and prone positioning.

DISCUSSION

Our data suggest that delayed application of positional therapy may diminish its beneficial effects on regional inflation. We used imaging to quantify the impact of the progression of experimental lung injury on the responses to body positioning: after supine non-protective ventilation for 24 hours, the prone position was less effective at re-inflating and recruiting posterior-caudal lung tissue than in early injury. Furthermore, the EIT measurements hint that prone positioning may be unable to improve posterior lung mechanics after prolonged ventilation in clinical ARDS.

Our large animal model mirrored the secondary progression of a primary lung insult. Previous small animal data showed that the evolution of lung injury led to a progressive loss of recruitability by higher PEEP [23]. Our study shows that the lungs' ability to respond to prone positioning was also altered over time, and that injury characteristics transitioned from reversible decrease of aeration to consolidative lesions.

To quantitate these evolving responses, we performed a detailed analysis of the effects of both prone positioning and PEEP on regional lung inflation. We used our registration method to map lung density shifts, including recruitment and derecruitment, with voxel-level resolution [14]. In early injury, switching position from supine to prone caused opposing changes in lung aeration in ventral vs. dorsal lung territories: a posterior region of the lungs was reinflated, while a large anterior territory was

deflated (**Figure 5A**), resulting in a stable EELV (**Table 1**) as in previous observations by our group [14] and others [24]. These changes were likely due to shifts of the gravitational and non-gravitational forces that deform the lungs [25]. Similar to our previous work [14], lung recruitment was prominent in the posterior-caudal territory during early injury (**Figure 5B, Figure 6**). This region was most likely well perfused [26], explaining the improved oxygenation in the prone position. However, after injury progression for over 24 hours, the posterior-caudal lung region became resistant to the forces that drive reinflation in the prone position (**Figure 5C, D**). Furthermore, anterior lung deflation was also visible in the prone images on the second day, with the net result of a smaller EELV than in the supine position.

Previous studies reported that opposite aeration shifts coexisted in the same subject when changing body position [27]. However, the relative contributions of recruitment and derecruitment cannot be separated and mapped when they are averaged within a large region of the lung [28,29]. By measuring aeration shifts in each individually registered voxel, we were able to show that, during early injury, derecruitment occurred in a smaller fraction of tissue than recruitment (**Table 2**). Derecruited voxels were mostly – but not exclusively – distributed in the anterior lung, a region with a smaller cross section than the posterior region. This geometric asymmetry can explain the net balance in favor of recruitment in prone subjects. On the second day, however, derecruitment by prone

positioning nearly offset recruitment, as the latter was smaller than in early injury. This suggests that the geometric factors that improve lung aeration in the acute stage of injury [25] do not guarantee a net beneficial effect of prone positioning when the posterior lung regions are consolidated.

Image registration also enabled us to observe that, when applied separately, PEEP and prone positioning recruited non-overlapping regions of lung tissue (**Figure 6A**). This was due to the fact that the tissue recruited at high PEEP was more anterior on Day 2 than on Day 1, since the posterior-caudal lung had become harder to reinflate (**Figure 5D**).

High PEEP worsened compliance on both days of the study despite a significant quota of recruitment, which could be explained by the fact that anterior aeration was not increased by higher PEEP (**Figure 6 A,C,** and **Figure 1** Online Supplement), suggesting maximal physiologic inflation in that region. This state was likely associated with unfavorable distribution of blood flow [30], contributing to worsening oxygenation at higher PEEP. Increased compliance with prone positioning on Day 1 can be explained by recruitment, although this mechanism does not completely account for the higher compliance also observed on Day 2, when both recruitment by prone positioning and EELV were decreased. It is possible that reduced inflation improved chest wall mechanics enough to offset the lack of net recruitment in the prone position [29].

Fibroproliferative responses occur early human [31] and experimental [32] lung injury, and are likely involved in the loss of positional responses in our patients [19]. However, fibrosis is unlikely to have measurable physiologic and radiologic consequences in the stages of injury explored in our animal studies. Using serial CT in injured rats, we previously reported that dependent areas of suboptimal and unstable inflation were progressively replaced by persistent loss of ventilation [8], a progression that was mitigated by prone positioning. This evolution was likely caused by concentration of lung strain, causing edema through capillary stress [33]. Edema could also explain the loss of posterior recruitability observed in our current study, but it is also possible that supine ventilation with relatively large tidal volume and low PEEP provoked induration of previously recruitable tissue, as described in an acid aspiration model [23]. This evolution is probably mediated by protein accumulation in the airspaces and resulting surfactant deterioration [23], which increases the tendency to derecruitment until gas loss becomes irreversible [34].

This study has potential clinical implications. The EIT measurements are explorative but hint to similarities between human and experimental ARDS in the evolution of imaging and physiological responses to positioning. In fact, the prone position improved regional compliance in the posterior lung regions of the early ARDS patients, likely indicative of lung recruitment in the same regions. Similar to the pigs, this effect was lost in late ARDS. Furthermore, the late ARDS subjects displayed a

decrease of anterior compliance in the prone position, suggesting worsened aeration. A large segment of the ARDS population is impervious to recruitment attempts [16]: e.g., Cornejo *et al.* showed smaller functional and radiologic effects of positioning in ARDS patients with low vs. high recruitability on chest CT [28]. Although other factors such as origin of injury [16] are likely contributors, our experimental and human results suggest that the stage of disease could contribute to variability of treatment responses.

The most successful clinical trial on prone positioning [5] showed a strong outcome benefit when treatment was applied within 72 hours of injury onset. Our results provide a physiological rationale to avoid delaying treatment. Furthermore, we suggest posterior lung recruitability as a possible early marker of the potential clinical success of prone positioning; this can better guide clinicians because oxygenation responses are not associated with survival [35]. Restrained inflation may limit stretch-induced injury in the anterior lung when subjects are prone [39], and may also reduce regional inflammation [7] in later injury stages. However, animal studies by our group [8] and by others show that improved inflation in the posterior lung may help contain early injury progression [36]. This regional response may be particularly relevant in obese patients, who suffer from posterior lung collapse and disproportionately benefit from positional therapy [37]. If our human findings are confirmed in clinical studies, EIT may provide bedside assessments of the likelihood

that positional therapy will improve regional lung mechanics –and potentially outcomes - in individual patients.

Our study has important limitations. In the absence of perfusion data, we can only speculate on the mechanisms through which prone positioning affected gas exchange in our study, but positional changes in ventilation and perfusion distributions are well documented [4,27]. We cannot discriminate the effects of chest wall mechanics on regional inflation and on respiratory compliance, respectively, in the absence of esophageal manometry.

We ventilated animals for 24 hours with non-protective settings to accelerate injury progression, which limits the clinical extrapolation of our results, although lung-protective ventilation did not prevent worsening of lung strain distribution in supine sheep [7]. Furthermore, the differences observed in EIT measurements between early and late ARDS suggest that lung protective ventilation may not avoid the degradation of positional effects on lung mechanics. During imaging, we chose a large gradient between tested PEEP levels because response to this PEEP range is a good predictor of maximum recruitability [16]. Furthermore, we wanted to reveal whether or not spatial patterns of response are superimposable between higher PEEP and prone positioning. However, a smaller PEEP difference could have produced better functional results. We chose different tidal volumes between tested PEEP levels to limit lung overdistension and barotrauma during high PEEP while avoiding lethal

hypoxemia during low PEEP. Finally, ventilator settings were applied in-scanner for only 15 minutes, although pilot studies showed that CT inflation patterns in our model were not substantially altered by longer wait times.

Faulty registration can induce errors in voxel-level measurements of inflation shifts due to higher PEEP and positional changes, but we have previously provided reassuring data showing that major airway structures [8,14], outer lung borders [38], and inflation distributions [8,14,39] are reasonably preserved after warping.

In conclusion, the results of this study support the hypothesis that evolving lung injury is characterized by a time-dependent loss of aeration response to prone positioning in the posterior lung. This deterioration probably contributes to variability in responses to positional therapy and might undermine the clinical outcome benefits of this treatment.

REFERENCES

1 Gattinoni L, Bombino M, Pelosi P, *et al.* Lung structure and function in different stages of severe adult respiratory distress syndrome. *JAMA* 1994;**271**:1772–9.

2 Matamis D, Lemaire F, Harf A, *et al.* Total respiratory pressure-volume curves in the adult respiratory distress syndrome. *Chest* 1984;**86**:58–66. doi:10.1378/chest.86.1.58

3 Network TARDS. Ventilation with Lower Tidal Volumes as Compared with Traditional Tidal Volumes for Acute Lung Injury and the Acute Respiratory Distress Syndrome. *New England Journal of Medicine* 2000;**342**:1301–8. doi:10.1056/NEJM200005043421801

4 Richter T, Bellani G, Harris RS, *et al.* Effect of Prone Position on Regional Shunt, Aeration, and Perfusion in Experimental Acute Lung Injury. *Am J Respir Crit Care Med* 2005;**172**:480–7. doi:10.1164/rccm.200501-004OC

5 Guerin C, Reignier J, Richard JC, *et al.* Prone positioning in severe acute respiratory distress syndrome. *The New England journal of medicine* 2013;**368**:2159–68. doi:10.1056/NEJMoa1214103;

6 Gattinoni L, Pelosi P, Vitale G, *et al.* Body position changes redistribute lung computed-tomographic density in patients with acute respiratory failure. *Anesthesiology* 1991;**74**:15–23.

7 Motta-Ribeiro GC, Hashimoto S, Winkler T, *et al.* Deterioration of Regional Lung Strain and Inflammation during Early Lung Injury. *Am J Respir Crit Care Med* 2018;**198**:891–902. doi:10.1164/rccm.201710-2038OC

8 Xin Y, Cereda M, Hamedani H, *et al.* Unstable Inflation Causing Injury. Insight from Prone Position and Paired Computed Tomography Scans. *American Journal of Respiratory and Critical Care Medicine* 2018;**198**:197–207. doi:10.1164/rccm.201708-1728OC

9 Bellani G, Laffey JG, Pham T, *et al.* Epidemiology, Patterns of Care, and Mortality for Patients With Acute Respiratory Distress Syndrome in Intensive Care Units in 50 Countries. *Jama* 2016;**315**:788–800. doi:10.1001/jama.2016.0291

10 Guérin C, Beuret P, Constantin JM, *et al.* A prospective international observational prevalence study on prone positioning of ARDS patients: the APRONET (ARDS Prone Position Network) study. *Intensive Care Medicine* 2018;**44**:22–37. doi:10.1007/s00134-017-4996-5

11 Goligher EC, Kavanagh BP, Rubenfeld GD, *et al.* Oxygenation response to positive end-expiratory pressure predicts mortality in acute respiratory distress syndrome. A secondary analysis of the LOVS and ExPress trials. *Am J Respir Crit Care Med* 2014;**190**:70–6. doi:10.1164/rccm.201404-0688OC

12 Artigas A, Camprubí-Rimblas M, Tantinyà N, *et al.* Inhalation therapies in acute respiratory distress syndrome. *Ann Transl Med* 2017;**5**. doi:10.21037/atm.2017.07.21

13 Grasso S, Mascia L, Del Turco M, *et al.* Effects of recruiting maneuvers in patients with acute respiratory distress syndrome ventilated with protective ventilatory strategy. *Anesthesiology* 2002;**96**:795–802. doi:10.1097/00000542-200204000-00005

14 Xin Y, Cereda M, Hamedani H, *et al.* Positional Therapy and Regional Pulmonary Ventilation: High-resolution Alignment of Prone and Supine Computed Tomography Images in a Large Animal Model. *Anesthesiology* Published Online First: 4 August 2020. doi:10.1097/ALN.0000000000003509

15 Gerard SE, Herrmann J, Kaczka DW, *et al.* Multi-resolution convolutional neural networks for fully automated segmentation of acutely injured lungs in multiple species. *Medical Image Analysis* 2020;**60**:101592. doi:10.1016/j.media.2019.101592

16 Gattinoni L, Caironi P, Cressoni M, *et al.* Lung Recruitment in Patients with the Acute Respiratory Distress Syndrome. *New England Journal of Medicine* 2006;**354**:1775–86. doi:10.1056/NEJMoa052052

17 Patroniti N, Bellani G, Manfio A, *et al.* Lung volume in mechanically ventilated patients: measurement by simplified helium dilution compared to quantitative CT scan. *Intensive Care Medicine* 2004;**30**:282–9. doi:10.1007/s00134-003-2109-0

18 Tustison NJ, Avants BB. Explicit B-spline regularization in diffeomorphic image registration. *Front Neuroinform* 2013;**7**. doi:10.3389/fninf.2013.00039

19 Fukuda Y, Ishizaki M, Masuda Y, *et al.* The role of intraalveolar fibrosis in the process of pulmonary structural remodeling in patients with diffuse alveolar damage. *Am J Pathol* 1987;**126**:171–82.

20 Costa EL, Lima RG, Amato MB. Electrical impedance tomography. *Current Opinion in Critical Care* 2009;**15**:18–24. doi:10.1097/MCC.0b013e3283220e8c

21 Introduction to Mixed Modelling: Beyond Regression and Analysis of Variance | Wiley. Wiley.com. https://www.wiley.com/en-

us/Introduction+to+Mixed+Modelling%3A+Beyond+Regression+and+Analysis+of+Variance-p-9780470035962 (accessed 13 Oct 2020).

22 Bates D, Mächler M, Bolker B, *et al.* Fitting Linear Mixed-Effects Models Using lme4. *Journal of Statistical Software* 2015;**67**:1–48. doi:10.18637/jss.v067.i01

23 Allen GB, Leclair T, Cloutier M, *et al.* The response to recruitment worsens with progression of lung injury and fibrin accumulation in a mouse model of acid aspiration. *American Journal of Physiology-Lung Cellular and Molecular Physiology* 2007;**292**:L1580–9. doi:10.1152/ajplung.00483.2006

24 Albert RK, Leasa D, Sanderson M, *et al.* The prone position improves arterial oxygenation and reduces shunt in oleic-acid-induced acute lung injury. *Am Rev Respir Dis* 1987;**135**:628–33. doi:10.1164/arrd.1987.135.3.628

25 Hubmayr RD, Walters BJ, Chevalier PA, *et al.* Topographical distribution of regional lung volume in anesthetized dogs. *J Appl Physiol Respir Environ Exerc Physiol* 1983;**54**:1048–56. doi:10.1152/jappl.1983.54.4.1048

26 Altemeier WA, McKinney S, Krueger M, *et al.* Effect of posture on regional gas exchange in pigs. *J Appl Physiol* 2004;**97**:2104–11. doi:10.1152/japplphysiol.00072.2004

27 Richard JC, Bregeon F, Costes N, *et al.* Effects of prone position and positive end-expiratory pressure on lung perfusion and ventilation. *Crit Care Med* 2008;**36**:2373–80. doi:10.1097/CCM.0b013e31818094a9

28 Cornejo RA, Díaz JC, Tobar EA, *et al.* Effects of Prone Positioning on Lung Protection in Patients with Acute Respiratory Distress Syndrome. *Am J Respir Crit Care Med* 2013;**188**:440–8. doi:10.1164/rccm.201207-1279OC

29 Galiatsou E, Kostanti E, Svarna E, *et al.* Prone Position Augments Recruitment and Prevents Alveolar Overinflation in Acute Lung Injury. *American Journal of Respiratory and Critical Care Medicine* 2006;**174**:187–97. doi:10.1164/rccm.200506-899OC

30 Musch G, Harris RS, Vidal Melo MF, *et al.* Mechanism by Which a Sustained Inflation Can Worsen Oxygenation in Acute Lung Injury. *Anesthesiology* 2004;**100**:323–30. doi:10.1097/00000542-200402000-00022

31 Chesnutt AN, Matthay MA, Tibayan FA, *et al.* Early detection of type III procollagen peptide in acute lung injury. Pathogenetic

and prognostic significance. *American Journal of Respiratory and Critical Care Medicine* 1997;**156**:840–5. doi:10.1164/ajrccm.156.3.9701124

32 Curley GF, Contreras M, Higgins B, *et al.* Evolution of the Inflammatory and Fibroproliferative Responses during Resolution and Repair after Ventilator-induced Lung Injury in the Rat. *Anesthesiology* 2011;**115**:1022–32. doi:10.1097/ALN.0b013e31823422c9

33 Katira BH, Giesinger RE, Engelberts D, *et al.* Adverse Heart-lung Interactions in Ventilator-induced Lung Injury. *Am J Respir Crit Care Med* Published Online First: 10 August 2017. doi:10.1164/rccm.201611-2268OC

34 Gaver III DP, Nieman GF, Gatto LA, *et al.* The POOR Get POORer: A Hypothesis for the Pathogenesis of Ventilator-Induced Lung Injury. *Am J Respir Crit Care Med* Published Online First: 10 June 2020. doi:10.1164/rccm.202002-0453CP

35 Albert RK, Keniston A, Baboi L, *et al.* Prone position–induced improvement in gas exchange does not predict improved survival in the acute respiratory distress syndrome. *American journal of respiratory and critical care medicine* 2014;**189**:494–496.

36 Broccard A, Shapiro RS, Schmitz LL, *et al.* Prone positioning attenuates and redistributes ventilator-induced lung injury in dogs. *Critical care medicine* 2000;**28**:295–303.

37 De Jong A, Molinari N, Sebbane M, *et al.* Feasibility and effectiveness of prone position in morbidly obese patients with ARDS: a case-control clinical study. *Chest* 2013;**143**:1554–61. doi:10.1378/chest.12-2115

38 Xin Y, Song G, Cereda M, *et al.* Semiautomatic segmentation of longitudinal computed tomography images in a rat model of lung injury by surfactant depletion. *Journal of Applied Physiology* 2015;**118**:377–85. doi:10.1152/japplphysiol.00627.2014

39 Cereda M, Xin Y, Hamedani H, *et al.* Tidal changes on CT and progression of ARDS. *Thorax* 2017;:thoraxjnl-2016-209833. doi:10.1136/thoraxjnl-2016-209833

Funding: This work was supported by NIH (Bethesda, MD, USA) grants R01-HL137389 and R01-HL139066, and by the Reginald Jenney Endowment Chair at Harvard Medical School and by Sundry Funds of the Anesthesia Center for Critical Care Research of the Department of Anesthesia, Critical Care and Pain Medicine of the Massachusetts General Hospital.

ONLINE SUPLLEMENT

ANIMAL EXPERIMENTS

Animal Preparation and Monitoring

Ten female Yorkshire pigs (30.7±1.1 kg) were anesthetized with intramuscular injection of ketamine (20–25 mg/kg) and xylazine (2 mg/kg); anesthesia was maintained by continuous intravenous infusion of ketamine (7–20 mg/kg/h), midazolam (0.2–0.7 mg/kg/h) and fentanyl (4–50 μg/kg/h) via a femoral vein catheter. Propofol (4–15 mg/kg/h) was used as an adjunct agent in case of inadequate anesthetic level. The femoral artery was catheterized for blood pressure and arterial blood gas monitoring. Femoral vessel cannulation was ultrasound-guided (Butterfly iQ, Guilford, CT). Pigs were intubated with a 6.5 mm cuffed endotracheal tube and mechanically ventilated (Servo-i, Maquet, Solna, Sweden). SpO_2, heart rate, blood pressure, end-tidal CO_2, and body temperature were continuously monitored (Cardell Max-12, Tampa, FL). The bladder was catheterized via the urethra. The urine output was collected and recorded hourly throughout the experiment. Rectal temperature was monitored continuously, and was actively maintained between 100 and 102 F with a circulating water pad. All animals received intravenous hydration with lactate Ringer's (10–20 ml/kg bolus and 1 mg/kg/h infusion). Hypotension (mean arterial blood pressure <60 mmHg) was treated by fluid bolus

administration and, if not responsive after two boluses, by epinephrine infusion. 5% dextrose was supplemented if blood glucose fell below 60 mg/dL, and potassium chloride was added for blood potassium below 4 mmol/L. Adequate anesthetic depth was monitored and recorded every 10 minutes and was maintained by increasing or decreasing the rates of ketamine/midazolam/fentanyl/propofol IV infusions. Immobility of respiratory muscles was monitored by visual analysis of ventilator tracings; during computed tomography (CT) scans, anesthetics were adjusted if motion artifacts were visible in the CT images.

HCl Instillation

After animal instrumentation and stabilization and the collection of healthy baseline physiological measurements, 3.5 ml/kg of hydrochloric acid (HCl, pH 1.0) was divided in 5 ml aliquots and instilled via bronchoscopy (Ambu Inc., Columbia, MD) into the lobar bronchi of each lung (approximately 10 injection each lung) to assure symmetric distribution of the acid. During HCl instillation, the pig was ventilated under pressure control ventilation (PEEP 5 cmH_2O, driving pressure 20 cmH_2O). The animals were then placed supine and stabilized while ventilated with pressure control ventilation (PEEP 10 cmH_2O, driving pressure 20 cmH_2O) for 2 hours.

Mechanical Ventilation

After the initial stabilization period, Day 1 CT scans were obtained. All animals were then ventilated supine for 24 hours on volume-controlled ventilation with PEEP 3 cmH_2O and tidal volume (V_T) 12 ml/kg. FiO_2 and respiratory rate were targeted to arterial oxygen saturation (>90%) and $PaCO_2$ (35–45 mmHg). However, to avoid dynamic hyperinflation, respiratory rate was not increased above 35 breaths per minute. After 24 hours, CT was repeated (Day 2). Respiratory mechanics (inspiratory airway resistance, intrinsic PEEP, and respiratory system compliance) were measured with an accepted technique [1] every hour, and arterial blood gases were measured every six hours. Animals were expeditiously transported to and from the CT scanner while manually ventilated with PEEP 5–10 cmH_2O.

Image Acquisition

CT scans were acquired with a Siemens SOMATOM Force scanner (Siemens Medical Systems, Erlangen, Germany). The settings were: 120 kVp, 200 mAs, pitch 0.95, slice thickness 0.75 mm, collimation 57.6x0.6 mm, estimated dosage 3–5 mSv. All images were reconstructed to a resolution of 1x1x1 mm with QR44 kernel. In the scanner, CT images and physiologic measurements were obtained after supine and prone ventilation with one of two settings randomly applied for 15 minutes: 1) low PEEP-high volume (PEEP 3 cmH_2O, V_T 12 ml/kg, rate 25 bpm), or 2) high PEEP-low volume (PEEP 15 cmH_2O, V_T 6 ml/kg, rate 40 bpm). Recruitment maneuvers were performed after arrival at the scanner and

again after each position change. The pigs lay unsupported when in the prone position. Lungs were scanned during 5-second-long end-inspiratory and end-expiratory pauses; however, only the expiratory images were used for analysis.

Image Analysis

To quantitatively analyze lung inflation, we first segmented (separated from non-pulmonary tissue) lung images using a validated deep-learning methodology [2]. This multi-resolution convolutional neural network can achieve an accurate and consistent segmentation across all the images, and has been validated on canine, porcine and ovine injured lung CTs [3]. Lung weights [4] and end-expiratory lung volumes (EELV) [5] were calculated using accepted methodology applied to the segmented images. We then registered (aligned) segmented CT scans obtained in the prone position (at low and high PEEP) and in the supine position (at high PEEP) to the supine low-PEEP images using deformable registration to align lung borders and internal features between images [6,7]. More specifically, due to the large difference between supine and prone images, two registration steps were performed as described in our published work [8]. First, the masks (outlines) of the images were aligned with rigid, affine and deformable registration algorithms, in sequence, to obtain a transform matrix (Φ_M). Second, deformable registration of prone to supine images was performed, building upon the previously acquired Φ_M. This allowed us to measure the effects of positioning and PEEP on the aeration of each

tissue voxel [8], which was quantified as the *voxelwise* change in density (HU) between the registered (warped) images (prone, high PEEP, or in combination) and the supine-low PEEP (target) image. Lung recruitment was defined as the non-aerated voxels in which aeration was restored, causing voxel density to decrease from >-100 Hounsfield units (HU) to any lower value when turning prone and/or increasing PEEP; conversely, voxels whose density increased to >-100 HU from a lower range were labeled as 'derecruitment' [8]. Recruited and derecruited voxels were identified and mapped in the registered images. Since all images were warped to match the same coordinates, the voxels recruited (or derecruited) by prone position, PEEP, and their combination could be spatially identified. All aeration changes were mapped and spatially analyzed in 10 anterior-posterior and 10 cranio-caudal equal-weight bins.

Histologic Analysis

After Day 2 CT imaging, animals were euthanized for autopsy. A total of 12 samples were acquired from each pig lung (lower/middle/upper lobes from each sides) and fixed in 10% formalin. Several 10-µm-thick slices excised from each section were stained with hematoxylin and eosin (H&E). The severity of lung injury in each slide was subsequently scored by two blinded operators. Injury was assessed by a combination of infiltration of polymorphonuclear cells (scale of 0–2: 0 = no infiltrate, 1 = infiltrate in the perivascular compartment, 2 = infiltrate in alveolar compartment), alveolar structure disruption (scale of 0–3: 0 = regular, 1 =

distorted, 2 = collapsed with torn capillary–alveolar membrane, 3 = collapsed with opacity), presence of hyaline membranes (scale of 0–5: 0 = None, 1 = detected in 1 or 2 areas, 2 = present in 3 or 4 areas, 3 = present in 5 or 6 areas, 4 = present in 7 or 8 areas and 5 = present in 9 or 10 areas) and edema (scale of 0–10: 0 = regular alveolus, through 10 = dilated vessels in alveolar walls and proteinaceous material in alveolus). All quantifications were performed using Leica microscope imaging software. Additional details can be found in our previously published paper [9].

Statistical Analysis

Data was prepared in Jupyter Notebook using Python 3.6. Statistical analysis was performed using RStudio 1.2.5001 (R Foundation for Statistical Computing; Vienna, Austria). No power analysis was performed due to the explorative nature of the study. Two-tailed paired T-tests with Bonferroni correction were performed for comparisons between different time points. Since each pig was imaged multiple times under different conditions, we used a mixed model approach (lme4, R package) [10,11]. Fixed effects were considered to be the effects of PEEP, positioning, and their combination on physiologic and imaging variables. To study the differences of within-subject factors as a function of time, we preferred to use separate models for each day. We assigned pig (as a subject term) as a random effect. We reported each estimate with its confidence intervals. Comparisons were assumed to be significant if the corrected 95% confidence interval did not contain zero. We also reported Cohen's d

effect sizes for each factor to show the clinical significance of positioning, PEEP, and their combination on different dependent variables. We have also reported an equivalent P-value (lmerTest, R package) [12] for readers unfamiliar with mixed models and the interpretation of confidence intervals. An experiment-wide Type I error level of 0.05 was used.

ARDS PATIENTS

The human studies were approved by the Investigational Review Board at the Massachusetts General Hospital (IRB 2019P001995). Data were obtained in 4 patients meeting acute respiratory distress syndrome (ARDS) criteria [13], who were studied either early (N=2) or late (N=2) after ARDS onset. The cutoff between early vs. late ARDS was set at seven days based on Fukuda et al. [14]. The authors of this study described rapid intra-alveolar fibroproliferation starting the second week after ARDS onset.

Regional lung mechanics were recorded using electrical impedance tomography (Enlight 1800, Timpel Medical, São Paulo, Brazil), as part of comprehensive monitoring by the Lung Rescue Team at Massachusetts General Hospital [15]. All patients were sedated, and ventilated in volume-controlled mode, tidal volume of 5–6 mL/Kg predicted body weight. EIT acquisitions were performed in the prone and in the supine position, at PEEP 15 cmH_2O. The time interval between the supine and the prone assessments was below 24h.

EIT images were reconstructed according to a 3D finite element model and plotted in a matrix of 32 x 32 pixels. Regions of interest (ROIs) were defined as each horizontal layer in the EIT matrix, where layer 1 was the most ventral and layer 32 the most dorsal (Figure 2). The impedance change induced by ventilation (ΔZ_V) was quantified in each ROI by averaging 20 respiratory cycles. EIT-regional compliance was calculated as the proportion of tidal ventilation in each ROI divided by the elastic recoil pressure of the respiratory system (Figure 2).

Patients #1, #2, #3 and #4 were 69, 35, 60, 62 years old, respectively. Days of mechanical ventilation, global respiratory system compliance (CRS), and oxygenation (PaO_2/FIO_2 ratio) are reported in Figure 7 of the main text.

REFERENCE

1 Bates JH, Baconnier P, Milic-Emili J. A theoretical analysis of interrupter technique for measuring respiratory mechanics. *J Appl Physiol (1985)* 1988;**64**:2204–14. doi:10.1152/jappl.1988.64.5.2204

2 Gerard SE, Herrmann J, Kaczka DW, *et al.* Transfer Learning for Segmentation of Injured Lungs Using Coarse-to-Fine Convolutional Neural Networks. In: Stoyanov D, Taylor Z, Kainz B, *et al.*, eds. *Image Analysis for Moving Organ, Breast, and Thoracic Images*. Springer International Publishing 2018. 191–201.

3 Gerard SE, Herrmann J, Kaczka DW, *et al.* Multi-resolution convolutional neural networks for fully automated segmentation of acutely injured lungs in multiple species. *Medical Image Analysis* 2020;**60**:101592. doi:10.1016/j.media.2019.101592

4 Hyde RW, Wandtke JC, Fahey PJ, *et al.* Lung weight in vivo measured with computed tomography and rebreathing of soluble gases. *Journal of Applied Physiology* 1989;**67**:166–73. doi:10.1152/jappl.1989.67.1.166

5 Patroniti N, Bellani G, Manfio A, *et al.* Lung volume in mechanically ventilated patients: measurement by simplified helium dilution compared to quantitative CT scan. *Intensive Care Medicine* 2004;**30**:282–9. doi:10.1007/s00134-003-2109-0

6 Tustison NJ, Avants BB. Explicit B-spline regularization in diffeomorphic image registration. *Front Neuroinform* 2013;**7**. doi:10.3389/fninf.2013.00039

7 Cereda M, Xin Y, Hamedani H, *et al.* Tidal changes on CT and progression of ARDS. *Thorax* 2017;:thoraxjnl-2016-209833. doi:10.1136/thoraxjnl-2016-209833

8 Xin Y, Cereda M, Hamedani H, *et al.* Positional Therapy and Regional Pulmonary Ventilation: High-resolution Alignment of Prone and Supine Computed Tomography Images in a Large Animal Model. *Anesthesiology* Published Online First: 4 August 2020. doi:10.1097/ALN.0000000000003509

9 Pourfathi M, Cereda M, Chatterjee S, *et al.* Lung Metabolism and Inflammation during Mechanical Ventilation; An Imaging Approach. *Scientific Reports* 2018;**8**:3525. doi:10.1038/s41598-018-21901-0

10 Introduction to Mixed Modelling: Beyond Regression and Analysis of Variance | Wiley. Wiley.com. https://www.wiley.com/en-us/Introduction+to+Mixed+Modelling%3A+Beyond+Regression+and+Analysis+of+Variance-p-9780470035962 (accessed 13 Oct 2020).

11 Bates D, Mächler M, Bolker B, *et al.* Fitting Linear Mixed-Effects Models Using lme4. *Journal of Statistical Software* 2015;**67**:1–48. doi:10.18637/jss.v067.i01

12 Kuznetsova A, Brockhoff PB, Christensen RHB. lmerTest Package: Tests in Linear Mixed Effects Models. *Journal of Statistical Software* 2017;**82**:1–26. doi:10.18637/jss.v082.i13

13 ARDS Definition Task Force, Ranieri VM, Rubenfeld GD, *et al.* Acute respiratory distress syndrome: the Berlin Definition. *JAMA* 2012;**307**:2526–33. doi:10.1001/jama.2012.5669

14 Fukuda Y, Ishizaki M, Masuda Y, *et al.* The role of intraalveolar fibrosis in the process of pulmonary structural remodeling in patients with diffuse alveolar damage. *Am J Pathol* 1987;**126**:171–82.

15 Spina S, Capriles M, De Santis Santiago R, *et al.* Development of a Lung Rescue Team to Improve Care of Subjects With Refractory Acute Respiratory Failure. *Respir Care* 2020;**65**:420–6. doi:10.4187/respcare.07350

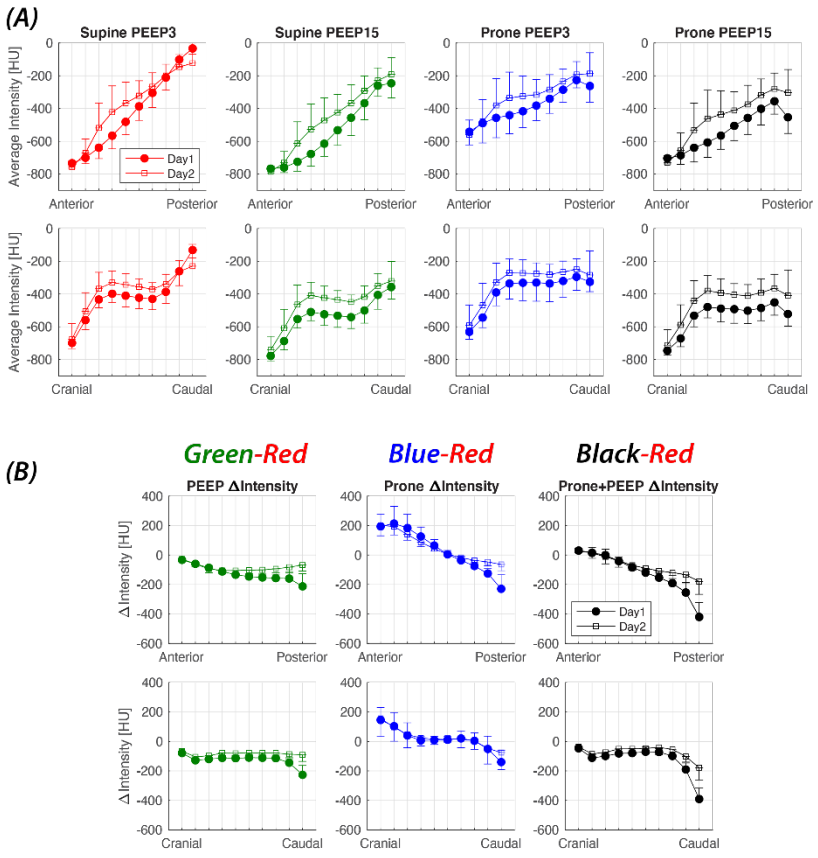

Figure 1. The regional distributions of average intensity (A) and intensity change due to tested treatments (PEEP, prone position, and their combination) (B) were analyzed by partitioning the lung into 10 segments of equal volume along the Anterior-Posterior and Caudal-Cranial axis. Day 1 (closed circles) and Day 2 (open squares) are shown in each plot.

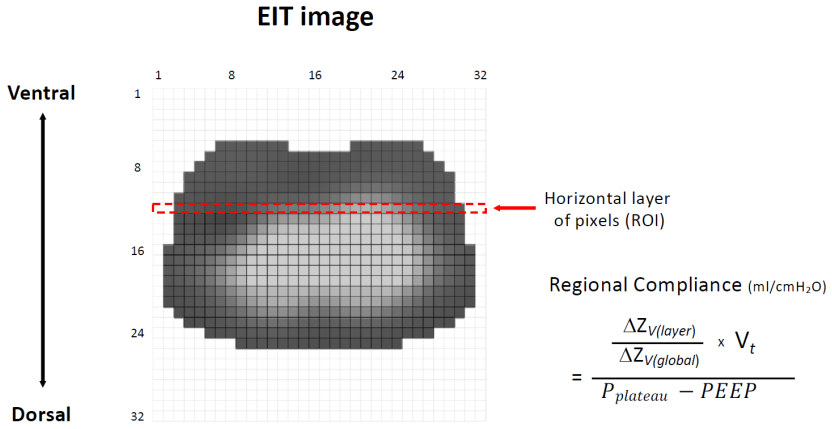

Figure 2. Functional images by electrical impedance tomography (EIT) were reconstructed in a matrix with 32 horizontal pixel layers and 32 vertical pixel columns (32 x 32). Regions of interest (ROIs) were composed of each horizontal bin layer in the EIT matrix, which is the maximum vertical resolution allowed by the instrument. The area outlined in red exemplifies a ROI selection. EIT-regional ventilation was calculated by multiplyng the fractional tidal change of impedance ($\Delta Z_{V(layer)}/DZ_{V(global)}$, averaged over 20 breaths) by the tidal volume (V_T, in ml). Then regional complaince was obtained by dividing this value by the driving pressure of the respiratory system ($P_{plateau}$ - PEEP).

	Healthy	HCl	12h	24h
pH	7.5±0.1	7.4±0.1	7.5±0.0	7.4±0.1
Lactic Acid (mmol/L)	0.7±0.4	1.0±0.3 †	0.7±0.2 ‡	0.7±0.4
Creatinine (mg/dL)	1.8±0.4	1.8±0.2	2.0±0.3 ‡	2.0±0.5
Blood Glucose (mg/dL)	83.0±17.1	76.0±21.2	82.4±19.6	78.5±21.5
FiO_2	0.5±0.0	0.6±0.2	0.5±0.1	0.7±0.2
SpO_2 (%)	99.5±0.7	98.4±1.1 †	97.4±1.6	96.3±2.3
Respiratory Rate	22.2±2.6	22.5±2.6	22.4±3.7	22.8±5.1
Peak Inspiratory Pressure (cmH_2O)	17.6±2.4	32.4±3.3 †	34.9±6.4	41.4±6.4 §
Plateau Pressure (cmH_2O)	12.9±2.5	25.3±4.3 †	26.6±5.6	32.2±3.9 §
Mean Airway Pressure (cmH_2O)	6.3±0.7	9.3±1.1 †	9.4±1.3	12.1±2.1 §
Auto PEEP (cmH_2O)	0.1±0.3	0.5±0.7	0.6±0.7	0.3±0.5
Airway Resistance	11.1±1.2	21.8±5.5 †	18.0±6.5	21.0±9.4
Total Fluids (ml)				3162.7±1284.6
Total Urine Output (ml)				2677.6±883.6
Mean Blood Pressure (mmHg)	87.9±14.6	75.6±13.0	72.0±13.3	67.5±10.4
$EtCO_2$ (mmHg)	34.3±1.7	36.0±3.6	35.0±2.9	35.9±5.0
Heart Rate	73.5±6.1	83.9±4.6 †	83.9±16.5	92.8±20.0

Table 1. Physiological and laboratory values before and after lung injury and during 24 hours of non-protective ventilation. †: P<0.05 healthy vs. HCl, ‡: P<0.05 HCl vs. 12h, §: 12h vs. 24h.

Fixed Effects	Estimate (95% CI)	Cohen's d	P-Value	Estimate (95% CI)	Cohen's d	P-Value	Estimate (95% CI)	Cohen's d	P-Value	Estimate (95% CI)	Cohen's d	P-Value	Estimate (95% CI)	Cohen's d	P-Value
	Compliance ml/cmH_2O			PaO_2/FiO_2 mmHg			$PaCO_2$ mmHg			Lung Volume ml			Mean Intensity HU		
Day 1															
Intercept	17.7 (15.9 , 19.4)			351.4 (272.4 , 430.4)			37.3 (32.1 , 42.5)			873.0 (799.1 , 946.8)			-539.4 (-565.2 , -513.6)		
Prone	3.9 (2.3 , 5.6)	**1.74**	**< 0.001**	101.7 (61.5 , 141.8)	**1.87**	**< 0.001**	0.4 (-3.3 , 4.1)	0.08	0.835	-29.0 (-68.7 , 10.6)	-0.54	0.163	17.3 (8.4 , 26.2)	**1.43**	**0.001**
PEEP	-6.1 (-7.8 , -4.5)	**-2.72**	**< 0.001**	-46.4 (-86.5 , -6.3)	**-0.86**	**0.032**	13.1 (9.3 , 16.8)	**2.60**	**< 0.001**	238.7 (199.0 , 278.3)	**4.45**	**< 0.001**	-55.0 (-63.9 , -46.0)	**-4.54**	**< 0.001**
Day 2															
Intercept	13.5 (10.8 , 16.3)			126.2 (83.6 , 168.8)			52.6 (41.1 , 64.1)			849.3 (760.8 , 937.7)			-493.8 (-525.1 , -462.6)		
Prone	2.3 (1.1 , 3.5)	**1.46**	**0.001**	-23.5 (-37.7 , -9.3)	**-1.22**	**0.003**	5.9 (1.4 , 10.5)	**0.96**	**0.017**	-106.0 (-142.7 , -69.2)	**-2.13**	**< 0.001**	29.0 (20.5 , 37.6)	**2.50**	**< 0.001**
PEEP	-5.1 (-6.3 , -3.9)	**-3.19**	**< 0.001**	13.7 (-0.5 , 27.9)	0.71	0.069	16.1 (11.5 , 20.7)	**2.61**	**< 0.001**	149.6 (112.9 , 186.3)	**3.01**	**< 0.001**	-41.6 (-50.1 , -33.0)	**-3.58**	**< 0.001**
Random Effects	Estimated SD (95% CI)			Estimate (95% CI)			Estimate (95% CI)			Estimate (95% CI)			Estimate (95% CI)		
Day 1															
Subject	1.5 (0.0 , 2.9)			110.60 (67.4 , 179.9)			16.8 (10.5 , 27.0)			102.0 (61.6 , 166.6)			38.2 (24.1 , 61.1)		
Residuals	2.7 (2.1 , 3.4)			64.87 (49.6 , 82.6)			7.4 (5.6 , 9.4)			64.1 (49.1 , 81.7)			14.5 (11.1 , 18.4)		
Day 2															
Subject	3.9 (2.44 , 6.3)			63.11 (40.0 , 101.0)			16.8 (10.5 , 27.0)			128.1 (80.0 , 206.3)			47.0 (30.0 , 74.9)		
Residuals	1.9 (1.46 , 2.4)			22.93 (17.5 , 29.2)			7.4 (5.6 , 9.4)			59.4 (45.4 , 75.6)			13.9 (10.6 , 17.7)		

Table 2. Comparisons of physiological characteristics of pigs at different PEEP levels and positions on different study days using a mixed-effect regression model, as detailed in the Statistical Analysis section.

Fixed Effects	Estimate (95% CI)	Cohen's d		Estimate (95% CI)	Cohen's d		Estimate (95% CI)	Cohen's d		Estimate (95% CI)	Cohen's d	
	Recruitment [%]			Derecruitment [%]			Recruitment by mass [%]			Derecruitment by mass [%]		
Day 1												
Intercept	13.34 (10.86 , 15.81)			0.71 (-1.11 , 2.52)			22.48 (18.86 , 26.10)			0.90 (-0.24 , 2.05)		
Prone+PEEP	3.30 (2.01 , 4.59)	**2.35**	**< 0.001**	1.14 (-1.18 , 3.47)	0.45	0.349	5.83 (3.75 , 7.92)	**2.58**	**< 0.001**	1.07 (-0.33 , 2.47)	0.70	0.154
Prone	-2.21 (-3.50 , -0.92)	**-1.57**	**0.004**	5.88 (3.56 , 8.20)	**2.33**	**< 0.001**	-3.55 (-5.63 , -1.46)	**-1.57**	**0.004**	4.98 (3.58 , 6.39)	**3.27**	**< 0.001**
Day 2												
Intercept	10.06 (8.77 , 11.35)			0.48 (-0.74 , 1.71)			15.77 (13.87 , 17.67)			0.58 (-0.52 , 1.68)		
Prone+PEEP	1.02 (-0.15 , 2.18)	0.80	0.106	1.31 (-0.13 , 2.74)	0.84	0.093	1.90 (-0.04 , 3.83)	0.90	0.072	1.24 (-0.13 , 2.60)	0.83	0.094
Prone	-5.41 (-6.57 , -4.24)	**-4.27**	**< 0.001**	5.85 (4.42 , 7.29)	**3.75**	**< 0.001**	-8.44 (-10.37 , -6.50)	**-4.01**	**< 0.001**	5.95 (4.59 , 7.32)	**4.01**	**< 0.001**
Random Effects	Estimate (95% CI)			Estimate (95% CI)			Estimate (95% CI)			Estimate (95% CI)		
Day 1												
Subject	3.58 (2.23 , 5.77)			1.34 (0.00 , 2.89)			5.16 (3.18 , 8.35)			0.97 (0.00 , 1.94)		
Residuals	1.48 (1.06 , 1.98)			2.66 (1.91 , 3.55)			2.39 (1.71 , 3.20)			1.61 (1.15 , 2.15)		
Day 2												
Subject	1.58 (0.82 , 2.69)			1.14 (0.00 , 2.18)			2.13 (0.88 , 3.75)			0.90 (0.00 , 1.84)		
Residuals	1.34 (0.96 , 1.79)			1.65 (1.18 , 2.20)			2.22 (1.59 , 2.97)			1.57 (1.12 , 2.10)		

Table 3. Recruited and derecruited lung tissue (as a percent of whole-lung volume and mass) as a result of applying high PEEP alone, prone position alone, and their combination in early (Day 1) and late (Day 2) injury. Comparisons were performed using a mixed-effect regression model, as detailed in the Statistical Analysis section.

CHAPTER 4: SUMMARY, CONCLUSION AND FUTURE PERSPECTIVES

4.1 SUMMARY AND CONCLUSIONS

Diaphragmatic dysfunction and pulmonary stress during mechanical ventilation are serious conditions that reducing positive outcomes and weaning successful in ICU patients.

Despite advances in the management of mechanical ventilation using of innovative strategies to overcome these problems and the development of novel pharmacological treatment, as Bellani have showed, the Acute Respiratory Distress Syndrome mortality is estimated as high as 40% [1].

The aim of the first study has been mainly focused on the effects of Angiotensin-(1-7) treatment in a rat model of diaphragmatic dysfunction induced by 8 hours of MV. To our knowledge, no studies investigated the role of Ang-(1-7) on the diaphragmatic injury. The main finding showed the ability of Ang-(1-7) to preserve the muscles fiber from atrophy event during the mechanical ventilation.

Our explanation for that observation it's that Ang-(1-7) was able to reduce the expression of Atrogin-1 and Muscle RING finger 1 (MuRF1), the two major muscle-specific E3 ubiquitin ligases that are increased transcriptionally in skeletal muscle under atrophy-inducing conditions.

Supporting that, the lower levels of Myogenin mRNA that we found, typically expressed by slow fibers.

The findings about the force generation muscle capability were not as evident as those about the fiber atrophy prevention. Indeed, treatment

with Angiotensin-(1-7) did not improve the diaphragmatic contraction, even if the two groups of rats treated with Mas and AT2R antagonists showed a greater contractility dysfunction, with less force developed at every frequency of stimulation. This may suggest that beneficial effects of Angiotensin-(1-7) are not correlated only to the prevention of fiber size but probably even about others physiological events. Therefore, future perspectives will be to investigate and evaluate the effects of Ang-(1–7) on the oxidative stress and confirm our findings in a model of ventilation more prolonged. However, these results encourage further preclinical studies direct to use angiotensin-(1–7) in human patients.

As is known, pulmonary stress during mechanical ventilation accelerates ARDS development [2].

The injury progression may limit the clinical efficacy of therapeutic and pharmacological treatments, limiting the opportunity of a positive outcomes. Indeed, during the ARDS management the timing of intervention with specific strategies is essential and fundamental to achieve a good level of success. Nowadays is unclear how lung injury progression during mechanical ventilation modifies pulmonary responses to prone positioning. The aim of this project was to understand and clarify if the progression of ARDS may decrease the beneficial effects of prone position to meliorate outcomes during the mechanical ventilation.

We compared the efficacy of prone positioning on regional lung aeration in late vs. early stages of lung injury.

Overall, the main findings of this study were promising showing for the first time that the progression of lung injury is strictly correlated with the stage of lung injury and the duration of ventilation. The results suggest that injury progression in ventilated lungs may lessen prone positioning's ability to improve aeration and recruit posterior lung regions. Indeed, we showed that there is a time-dependent loss of aeration response to prone positioning in the posterior lung. The decline of this event may generate a variability in responses to pronation therapy and might limit the clinical efficacy of this important treatment. Furthermore, EIT measurements hint that pronation may be unable to improve posterior lung mechanics after prolonged ventilation in clinical ARDS.

Therefore, the beneficial effects of pronation on the regional physiology are time dependent and with our results providing an important rationale to avoid delaying treatment.

4.2 FUTURE PERSPECTIVES

The future goals are to combine the heterogenic knowledges that I acquired during my research period in Milan and Philadelphia to evaluate the effect of pronation on the diaphragmatic dysfunction during a mechanical ventilation.

The overdistention of the lung is one of the most important mechanisms that damages tissue during a mechanical ventilation, in addition the release of and/or activation of cytotoxic and inflammatory cascades worsen the medical case [3].

Although the prone position is often considered a non-physiological posture for human beings, it reconfigures the diaphragm profile in ways that could improve its function and biology. Due to redistribution of abdominal pressures, we think that the dorsal part of the diaphragm undergoes more sustained stretch than in the supine position. This stretch may attenuate the progressive loss of muscle mass during prolonged mechanical ventilation, by maintaining a state of tension on the muscle fibers. Preclinical studies showed a decrease of diaphragm fiber apoptosis in prone vs. supine sheep [4].

In this respect, we hypothesize that the prolonged stretch that occurs during pronation could makes the inactivity more tolerable mitigating the detrimental effects about the diaphragm during the mechanical ventilation.

Our future aim is to study the effects of body position on the diaphragmatic dysfunction due to prolonged mechanical ventilation. The potential role of pronation to mitigate the adverse effects of prolonged mechanical ventilation represents a major leap forward in developing effective, personalized approaches to ICU patients. Investigate the effects of pronation on the diaphragmatic dysfunction, at different conditions, could suggest if a personalized ventilation can determinate an improvement in weaning outcome.

Our primary hypothesis is that, in the prone position prolonged stretch of the posterior region of the diaphragm mitigates the detrimental effects of inactivity on its muscle fibers. Ventilation in prone position might improves diaphragm tolerance by modifying the muscle profile compared to ventilation in supine position, and it could protect the diaphragm, through a different respiratory mechanics, from the pressure load due to ventilation. If it's confirmed, the mitigating effect of prone positioning on VIDD represents a major leap towards developing more effective and personalized strategies to control the adverse effects of prolonged ventilation and to limit ventilator dependence. Using imaging and biological methodologies, we will test this hypothesis in a model of rat.

Moreover, the second future goal it will be to investigate if the progression of ARDS exasperated by the ventilatory parameters could worsen the diaphragm muscle physiology.

REFERENCES

1. Bellani G, Pham T, Laffey J; LUNG-SAFE Investigators; ESICM Trials Group. Incidence of Acute Respiratory Distress Syndrome--Reply. JAMA. 2016 Jul 19;316(3):347.
2. Network TARDS. Ventilation with Lower Tidal Volumes as Compared with Traditional Tidal Volumes for Acute Lung Injury and the Acute Respiratory Distress Syndrome. New England Journal of Medicine 2000;342: 1301–8.
3. Dos Santos CC, Slutsky AS. Invited review: mechanisms of ventilator-induced lung injury: a perspective. J Appl Physiol (1985). 2000 Oct;89(4):1645-55.
4. Nakos G, Batistatou A, Galiatsou E, Konstanti E, Koulouras V, Kanavaros P, Doulis A, Kitsakos A, Karachaliou A, Lekka ME, Bai M. Lung and 'end organ' injury due to mechanical ventilation in animals: comparison between the prone and supine positions. Crit Care. 2006 Feb;10(1): R38.

CHAPTER 5: PUBBLICATIONS

5.1 PAPERS

Zambelli V, Sigurtà A, Rizzi L, Zucca L, Delvecchio P, Bresciani E, Torsello A, Bellani G. **Angiotensin-(1-7) exerts a protective action in a rat model of ventilator-induced diaphragmatic dysfunction**. Intensive Care Med Exp. 2019 Jan 18;7(1):8.

Zambelli V, Rizzi L, Delvecchio P, Bresciani E, Molteni L, Meanti R, Pascal V, Fehrentz JA, Omeljaniuk RJ, Bellani G, Torsello A. **JMV5656, a short synthetic derivative of TLQP-21, alleviates acid-induced lung injury and fibrosis in mice**. Pulm Pharmacol Ther. 2020 Jun;62:101916.

Vanessa Zambelli, Laura Rizzi, Paolo Delvecchio, Elena Bresciani, Laura Molteni, Ramona Meanti, Maria Serena Cuttin, Giorgio Bovo, Coco Silvia, Robert J. Omeljaniuk, Vittorio Locatelli, Giacomo Bellani, Antonio Torsello. **Acute hexarelin treatment modulates lung fibrosis in a murine ARDS model; the potential for growth hormone secretagogues in treatment of COVID-19 pneumonia-associated ARDS.** Submitted

Yi Xin, Kevin Martin, Caio C.A. Morais, Paolo Delvecchio, Sarah E. Gerard, Hooman Hamedani, Jacob Herrmann, Nicholas Abate, Austin Lenart, Shiraz Humayun, Uday Sidhu, Mihail Petrov, Kristan Reutlinger, Tal Mandelbaum, Ian Duncan, Nicholas Tustison, Stephen Kadlecek, Shampa Chatterjee, James C. Gee, Rahim R. Rizi, Lorenzo Berra, Maurizio Cereda.

Diminishing Efficacy of Prone Positioning with Late Application in Evolving Lung Injury. submitted

M. Connell, Y. Xin, S. Gerard, J. Herrmann, P. K. Shah, K. T. Martin, E. Rezoagli, D. Ippolito; J. Rajaei, R. Baron; P. Delvecchio, S. Humayun, G. Bellani, R. R. Rizi, M. Cereda. **Unsupervised Segmentation and Quantification of COVID-19 Lesions on Computed Tomography Scans Using CycleGAN.** submitted

5.2 ORAL PRESENTATIONS

Delvecchio P., Zambelli V., BEllani G. **Preclinical model and therapeutic strategies for Ventilatory Induced Diaphragmatic Dysfunction**. DIMET open day 2018.

5.3 POSTERS

Delvecchio P., Zambelli V., Rizzi L., Zucca L., Sigurtà A., Bresciani E., Torsello A.B., Bellani G. **Angiotensin-(1-7) effects in a rat model of**

ventilator-induced diaphragmatic dysfunction (VIDD). AISAL Congress 2017.

A.C. Ionescu, M.D.S. Chiari, V. Zambelli, R.R. Braga, P. Delvecchio, S. Scolavino, E. Brambilla. **DCPD-containing composites prevent secondary caries, an in-vitro biofilm model**. ADM 2018.

Delvecchio P., Zambelli V., Bellani G. **Angiotensin-(1-7) effects in a rat model of ventilator-induced diaphragmatic dysfunction (VIDD).** DIMET open day 2019.

5.4 ABSTRACTS

Zambelli V., Rizzi L., Zucca L., Sigurtà A., Delvecchio P., Bresciani E., Torsello A.B., Bellani G. Angiotensin-(1-7) effects in a rat model of ventilator-induced diaphragmatic dysfunction (VIDD). ERS congress. Zambelli V., Rizzi L., Zucca L., Sigurtà A., Delvecchio P., Bresciani E., Torsello A.B., Bellani G. **Effetti del trattamento con Angiotensina-(1-7) in un modello sperimentale di insufficienza diaframmatica indotta dalla ventilazione meccanica prolungata (VIDD)**. 28th SMART Congress.

Rizzi L., Zambelli V., Delvecchio P., Bresciani E., Molteni L., Torsello A., Locatelli V., Bellani G. **Effetti del trattamento con Hexarelin in un modello sperimentale di insufficienza respiratoria acuta.** 28th SMART Congress.

Delvecchio P., Xin Y., Martin K., Gerard S., Hamedani H., Herrman J., Humayun S., Lenart A., Sidhu U., Pretov M., Abate N., Reutlinger K., Staley M., Esposito S., Tustison N., Gee J., Rizi R., Cereda M**. A clinically relevant and reliable model for preclinical research of ARDS syndrome.** ATS 2021.

Xin Y., Herrman J., Gerard S., Delvecchio P., Martin K., Hamedani H., Humayun S., Lenart A., Sidhu U., Pretov M., Abate N., Reutlinger K., Staley M., Esposito S., Tustison N., Gee J., Rizi R., Cereda M**. Non-linear Inflation Dynamics Increase During Progression of Experimental Lung injury.** ATS 2021.

Xin Y., Herrman J., Martin K., Gerard S., Delvecchio P., Hamedani H., Humayun S., Lenart A., Sidhu U., Pretov M., Abate N., Reutlinger K., Staley M., Esposito S., Tustison N., Gee J., Rizi R., Cereda M. **Prone Ventilation in Lung Injury: The Declining Benefits of Vertical Axis Ventilation and Perfusion Matching at Late Stages of Injury.** ATS 2021.

Martin K., Xin Y., Herrman J., Gerard S., Delvecchio P., Hamedani H., Humayun S., Lenart A., Sidhu U., Pretov M., Abate N., Reutlinger K., Staley M., Esposito S., Tustison N., Gee J., Rizi R., Cereda M. **Diminished Redistribution of Aeration and Perfusion with Prone Ventilation in Late Stage Experimental Lung Injury.** ATS 2021.

Connell M., Xin Y., Gerard S., Herrman J., Shah K., Martin K., Rezoagli E., Ippolito D., Rajaei J., Baron R., Delvecchio P., Humayun S., Bellani G., Rizi R., Cereda M. **Unsupervised Segmentation and Quantification of COVID-19 Lesions on Computed Tomography Scans Using CycleGAN.** ATS 2021.

Xin Y., Lenart A., Martin K., Delvecchio P., Gerard S., Hamedani H.,Herrman J., Humayun S., Lenart A., Sidhu U., Pretov M., Abate N., Reutlinger K., Staley M., Esposito S., Tustison N., Gee J., Rizi R., Cereda M. **High-Resolution Responses to Prone Positioning and PEEP Therapy in a Large Animal Model of Evolving Lung Injury.** ATS 2021.

M. Connell, Y. Xin, P. Delvecchio, A. Kajanaku, N. Abate, U. Sidhu, A. Lenart, S. Esposito, M. Petrov, K. Reutlinger, T. Mandelbaum, K. Martin, M. Del Signore, C. Ellis, D. Jaye, M. Staley, H. Profka, N. Tustison, J. Gee, R.

Rizi, M. Cereda; **Whole-lung And Lobar Segmentation Of Lungs With Severe ARDS Using Deep Convolutional Neural Networks.** ATS 2020

Y. Xin, N. Abate, A. Lenart, P. Delvecchio, U. Sidhu, A. Kajanaku, S. Esposito, M. Petrov, M. Connell, K. Reutlinger, T. Mandelbaum, K. Martin, M. Del Signore, C. Ellis, D. Jaye, M. Staley, H. Profka, N. Tustison, J. Gee, R. Rizi, M. Cereda; **The Efficacy Of Prone Positioning Deteriorates In Late Stages Of Lung Injury .** ATS 2020.

Y. Xin, N. Abate, A. Lenart, P. Delvecchio, U. Sidhu, A. Kajanaku, S. Esposito, M. Petrov, M. Connell, K. Reutlinger, T. Mandelbaum, K. Martin, M. Del Signore, C. Ellis, D. Jaye, M. Staley, H. Profka, N. Tustison, J. Gee, R. Rizi, M. Cereda;**A Realistic And Reproducible Model Of Progressive Lung Injury In Ventilated Pigs.** ATS 2020

T. Mandelbaum**,** Y. Xin, N. Abate, A. Lenart, P. Delvecchio, U. Sidhu, A. Kajanaku, S. Esposito, M. Petrov, M. Connell, K. Reutlinger, T. Mandelbaum, K. Martin, M. Del Signore, C. Ellis, D. Jaye, M. Staley, H. Profka, N. Tustison, J. Gee, R. Rizi, M. Cereda;**A Novel Method Of**

Detecting Pulmonary Overdistention Using Lung Ultrasound Pilot Study.

ATS 2020